UNIVERSITY OF CALIFORNIA, SAN DIEGO

Cellular Defenses and Viral Counterattacks During Herpes Simplex Virus Infection

A dissertation submitted in partial satisfaction of the

requirements for the degree Doctor of Philosophy

in

Biology

by

Mira Suresh Chaurushiya

Committee in charge:

Professor Matthew D. Weitzman, Chair
Professor Daniel Donoghue
Professor Tony Hunter
Professor Richard Kolodner
Professor Suresh Subramani

2011

The dissertation of Mira Suresh Chaurushiya is approved, and it is acceptable in quality and form for publication on microfilm and electronically:

_____

_____

_____

_____

_____

_____
Chair

University of California, San Diego

2011

DEDICATION

For my mother, my father, my sister, and my wife.

Without them, none of this would be worth it.

TABLE OF CONTENTS

LIST OF FIGURES

Chapter 1

Chapter 2

Chapter 3

Chapter 4

Chapter 5

Appendix

LIST OF TABLES

Chapter 4

ACKNOWLEDGEMENTS

I must first thank Matthew Weitzman, my advisor, for his support throughout my graduate training. He had an unwavering belief that I would always "figure it out in the end," even when I did not think I would. He let me do things my own way but was always waiting in the wings in case I needed help. The reason he did not have to save me too often was because of Caroline Lilley, who I thank for her friendship as well as her mentorship. It was through our many, many arguments that I learned how to ask and answer good questions. We often picked up experiments where the other left off, which requires a special kind of trust that will be hard to come by in the future. I thank her as well as the graduate students who were in the lab with me, Rachel, Seema, and Nicole, for making the lab my home away from home and a wonderful place to do science. The postdoctoral fellows in the lab were a continual resource for me. I thank Junghae Suh for her mentorship during my rotation through the lab. Brandon Lamarche, a talented biochemist, was invaluable when my project required biochemical techniques with which I was unfamiliar. Sebastien Landry and Inigo Narvaiza always had useful suggestions that strengthened the projects, and I also thank Inigo for some crucial late night rides home from the lab.

I am grateful to collaborators and co-authors including Caroline Lilley, Junghae Suh, Simina Ticau, and Sebastien Landry from the Weitzman Lab, Jill Meisenhelder and Aaron Aslanian from Tony Hunter's lab, Roger Everett and Chris Boutell from the MRC Virology Unit in Glasgow, Steffi Panier and Daniel Durocher from the Samuel Lunenfeld Research Institute at the University of Toronto, and Grant

Stewart at Cancer Research UK in Birmingham. I also thank Brenda Schulman, who gave me the opportunity to work in her lab at St. Jude Children's Research Hospital to generate some of the data presented in this Dissertation. She has since become a wonderful collaborator and mentor, and is a continual source of encouragement.

Some of the data in Chapter 2 are reprints as they appear in EMBO J. 2010, Lilley CE, Chaurushiya MS, Boutell C, Landry S, Suh J, Panier S, Everett RD, Stewart GS, Durocher D, and Weitzman MD, A viral E3 ligase targets RNF8 and RNF168 to control histone ubiquitylation and DNA damage responses, 29:943-955, and PLoS Pathogens, 2011, Lilley CE, Chaurushiya MS, Boutell C, Everett RD, and Weitzman MD, The Intrinsic Antiviral Defense to Incoming HSV-1 Genomes Includes Specific DNA Repair Proteins and is Counteracted by the Viral Protein ICP0, 7(6): e1002084. The Dissertation author was a researcher and author on these papers.

Chapter 3, in full, has been submitted for publication for material as it may appear in Molecular Cell, 2011, Viral E3 ubiquitin-mediated degradation of a cellular E3: viral mimicry of a cellular phosphorylation mark to target cellular FHA domain proteins, Chaurushiya MS, Lilley CE, Aslanian A, Meisenhelder J, Ticau S, Boutell C, Yates JR III, Schulman BA, Hunter T, and Weitzman MD. The Dissertation author was the primary researcher and author of this paper.

I thank the members of my thesis committee, Daniel Donoghue, Ananda Goldrath, Tony Hunter, Richard Kolodner, and Suresh Subramani, who always provided challenging and insightful discussions during my annual committee meetings. The work presented in this Dissertation has greatly benefited from their

suggestions, experience, and advice. I thank Tony Hunter in particular for critical reading of manuscripts that improved the quality of the papers submitted for publication.

I thank the H.A. and Mary K. Chapman Foundation and the UCSD Growth Regulation and Oncogenesis Training Grant (NIH T32) for providing financial support during my graduate training.

Finally, none of this would have been possible without the wonderful friends I have made in San Diego. They have unwaveringly supported me through the ups and downs of life events during my time in graduate school, and for that I am forever grateful.

VITA

2011	Ph.D., Biological Sciences Division, University of California, San Diego
2005-2011	Graduate Student, Biological Sciences Division, University of California, San Diego
2006-2009	Teaching Assistant, Biological Sciences Division, University of California, San Diego
2003-2005	Research Assistant, Pediatric Infectious Diseases Department, The University of Chicago
2002-2003	Research Assistant, Laboratory for Cancer Biology, The Rockefeller University
2002	B.A., *cum laude*, Department of Biology, Carleton College
2001	Summer Intern, Department of Laboratory Medicine and Pathology and the Supercomputer Institute, The University of Minnesota
2000-2002	Undergraduate Intern, Department of Biology, Carleton College

PUBLICATIONS

Chaurushiya MS, Lilley CE, Aslanian A, Meisenhelder J, Ticau S, Boutell C, Yates JR III, Schulman BA, Hunter T, Weitzman MD. Viral E3 ubiquitin-mediated degradation of a cellular E3: viral mimicry of a cellular phosphorylation mark to target cellular FHA domain proteins. 2011, *submitted.*

Weitzman MD, Lilley CE, Chaurushiya MS. Changing the ubiquitin landscape during viral manipulation of the DNA damage response. 2011. FEBS Letters, *in press*.

Lilley CE, Chaurushiya MS, Boutell C, Everett R, Weitzman MD. The Intrinsic Antiviral Defense to Incoming HSV-1 Genomes Includes Specific DNA Repair Proteins and Is Counteracted by the Viral Protein ICP0. 2011. PLoS Pathogens, 7(6): e1002084.

Weitzman MD, Lilley CE, Chaurushiya MS. Genomes in conflict: maintaining genome integrity during virus infection. Annual Review of Microbiology. 2010. 64:61-81.

Lilley CE, Chaurushiya MS, Boutell C, Landry S, Suh J, Panier S, Everett RD, Stewart GS, Durocher D, Weitzman MD. A viral E3 ligase targets RNF8 and RNF168 to control histone ubiquitylation and DNA damage responses. 2010. EMBO J. 29(5):943-55.

Lilley CE, Chaurushiya MS, and Weitzman MD. Chromatin at the intersection of viral infection and DNA damage. 2010. Biochim Biophys Acta. 1799(3-4):319-27.

Chaurushiya MS and Weitzman MD. Viral manipulation of DNA repair and cell cycle checkpoints. DNA Repair (Amst). 2009. 8(9):1166-76.

Stoffel A, Chaurushiya M, Singh B, Levine AJ. Activation of NF-kB and inhibition of p53- mediated apoptosis by API2/mucosa-associated lymphoid tissue 1 promote oncogenesis. 2004. Proceedings of the National Academy of Sciences USA 101(24):9097-84.

ABSTRACTS SELECTED FOR ORAL PRESENTATION

Chaurushiya MS, Lilley CE, Aslanian A, Ticau S, Yates JR III, Schulman BA, Hunter T, Weitzman MD. A viral ubiquitin ligase mimics a cellular phosphorylation mark to modulate the DNA damage response and relieve transcriptional silencing. The Sixth Cold Spring Harbor Meeting on the Ubiquitin Family, May 2011, Cold Spring Harbor Laboratory, NY

Chaurushiya MS, Lilley CE, Ticau S, Weitzman MD. ICP0 targets RNF8 for degradation via phosphorylation dependent interaction with RNF8 FHA domain. 35th International Herpesvirus Workshop. Jul 2010, Salt Lake City, UT

Chaurushiya MS, Lilley CE, Aslanian A, Boutell C, Yates JR III, Hunter T, Weitzman MD. A viral E3 ubiquitin ligase targets cellular E3 ubiquitin ligases to modulate histone ubiquitylation: implications for viral latency and reactivation. 5th International Conference on SUMO, Ubiquitin, UBL proteins: Implications for Human Diseases. Feb 2010, Houston, TX

ABSTRACT OF THE DISSERTATION

Cellular Defenses and Viral Counterattacks During Herpes Simplex Virus Infection

by

Mira Suresh Chaurushiya

Doctor of Philosophy in Biology

University of California, San Diego, 2011

Matthew D. Weitzman, Chair

Viruses rely on host cell resources to execute the diverse functions required for propagation, and they must simultaneously counteract intrinsic antiviral defenses deployed by the cell. To commandeer and overtake cellular processes, viruses encode regulatory proteins able to bind and redirect host proteins that function at key nodes in cellular pathways. Many viruses harness the cellular ubiquitin-proteasome system to execute their counterattacks. Herpes simplex virus-1 (HSV-1) encodes a RING domain E3 ubiquitin ligase, ICP0, which promotes lytic infection and reactivation from latency by targeting cellular proteins for ubiquitylation and degradation. In the work presented in this Dissertation, we identify two novel substrates of ICP0, the cellular E3 ligases and DNA damage response (DDR) proteins RNF8 and RNF168. In

uncovering why these cellular proteins are targeted, we demonstrate that the cell is able to deploy the DDR not only to recognize damage to the host genome, but also to recognize incoming HSV-1 genomes and repress transcription from the viral genome. As such, we define the DDR to function as an intrinsic antiviral defense, coordinated through RNF8 and ubiquitin-dependent mechanisms. The degradation of RNF8 and RNF168 serves as the viral counterattack, as this prevents recruitment of DDR proteins to sites of incoming viral genomes, induces loss of ubiquitylated H2A and H2AX, relieves transcriptional repression of the viral genome, and promotes viral infection. We further elucidate the mechanism by which ICP0 targets RNF8 and demonstrate that ICP0 mimics a cellular phosphosite normally induced on cellular proteins in response to DNA damage to bind the RNF8 FHA domain. We demonstrate a role for the cellular CK1 kinase in catalyzing phosphorylation on ICP0 to facilitate the RNF8-ICP0 interaction. These observations highlight the power of viral mimicry in targeting cellular proteins and pathways during infection and suggest that other viruses may mimic cellular post-translational marks to insert themselves into key cellular pathways. Finally, our findings demonstrate that the ubiquitin system plays prominent roles in both cellular defense and viral counterattack during infection.

Chapter 1. Introduction

Virus-host interactions and intrinsic antiviral defense

Viruses have an intimate relationship with the host cells that they infect. As obligate intracellular parasites, they have evolved directed mechanisms by which to take advantage of host cell proteins and processes to promote their own replication. Viruses cannot metabolize environmental energy sources to generate the ATP required to propagate, and instead rely on cellular metabolic pathways for ATP. Similarly, they harness cellular enzymes and machinery to execute the many tasks required for viral progeny production. While taking advantage of these cellular resources, viruses must also inactivate those cellular proteins and pathways that pose barriers to infection.

The acquired and innate immune systems are often viewed as the primary barriers against pathogenic infections in an organismal context, but a growing body of evidence has demonstrated that intracellular proteins can perform dual functions, executing cellular tasks in the absence of infection and redirecting their efforts to quench a virus in the event of infection. Such mechanisms have been termed intrinsic antiviral defenses (Bieniasz, 2004). Three key features define proteins that can function as intrinsic antiviral defenses. First, the cellular proteins are constitutively expressed and not induced upon viral infection. Second, the cellular proteins are restrictive to viral infection. Finally, in most cases the virus has evolved a mechanism by which to counter the intrinsic antiviral defense. This counterattack often comprises the encoding of viral proteins that inactivate the restrictive cellular factors. Thus there

exists a continual battle between viral and cellular proteins for control of host cell resources during infection of the cell.

The viral counterattack often takes advantage of the cellular ubiquitin-proteasome system (UPS), which can target proteins for degradation. Viruses encode UPS components to directly and specifically target restrictive cellular proteins for degradation. Adenovirus (Ad), Human Papillomavirus (HPV), Epstein-Barr virus (EBV), Herpes simplex virus (HSV), and Human immunodeficiency virus (HIV) are just a few of the viruses that hijack the UPS to promote infection (Boutell et al., 2002; Masucci, 2004; Querido et al., 2001; Scheffner et al., 1993; Yu et al., 2003b). The targeting mechanisms and cellular substrates of the viral proteins interfacing with the UPS are often unknown, and have the potential to provide novel insights into the mechanisms governing virus takeover of the host cell. Furthermore, as viruses often target key nodes of cellular pathways, the identification of cellular targets can also provide insight into the mechanisms by which cellular pathways function.

Recent work from a number of labs has demonstrated that the cellular DNA damage response (DDR) pathway is activated during many types of viral infection (reviewed in (Weitzman et al., 2010)), likely due to recognition of abnormal viral DNA structures. In some cases viruses harness the DDR to promote infection, and in others the DDR poses a barrier that must be overcome (Lilley et al., 2007). Work described in this Dissertation explores the interplay between Herpes simplex virus type-1 (HSV-1), the cellular DNA damage response, and the HSV-1 encoded ubiquitin

ligase ICP0, revealing that the DDR functions as an intrinsic antiviral defense that is counteracted through ICP0.

Herpes Simplex Virus -1

Disease and Treatment

Herpes simplex virus type-1 (HSV-1) and type-2 (HSV-2) are ubiquitious human pathogens that infect up to 80% of the world population and subsist for the lifetime of the infected individual. As with all herpesviruses, HSV-1 and HSV-2 possess the ability to transition between latent and lytic states. The initial infection is lytic and occurs in the oral or genital mucosal epithelial tissues, resulting in production of viral progeny and cell death. These primary infections can result in lesions in the oral or genital tissues, but are often asymptomatic. Latent infections stem from the initial infection and occur in the neurons innervating the original site of infection. In contrast to lytic infections, latent infections do not result in production of viral progeny or neuronal death, allowing the virus to remain in the body in a silent reservoir without causing visible disease. HSV-1 is more prevalent in oral mucosa while HSV-2 is more prevalent in the genital tissues. However, both viruses are able to infect the oral and genital tissues and establish latency in the trigeminal and sacral ganglia, respectively.

Recurrent infection can occur when the latent virus reactivates, and as in the primary infection, recurrent infection can be symptomatic or asymptomatic. HSV is

often transferred via skin-to-skin contact during asymptomatic recurrence, when the virus is present in the saliva and mucosa, but does not present with obvious lesions.

HSV can cause more serious disease in infants and can be acquired congenitally or neonatally (Corey and Wald, 2009). HSV replication in the neurons can cause encephalitis (Dennett et al., 1997), and HSV infection has been correlated with an increased risk for acquiring HIV (Wald and Link, 2002), although the causal relationship is still debated (Corey, 2007). Increased HIV susceptibility may be due to the higher number of activated T-cells and macrophages present in the genital mucosa, which are more susceptible to HIV infection than resting T-cells and macrophages. The ability of genital HSV lesions to compromise the integrity of the genital tissues may also facilitate HIV entry into the body (Wald and Link, 2002).

HSV infections can be treated using a nucleoside analogue, acyclovir, which is activated in an infected cell by phosphorylation via the viral thymidine kinase (TK). Cellular kinases then facilitate the formation of a triphosphate version of acyclovir, which can then interfere with the viral polymerase and act as a chain terminator, preventing replication of the viral genome (Elion, 1983). Acyclovir and related therapies reduce the severity and length of an outbreak as well as prolong the time period between outbreaks. While therapeutic interventions exist, there are currently no vaccines to prevent acquisition of HSV. Understanding the relationship between HSV and its host, particularly on the molecular level, is integral for the rational design of novel intervention strategies.

Genome Organization and Virion Structure

HSV-1 is an enveloped virus that contains a double stranded, linear DNA genome of approximately 152 kb. It is composed of unique long (U_L) and unique short (U_S) subunits bounded by inverted and terminal repeat regions (IR_L/TR_L and TR_S/IR_S) and encodes at least 72 genes. During infection, the U_L and U_S subunits can be inverted, giving rise to four possible isomers of the genome **(Figure 1-1A).** It has been empirically determined that all four isomers exist in equimolar ratios in an infected cell (Roizman, 1979). While most genes exist in a single copy, genes encoded in the terminal repeat regions exist in two copies; of relevance to this thesis, the RNA species known as the latency associated transcripts (LATs) and ICP0 are encoded in the R_L regions **(Figure 1-1B)**.

The viron particle consists of the viral genome housed in an icosahedral capsid, a lipid bilayer embedded with glycoproteins, and a region between the viral capsid and envelope called the tegument **(Figure 1-1C)**. The tegument consists of viral proteins that are required early during infection, before viral gene expression.

Life Cycle

Like all herpesviruses, HSV-1 undergoes lytic and latent stages of infection. The primary lytic infection occurs in mucosal epithelial tissues and is characterized by a cascade of viral gene expression, genome replication, virion assembly, and egress. Following primary infection, some of the viral progeny enter the axons of neurons innervating the site of infection and are transported to the neuronal nucleus. During

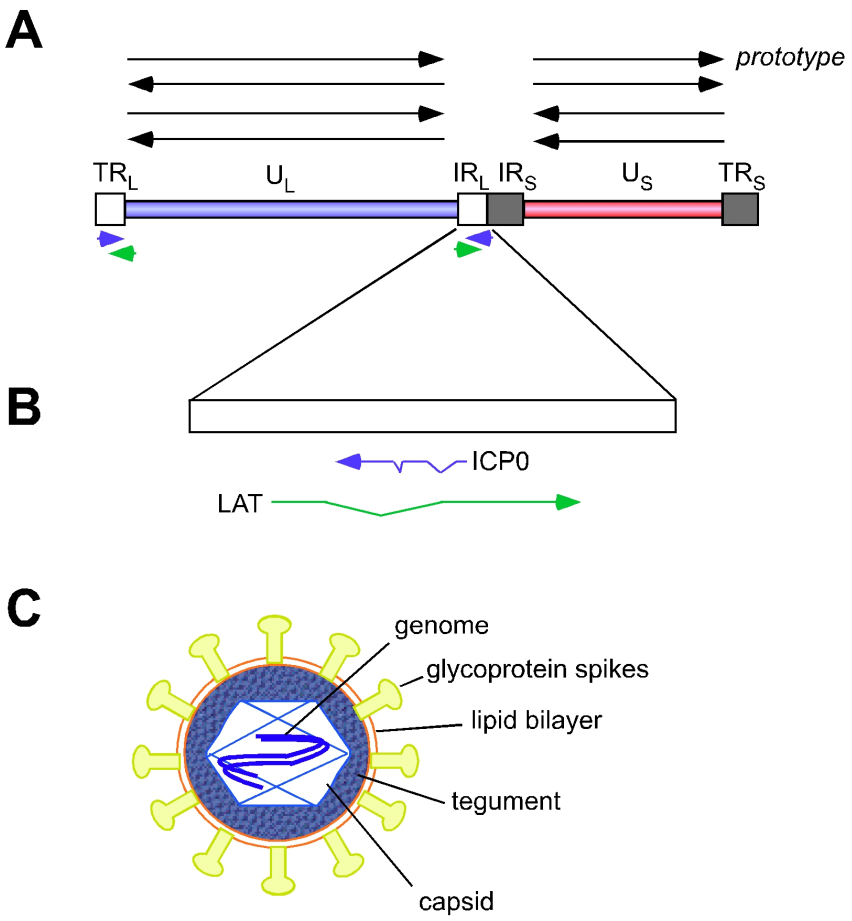

Figure 1-1. HSV-1 genome organization and virion structure. A. The HSV-1 genome is composed of unique long and unique short regions that can be inverted to yield four different isoforms of the genome. While there is only one U_L and U_S unit per genome, the repeat regions exist in terminal and internal copies, and thus genes encoded in these regions exist in two copies. Notably, ICP0 (blue arrow) and LAT (green arrow) are encoded in two copies as indicated. **B.** Location of ICP0 and LAT in the repeat region. The ICP0 coding region is complementary to the LAT coding region and both are depicted as they are oriented in the prototype isoform. **C.** The viral particle is composed of an icosahedral capsid, which houses the viral genome and is enveloped by a lipid bilayer (orange) containing glycoprotein spikes (yellow), which are used for binding and adsorption into target cells. Between the lipid bilayer and capsid is a mixture of proteins called the tegument (dark blue).

latency, no viral proteins are produced and the genome is largely transcriptionally silent, except for expression of the LATs. The LATs encode RNAs that have been shown to function as micro RNAs (miRNAs), interfering with lytic gene expression during latency (Umbach et al., 2008) and promoting neuronal survival (Perng et al., 2000). Periodically, due to stress factors including UV exposure, trauma, or stress, the virus reactivates and exits latency, establishing another round of lytic infection at the primary site of infection (Whitley, 2001) **(Figure 1-2)**. The molecular mechanisms governing the establishment of and reactivation from latency are still unclear and are studied in a variety of herpesvirus systems.

Lytic infection is characterized by the temporal expression of immediate-early (IE), early (E), and late (L) genes (Honess and Roizman, 1974; Roizman and Knipe, 2001). The IE genes generally function as transcriptional regulatory proteins to promote E gene expression. The E gene products are involved in replication of the viral genome, and L genes encode the proteins involved in capsid and virion assembly (Roizman and Knipe, 2001).

After adsorption and entry into the host cell, the viral capsid migrates through the cytoplasm to the nucleus, where it is thought to dock with the nuclear pore complex and inject the viral DNA into the nucleus, leaving the empty capsid in the cytoplasm (reviewed in (Liashkovich et al., 2011)). The viral DNA initially exists in its virion form, as double-stranded, linear molecule. VP16, a virally encoded transcriptional transactivator, is packaged in the virion as part of the tegument and therefore enters the cell as a fully functional protein. It also enters the nucleus, and

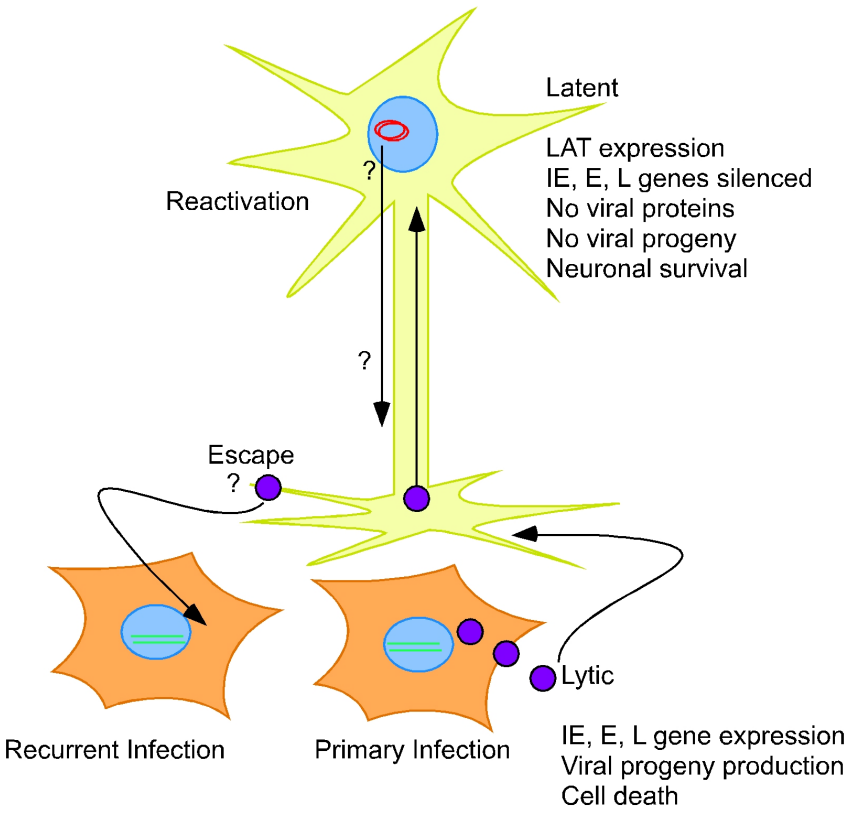

Figure 1-2. The HSV-1 life cycle. Primary infection occurs in the epithelial cells (orange) and results in transcriptional activation of the viral genome (green), viral protein synthesis, and progeny production (purple). Progeny virions can enter the axons of neurons innervating the site of infection and are transported to the neuronal body, where a latent infection is established. During latency the viral genome exists as a largely transcriptionally silent episome (red) and no viral proteins or progeny are detected. Upon reactivation, the virus escapes the neuron and enters another round of lytic infection in the epithelial cells, establishing a recurrent infection. The molecular mechanisms governing reactivation and escape are unclear.

there it recruits the cellular Oct-1 and HCF-1 transcription factors to bind IE gene promoters at conserved TAATGARAT sequences and promote transcription of the five IE genes (reviewed in (Wysocka and Herr, 2003)). Four of these, ICP4, ICP27, ICP22 and ICP0, promote the timely expression of the three classes of genes (Roizman and Knipe, 2001) **(Figure 1-3)**, whereas the fifth, ICP47, is involved in immune evasion (Hill et al., 1995; York et al., 1994).

The structure of the replicating genome and the mechanism by which it is replicated are currently the subject of controversy (Sandri-Goldin, 2003). Several biochemical studies have indicated that the genome is circularized (Garber et al., 1993; Strang and Stow, 2005) and undergoes a rolling circle mechanism of replication (Roizman, 1979; Skaliter et al., 1996). This could explain the observed concatemerization of the genome, which must be cleaved before packaging, as well as the generation of the four isomers. However, other studies report that this circular form does not exist (Jackson and DeLuca, 2003), at least during lytic infection, and differences in biochemical assays may be responsible for these conflicting results. Replication of the viral genome occurs in distinct sub-nuclear sites that can be visualized using immunofluorescence against the viral ssDNA binding protein ICP8 (Quinlan et al., 1984). Biochemical and immunofluorescence based experiments have found that many cellular proteins, particularly those involved in DNA replication and repair, are recruited to these sites (Lilley et al., 2005; Shirata et al., 2005; Taylor and Knipe, 2004; Wilkinson and Weller, 2004). Here, they may aid in viral DNA processing, replication, recombination, and concatemer cleavage before packaging.

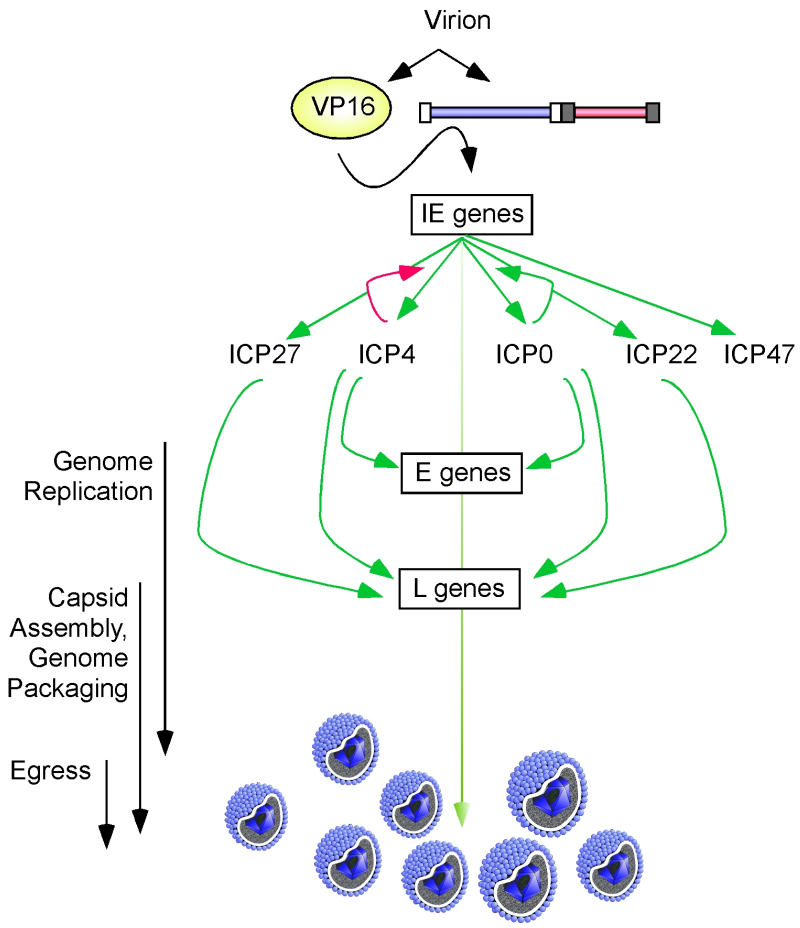

Figure 1-3. Lytic HSV-1 infection occurs via a cascade of gene expression. The virion delivers the viral genome and the VP16 transactivator into the cell. VP16 recruits cellular transcriptional activators to IE gene promoters. The IE gene products transactivate E and L genes as indicated. Green arrows indicate activation of the target genes, whereas red arrows indicate a repression of the indicated target genes. L gene transcription takes place after genome replication is complete. The genome is then packaged into viral capsids and egress results in the enveloped viral progeny budding from the cell.

Capsid proteins are encoded by the L genes and assemble within the nucleus of the infected cell. The replicated genomes are cleaved and packaged into capsids, and the viral capsids then begin the complicated process of egress. This involves escaping the nucleus via budding through the inner and outer nuclear membranes, traversing the cytoplasm through envelopment into the trans golgi network, and release through endosomal budding from the plasma membrane, becoming enveloped in the host cell membrane in the process (reviewed in (Johnson and Baines, 2011)).

ICP0 contribution to HSV-1 infection

During HSV-1 infection, ICP0 promotes the ability of the virus to enter a replicative cycle and also plays important roles in reactivation from latency. These effects can be studied in a variety of tissue culture systems and animal models, which combined have helped elucidate the contribution of ICP0 to HSV-1 infection.

In mouse models, ICP0 mutant viruses can replicate when inoculated into the eye and are able to establish latency in the murine trigeminal ganglia (TG), though less efficiently than WT viruses. However, they are greatly impaired in their ability reactivate from latency (Cai et al., 1993; Clements and Stow, 1989; Leib et al., 1989). In tissue culture systems, ICP0-null (ΔICP0) viruses are impaired for viral progeny production compared to WT virus, although these effects are apparent only when very low amounts of virus are used. When high amounts of virus are used, the requirement for ICP0 is negligible. These observations support a hypothesis whereby restrictive cellular factors can be titrated out by the presence of enough viral genomes, or in the

more physiological context of fewer viral genomes, by ICP0. Importantly, the defects of an ICP0-null virus can vary depending on the cell type. Most notably, ΔICP0 viruses exhibit no growth defect in U2OS (human osteosarcoma) cells (Yao and Schaffer, 1995), and the mechanisms underlying this observation are still unclear.

Several tissue culture systems have been developed in order to assess the contribution of ICP0 to reactivation from latency. HSV-1 viruses have been constructed that enter an abortive infection and establish a transcriptionally silent state when used to infect tissue culture cells. These can be temperature sensitive mutants, mutants defective for of all five of the IE genes, or mutants in which VP16 is unable to transactivate IE genes. In these systems, ICP0 expression *in trans* facilitates the ability of the virus to emerge from quiescence (Harris et al., 1989; Hobbs et al., 2001; Samaniego et al., 1998). Viral DNA transfection can also recapitulate a reactivation-like scanario (Cai and Schaffer, 1989). It mimics the situation thought to exist during latency for two reasons. First, the viral genome is present in the cell, but viral proteins that are usually delivered in the virion (such as VP16) are not. Second, the number of genomes per cell (MOI) is very low, which may be more similar to the small number of neurons carrying the latent genome in the organism. In this system, WT HSV-1 DNA yields infectious viral particles much earlier and at much higher titer than HSV-1 DNA lacking ICP0 (Cai and Schaffer, 1989), indicating that ICP0 contributes to *de novo* expression of viral proteins and subsequent viral replication.

Chromatin, latency, and ICP0

The HSV-1 genome is devoid of histones or nucleosome structures in its virion state (Oh and Fraser, 2008; Pignatti and Cassai, 1980; Placek and Berger, 2010). However, upon infection the genome becomes rapidly associated with histones and nucleosomes. This has been demonstrated using microccocal nuclease digestion, which cleaves DNA that is not protected by a nucleosome structure (Greil et al., 1976). Both the lytic and latent genomes are associated with nucleosomes, although the chromatin structures and epigenetic marks are distinct, and the virally encoded LATs and ICP0 affect the nucleosome and epigenetic landscape of the viral genome.

The latent genome associates with nucleosomes characteristic of those observed in the cellular chromatin (Deshmane and Fraser, 1989). There appears to be no difference in the nucleosome occupancy of the LAT promoters, which are active during latency, and the promoters of lytic genes, which are silenced. Furthermore, the latent viral genome itself does not appear to be methylated, which is a marker of silenced regions (Kubat et al., 2004). However, analysis of epigenetic marks reveals that the promoter regions of the LATs are enriched for transcriptionally permissive, euchromatin-associated marks such as acetyl H3K9 and K14, and dimethyl H3K4 (Kubat et al., 2004; Kwiatkowski et al., 2009). In contrast, lytic gene promoters such as ICP4 and ICP0 do not contain euchromatin marks and are enriched for transcriptionally repressive facultative and constitutive heterochromatin marks, including trimethyl H3K9 and H3K27, and macro H2A (Cliffe et al., 2009; Kwiatkowski et al., 2009). Additionally, chromatin-modifying proteins such as Bmi1

have been found to be associated with the latent genome (Kwiatkowski et al., 2009), providing evidence that the latent genome is silenced through chromatinization and deposition of silencing epigenetic marks through cellular pathways. Intriguingly, expression of the LATs appears to affect the epigenetic state of the latent genome, though different HSV-1 strains may assume different epigenetic profiles in response to LAT expression. In strain 17 *syn*+, which is a highly reactivating virus, the presence of the LATs reduces the amount of facultative heterochromatin on the viral genome (Kwiatkowski et al., 2009). In contrast, in strain KOS, which reactivates less frequently, the LATs promote heterochromatin formation on the lytic promoters (Cliffe et al., 2009).

Compared to the latent genome, the nucleosome structure of the lytic genome appears to be composed of destabilized and disordered nucleosome structures (Kent et al., 2004; Lacasse and Schang, 2010), and enriched for transcriptionally permissive epigenetic marks (Kent et al., 2004). These include acetyl H3K9 and K14 at the promoter regions of the ICP0, VP16, and TK genes, and trimethyl H3K4 at the 5' end of the ORFs of these genes. Along with changes in specific epigenetic marks, the overall histone occupancy at IE gene promoters appears reduced compared to other regions of the lytic viral genome, and chromatin-remodeling co-activators that promote transcription are recruited in a VP16 dependent manner (Herrera and Triezenberg, 2004).

ICP0 affects the chromatin state of the lytic and latent viral genomes, particularly during reactivation and lytic infection. In quiescence models mimicking

the transcriptionally repressed, latent state of the virus, ICP0 expression *in trans* is able to remove silencing heterochromatin marks from the promoters of lytic genes, concurrent with gene activation and emergence from quiescence (Ferenczy and DeLuca, 2009, 2011). ICP0 expression decreases histone occupancy on lytic promoters of latent genomes, indicating that ICP0 promotes genome transition from its latent chromatin state to a chromatin state more reminiscent of lytic infection. ICP0 also promotes histone removal during lytic infection, and ICP0 expression results in the deposition of activating acetylation marks on the nucleosomes (Cliffe and Knipe, 2008). Combined, these observations suggest that the chromatin state of the viral genome affects the establishment of and reactivation from latency, and that ICP0 plays key roles in modulating the epigenetic marks during reactivation and lytic infection. However, the mechanisms by which ICP0 affects these epigenetic marks are unclear.

Molecular and biochemical functions of ICP0

Several studies using promoters fused to reporter genes found that ICP0 transcriptionally transactivates all the classes of HSV-1 promoters (Cai and Schaffer, 1992; Cai and Schaffer, 1989) and promotes the transactivator function of ICP4 (Everett, 1987). In these studies, mutant analysis of ICP0 demonstrated that the N-terminal half of the protein is most important for these functions. In animal model systems as well as tissue culture systems, analysis of mutant forms of ICP0 established that the N-terminal half of the protein is also most important for its contribution to efficient HSV-1 replication, emergence from quiescence, and reactivation from

latency (Cai and Schaffer, 1989). Thus, the transactivator capability of ICP0 mutants correlates closely with the ability to promote HSV-1 infection.

Early bioinformatics analysis revealed that the N-terminal half of ICP0 contains a cysteine rich zinc-coordinating region. While it was suggested that this region could be important for DNA binding (Everett, 1987), purification of recombinant ICP0 protein revealed that it could not directly bind DNA in solution (Everett et al., 1991). The cysteine rich zinc-coordinating region was subsequently identified to contain sequences characteristic of the RING (Really Interesting New Gene) domain, which associates with E2 ubiquitin conjugating enzymes to target cellular proteins for ubiquitylation. This suggested that ICP0 could interface with the cellular ubiquitin-proteasome system. Supporting this hypothesis, ICP0 was demonstrated to promote the accumulation of co-localizing conjugated ubiquitin, and the addition of proteasome inhibitors prevented the ability of ICP0 to transactivate promoters and promote reactivation (Everett et al., 1993; Everett et al., 1998b). Thus it appeared that the primary functions of ICP0 were dependent on the cellular UPS.

Biochemical analysis of recombinant ICP0 protein revealed that it could promote conjugation of polyubiquitin chains *in vitro* in cooperation with cellular ubiquitin activating and conjugating enzymes, and that its RING domain was necessary and sufficient for this function (Boutell et al., 2002). Thus ICP0 was determined to be an HSV-1 encoded E3 ubiquitin ligase, with the N-terminal RING domain conferring its E3 ligase activity. C-terminal portions of the protein have been shown to target ICP0 to at least some of its substrates **(Figure 1-4A)**.

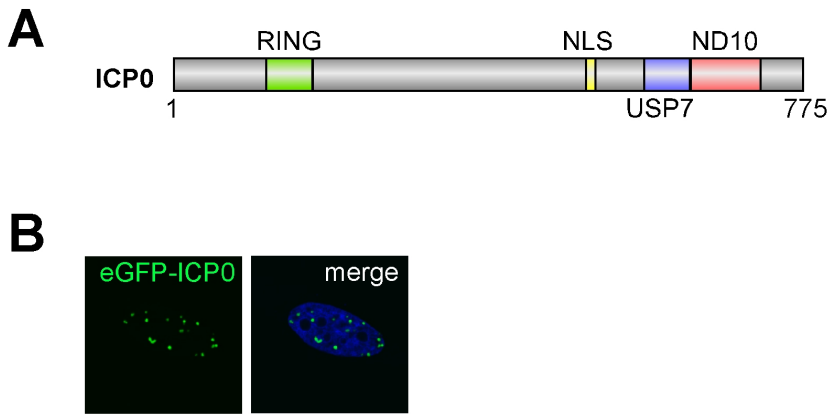

Figure 1-4. Domain structure and subcellular localization of ICP0. A. ICP0 contains a RING domain at its N terminus that confers E3 ubiquitin ligase activity. The C-terminal region contains the nuclear localization signal (NLS) as well as sequences that target ICP0 to two of its degradation targets, USP7 and PML bodies (PML and Sp100). Numbers represent amino acid positions. **B.** ICP0 localizes to distinct nuclear foci corresponding to PML bodies. eGFP-ICP0 was transfected into HeLa cells, fixed 24 h post-transfection, and visualized using GFP fluorescence.

Several ICP0 ubiquitylation and degradation targets have been identified. The ubiquitin-specific protease USP7 binds the ICP0 C-terminus and is degraded during infection in an ICP0-dependent manner (Boutell et al., 2005; Everett et al., 1999b; Everett et al., 1997; Meredith et al., 1995; Meredith et al., 1994). In cells, ICP0 localizes to discrete foci in the nucleus that coincide with promyelocitic leukemia (PML) bodies (Everett and Maul, 1994; Maul and Everett, 1994), and this is dependent on a C-terminal region of the protein **(Figure 1-4B)**. PML bodies are nucleated by several PML isoforms through SUMO-dependent interactions. Upon ICP0 expression, PML bodies are dispersed and the accumulation of conjugated ubiquitin can be detected at ICP0 foci (Everett, 2000a; Everett et al., 1998a; Everett and Maul, 1994; Everett and Murray, 2005; Maul and Everett, 1994). Consistent with these observations, ICP0 mediates the proteasome-dependent degradation of several PML isoforms and Sp100, another component of PML bodies (Everett et al., 1998a). In mitotic cells, ICP0 can also be visualized at the kinetochore, where it mediates the degradation of several centromeric proteins (Everett et al., 1999a; Lomonte and Morency, 2007; Lomonte et al., 2001). While *in vitro* ubiquitylation of p53 has been observed, p53 is stabilized during HSV-1 infection, and so the significance of this ubiquitylation is unclear (Boutell and Everett, 2003, 2004). Finally, ICP0 has been shown to mediate degradation of the catalytic subunit of the DNA-dependent protein kinase (DNA-PKcs) (Lees-Miller et al., 1996; Parkinson et al., 1999), although an interaction between ICP0 and DNA-PKcs has not been detected.

In several cases, the cellular proteins targeted by ICP0 have been shown to be restrictive to HSV-1 infection. The replication of ΔICP0 viruses is increased in cells where expression levels of the PML body components PML, Sp100, ATRX, or hDaxx are attenuated (Everett et al., 2008; Everett et al., 2006; Lukashchuk and Everett, 2010). During infection with ΔICP0 virus, PML and associated components can be visualized at sites associated with incoming viral genomes (Everett and Murray, 2005), suggesting that they can recognize and repress the genome. ΔICP0 infection is also enhanced in cells lacking DNA-PKcs (Parkinson et al., 1999), indicating that this degradation target is also a restrictive factor during HSV-1 infection. While in these cases the targeted cellular proteins are restrictive to infection, the restrictive effects are often are subtle, indicating that it is a combinatorial targeting of multiple cellular proteins by ICP0 that is likely responsible for the effects of ICP0.

The ICP0 requirement for reactivation from latency, its role in modifying the chromatin state of the viral genome, its function as a transcriptional transactivator, and its ability to target restrictive cellular proteins for degradation via its E3 ligase activity suggests that ICP0 promotes early transcription events via cellular protein degradation to facilitate HSV-1 infection (Everett, 2000b). Its main function in this scenario would be to titrate out repressive cellular factors, which is most important at times where very few viral genomes exist: the early stages of lytic infection and during reactivation from latency. It is unclear exactly how the currently identified substrates restrict HSV-1 infection or how they contribute to the transcriptional transactivation functions attributed to ICP0. Furthermore, it remains likely that there are as-yet

undescribed targets of ICP0 that are critical for the ability of ICP0 to promote these events.

Ubiquitylation and substrate targeting

The UPS regulates protein function via covalent modification of proteins by ubiquitin. Ubiquitin is an abundantly expressed protein in eukaryotic cells. It is conjugated to targets via a chain of enzymatic reactions, in a targeted, inducible, and reversible manner. The UPS regulates diverse cellular functions including cell cycle and the DDR, and is often deregulated in diseases and hijacked by pathogens (reviewed in (Ciechanover and Schwartz, 2004)).

Ubiquitin comprises 76 amino acids and can be covalently attached to Lys residues of target proteins via its C-terminal Gly residue. The conjugation of ubiquitin to a substrate occurs through an ATP-dependent pathway consisting of E1, E2, and E3 enzymes. Activation of ubiquitin occurs via the E1 activating enzyme, which forms a high-energy thioester bond with ubiquitin. The ubiquitin molecule is transferred from the E1 to an E2 conjugating enzyme, and conjugation to the target substrate is directed and mediated by E3 ligases. E3 ligases interact with E2s by virtue of the RING or HECT (Homologous to E6AP C-terminal) domains. RING domain E3 ubiquitin ligases can transfer ubiquitin directly from the E2 onto the target Lys of the substrate, whereas HECT domain E3 ligases transfer the ubiquitin to an active site Cys within the HECT domain before transfer to a Lys residue of the targeted substrate **(Figure 1-5A)**.

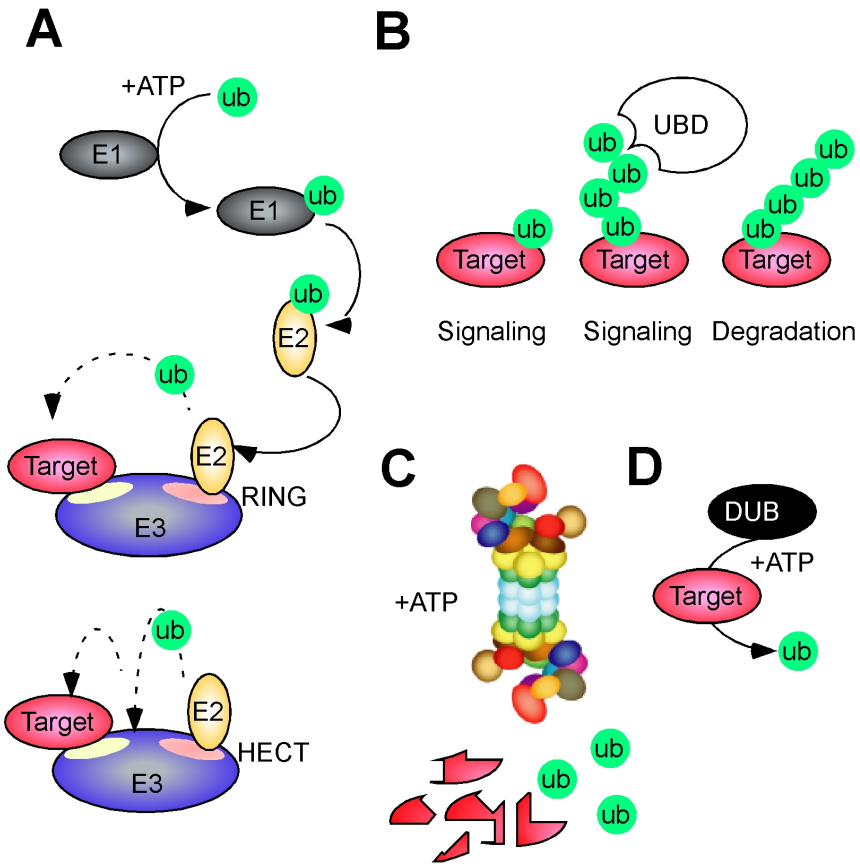

Figure 1-5. The ubiquitin proteasome system. A. Mechanism of ubiquitin conjugation. Ubiquitin is activated via a high-energy thioester linkage to the E1 activating enzyme. It is transferred to the E2 conjugating enzyme and is targeted to its substrate via E3 ligases, which bind the E2 and target. RING domain E3 ligases mediate direct transfer from the E2 to the substrate, where as HECT domain ligases are conjugated to the ubiquitin molecule before transfer to the substrate. **B.** Different ubiquitin linkages result in different protein fates. Mono ubiquitin or various lysine linkage chains can serve as signaling marks, most notably by binding ubiquitin binding domains (UBD). K48 linkages generally target the protein for proteasome mediated degradation. **C.** The proteasome cleaves the target substrate in an ATP dependent manner yielding cleaved peptides and unconjugated ubiquitin. **D.** Deubiquitinating enzymes can deubiquitylate proteins, making this a reversible process.

Substrate specificity within the ubiquitin system is endowed by the hundreds of E3 ligases expressed in cells, each of which contain distinct protein-protein interaction domains to target unique substrates. In some cases, the E3 does not mediate both the E2 and substrate binding, but rather coordinates with multi-subunit complexes to identify targets (reviewed in (Cardozo and Pagano, 2004)). Adding complexity to the system, ubiquitin chains can be generated through the linkage of ubiquitin to itself via one of its seven Lys residues, yielding many permutations and combinations of structurally distinct ubiquitin chains **(Figure 1-5B)**. The type of ubiquitin chain generated is usually specified by the E2 used in the reaction (Ye and Rape, 2009). K48 linkage chains canonically direct the ubiquitylated protein to the proteasome, which degrades the targeted protein via ATP-dependent cleavage. This process also cleaves ubiquitin chains into monomer units available for another round of activation, conjugation, and ligation **(Figure 1-5C)**. Monoubiquitylation and K63 linkages have been implicated in altering protein function, particularly within the endocytic and DNA damage response pathways, respectively. Ubiquitin chains can serve as a binding site for ubiquitin-binding domains (UBDs) of other proteins, facilitating protein-protein interactions that can transduce cellular signals. Deubiquitinating enzymes (DUBs), also known as ubiquitin-specific proteases (USPs), can catalyze the deconjugation of ubiquitin from substrate proteins, thus making the ubiquitin pathway both inducible and reversible **(Figure 1-5D)**.

In recent years many ubiquitin-like proteins (UBLs) have been identified. Among others, these include SUMOs (Small Ubiquitin-Like Modifier), Nedd8 (Neural

precursor Expressed, Developmentally Downregulated 8), and ISG15 (Interferon Stimulated Gene 15). Like ubiquitin, they can be conjugated to proteins by E1/E2/E3 cascades. It is becoming clear that crosstalk between these and other post-translational modifications, including phosphorylation, acetylation, and methylation, facilitates substrate targeting and regulation within the UPS, enabling the regulation of diverse cellular signals (Hunter, 2007). ICP0 has been shown to contain SUMO-interacting motif-like sequences (SLSs) that can bind SUMO. It appears that ICP0 targets PML for ubiquitylation by binding SUMOylated PML via its SLS sequences, functioning as a SUMO-targeted ubiquitin ligase (C. Boutell, personal communication). In this way, ICP0 constitutes an elegant example of crosstalk between post-translational modifications that facilitate substrate targeting within the UPS. Intriguingly, a role in substrate targeting via any of its many phosphorylated residues has not been described.

To date, many E3 ubiquitin ligases have been identified, either by proteomics, bioinformatics, and/or biochemical approaches. However, the substrates of these E3s are often unknown. The identification of E3 ligase targets is essential for understanding the effects of different E3s on cellular pathways, as well as how they can be deregulated in infection and disease. E3s often contain binding motifs for their substrates, and thus novel targets can be identified via biochemical association with an E3 of interest. Because many viruses hijack the UPS to commandeer cellular processes, identifying substrates of virally encoded E3 ligases, and the mechanisms by which they interact with and identify their substrates, is integral to understanding the mechanisms governing viral infection.

Protein-protein interactions and the FHA domain

Cellular signals are often transduced via protein-protein interactions that target enzymes to their substrates, and can include the *de novo* assembly of multi-subunit complexes. Protein-protein interactions are orchestrated through a diverse array of structured domains that can bind to each other or to short linear motifs, which are often less than ten amino acids in length. Among other mechanisms, short linear motifs can be induced by phosphorylation events and bound by phospho-binding domains (Pawson and Scott, 1997; Ren et al., 2008). For example, fork-head associated (FHA) domains bind pThr motifs (Durocher et al., 1999), BRCA C-terminal (BRCT) domains bind pSer motifs (Yu et al., 2003a), and Src homology 2 (SH2) domains bind pTyr motifs (Songyang et al., 1993). These domains do not have affinity for an unphosphorylated region of an otherwise conforming consensus sequence, and generally contain little affinity for other phosphorylated residues. Structural variation within these families results in specific preferences for the context in which the phosphorylated residue is presented; thus short linear motifs that are differentiated by a few amino acids can recruit distinct members of the same phospho-binding family (Durocher et al., 2000; Rodriguez et al., 2003).

Structures of FHA domains have revealed they composed of antiparallel β strands forming a β sandwich, with the N- and C- termini in close proximity to each other on one end of the sandwich. At the other end, loops connecting the β strands contain conserved residues that mediate pThr binding (Durocher et al., 2000) **(Figure 1-6)**. Oriented peptide screens have found that the most common mechanisms by

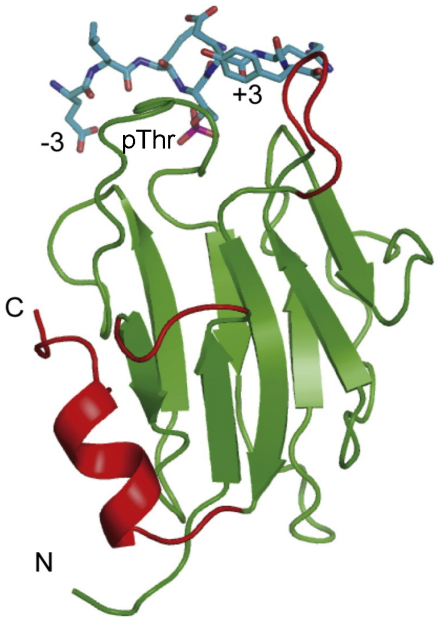

Figure 1-6. Structure of the RNF8 FHA domain and pThr binding. FHA domains contain characteristic antiparallel β-strands that form a β- sandwich (green). The N and C termini are located in close proximity at one end of the sandwich, whereas flexible loop regions at the opposite contain conserved residues that mediate phospho-Thr (purple) binding. Amino acids in the pT-3 to pT+3 positions (blue) contribute to the ability to target different FHA domains. In the case of RNF8, the FHA domain prefers pThr with Phe or Tyr in the pT+3 position (reprinted directly from Huen et al., 2008).

which FHA domains select their pThr binding partners is through specific preferences for the residue in the pT+3 position. For example, the RING-finger 8 (RNF8) FHA domain selects specifically for Phe or Tyr at pT+3 (Huen et al., 2007). However, substrate selection can also occur via residues anywhere between the pT-3 to pT+3 positions. The FHA domain of the Nijmegen breakage syndrome protein (Nbs1) appears to differentiate substrates via a preference for Asp at pT+1 (Lloyd et al., 2009; Williams et al., 2009). In contrast, polynucleotide kinase (PNK) displays little tolerance for sequence variations in the pT-2 and pT-3 positions, while residue substitutions at pT+3 are better tolerated (Koch et al., 2004).

The FHA domain was originally identified as a region of sequence similarity in forkhead transcription factors from yeast, but is found in functionally diverse proteins in a wide variety of organisms (Hofmann and Bucher, 1995). The original study, using computer-aided sequence alignments, identified 18 proteins in 8 species, but there are now at least 168 FHA domain proteins in 32 species, ranging from bacteria to human. Over 30 FHA domain proteins are present in humans (Uniprot protein knowledge database, www.uniprot.org), and many of their functions are as yet uncharacterized. Most of the characterized FHA domain proteins are nuclear and function in cell signaling pathways, including those regulating cell cycle and DNA damage responses. In mammalian cells, FHA domains are found on many DNA damage response proteins including Nbs1, Chk2, RNF8, and Mdc1, and as described in the next several sections, these proteins and their FHA domains play important roles in transduction of DDR signals.

DNA damage and repair

The cellular genome is subjected to tens of thousands of lesions per day that must be resolved in order to maintain genome integrity. These lesions can occur from endogenous and exogenous sources resulting in a variety of structural abnormalities within the DNA. Induction of DNA damage can lead to loss of genetic information and chromosomal translocations that threaten cell viability and contribute to diseases ranging from immune deficiencies and aging defects to cancer and neurodegenerative disorders (Jackson and Bartek, 2009). Thus the cell has evolved sophisticated pathways to recognize the presence of aberrant DNA and chromosomal structures and signal for DNA repair, enabling it to continually survey and maintain genome fidelity.

Lesions in the cellular DNA can occur spontaneously during replication or be induced by endogenous and exogenous sources. Within the cell, reactive oxygen species (ROS) accumulate as a byproduct of oxidative respiration or as the result of immune responses. These products can react with the cellular DNA and generate DNA structures that impair the ability of replicative or transcriptional polymerases to pass through the region. The most common types of lesions comprise single base deletions, single stranded nicks, or nucleotide mismatches, and arise spontaneously during the cell cycle. These can be recognized and resolved through nucleotide excision repair, base excision repair, or translesion synthesis pathways. Replicative stresses such as stalled replication forks induce single-stranded regions of DNA (ssDNA) that can also lead to double stranded breaks (DSBs). DSBs are particularly challenging to repair as the complementary strand upon which to model repair is also

disrupted. They are also particularly toxic, as the inability to properly repair DSBs can lead to chromosome translocations and gross chromosomal abnormalities. Importantly, DSBs can also be induced via programmed pathways using cellular nucleases and subsequently re-ligated using DNA repair pathways. This is particularly evident in programmed genome altering events that occur during meiotic recombination (Richardson et al., 2004) and class switch recombination during development of the B- and T- lymphocytes of the immune system (Chaudhuri and Alt, 2004). Exogenous sources of DNA damage include UV and gamma irradiation, as well as chemicals such as those contained in chemotherapeutics for cancer. These sources induce a variety of lesions in the cellular genome, including ssDNA regions and DSBs. A collective hierarchy of signals within the DDR facilitates the processing and repair of damaged DNA and coordinates with other cell signaling pathways to halt DNA replication, cell cycle, and transcription at the chromatin surrounding the break.

The pathway chosen for DSB repair depends on the type of lesion incurred as well as the stage of the cell cycle, and in general are spearheaded by the PI3K-like kinases DNA-PKcs, ATM, and ATR. Repair of DSBs occurs through non-homologous end joining (NHEJ) or homologous recombination (HR) pathways coordinated by DNA-PKcs and ATM, respectively. ATR signaling is induced by ssDNA regions that are a result of replication stresses, or processed from other forms of DNA damage, including DSBs. While ATM and ATR share a subset of substrates, they are activated by distinct mechanisms and in response to distinct forms of DNA damage and stress. More recent work has also indicated that there is likely crosstalk

between these pathways. This is particularly apparent in the requirement for the Mre11-Rad50-Nbs1 (MRN) complex and ATM for full activation of ATR (Carson et al., 2009), and the ability of ssDNA intermediates from resected DSBs to be coated by the ssDNA binding protein RPA, recognized by the ATR-ATRIP complex, and initiate ATR-dependent phosphorylation cascades (reviewed in (Cimprich and Cortez, 2008)).

NHEJ involves the recognition of a DSB by the Ku protein heterodimer, composed of the Ku70 and Ku80 subunits. These proteins recruit DNA-PKcs, followed by recruitment of the DNA ligase IV-XRCC4 complex and XLF (Grawunder et al., 1998; Sibanda et al., 2001), which ligate the broken DNA ends together (Robins and Lindahl, 1996; Wilson et al., 1997). Because it does not use a complementary DNA template for repair, NHEJ can occur during any stage of the cell cycle. However, this is an error prone pathway as information contained within the break can be lost or mutated. In contrast, HR uses the sister chromatid as template for repair, which is accessible during S and G_2 phases of the cell cycle. This process involves end resection of the DSB via the MRN complex and CtIP (reviewed in (Paull, 2010)), to yield a 5' single-stranded DNA (ssDNA) overhang region that can invade the sister chromatid, which is then used as the template for repair. HR is thus an error-free method of DSB repair, although it can only occur at certain stages of the cell cycle. Pathway choice between NHEJ and HR possibly occurs through competition of the MRN and Ku complexes binding the ends of the DSB.

While DNA processing and repair functions are one consequence of DDR signaling, other DDR-regulated functions are essential to maintain the cell in a viable

state while the DNA is repaired. Among other events, the ATM and ATR-induced signaling cascades control cell cycle checkpoints, apoptosis, transcription, and chromatin remodeling at the site of the break. These cascades are characterized by protein-protein interactions through post-translational modifications that facilitate localization of DDR proteins to sites of DNA damage.

Protein-protein interactions and signaling cascades in response to DNA damage

The DDR is characterized by the sequential and orchestrated recruitment of DDR proteins to sites of DNA damage, facilitating processing and repair of the DNA and integrating with signaling pathways mediating effector functions such as cell cycle and transcriptional regulation. The signals are propagated through ATM- and ATR-mediated phosphorylation, resulting in checkpoint kinase activation and DDR protein recruitment to the site of the break. More recently, the contribution of other post-translational modifications, including ubiquitylation, SUMOylation, methylation, and acetylation, have been described (reviewed in (Polo and Jackson, 2011)), and the catalog of cellular DDR proteins facilitating these post-translational modifications and protein-protein interactions is expanding.

The accumulation of proteins at sites of DNA damage, which is a common feature of many DDR proteins, can be visualized by fluorescence microscopy. Damage induced in response to ionizing radiation results in the formation of discrete focal structures in the nucleus where DDR proteins accumulate, termed irradiation-induced foci (IRIF) **(Figure 1-7A)**. Damage can also be induced in a defined

subnuclear region and analyzed in real-time by exposure to "laser scissors," accomplished by subjecting sensitized cells (via DNA-intercalating agents) to high-powered, near-UV wavelength lasers on a confocal microscope (Bekker-Jensen et al., 2005) **(Figure 1-7B)**. In this case, the recruitment of fluorescently tagged proteins can be analyzed in real time after induction of damage. The types of damage generated at IRIF and laser scissor lines likely comprises a mixture of lesions, including DSBs. In both cases the recruitment of DNA damage proteins can be visualized at the site(s) of damage, and DDR proteins exhibit similar requirements for recruitment. The temporal aspects of recruitment, analyzed using laser scissors, generally coincide with the molecular and genetic requirements. Overall it appears that phosphorylation dependent interactions coordinate recruitment at the earlier stages of the DDR and continue through later stages, while ubiquitin dependent interactions are dependent on the early phosphorylation events, and contribute during the later stages **(Figure 1-7C)**.

Phosphorylation dependent interactions at sites of DNA damage

ATM normally exists in the cell as an inactive dimer (Bakkenist and Kastan, 2003). While the exact mechanisms governing its activation are still unclear, ATM activation and localization to sites of DNA damage are dependent on the MRN complex (Carson et al., 2003; Uziel et al., 2003). Upon initial activation, the dimer

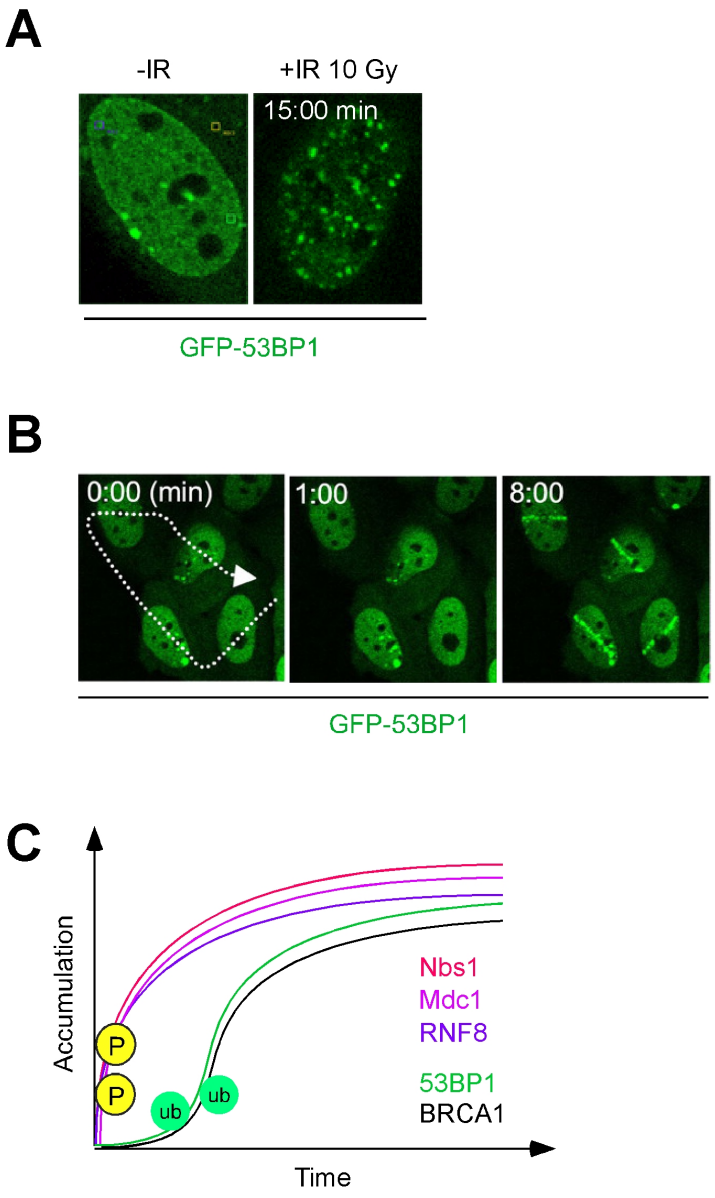

Figure 1-7. Methods of analyzing DNA damage responses. A. DDR proteins are normally diffusely nuclear and are relocalized to IRIF after exposure to ionizing radiation. The DDR protein 53BP1 is used as an example here. **B.** The laser scissors method induces a defined area of damage (dashed line). Time lapse microscopy measures recruitment of GFP-tagged 53BP1 (From Bekker-Jensen et al., 2005). **C.** Quantitative analysis of DDR protein recruitment to laser scissors lines reveals that different DDR proteins are recruited at different times post damage. Notably, proteins that are phosphorylation dependent, such as Nbs1, Mdc1, and RNF8, are recruited early. After a brief delay, ubiquitin-dependent protein recruitment, such as 53BP1 and BRCA1, occurs (adapted from Bekker-Jensen and Lukas, 2010).

dissociates and ATM autophosphorylation yields the catalytically active form of ATM, as the kinase domain becomes accessible to its substrates (Bakkenist and Kastan, 2003). Full ATM activation requires MRN-dependent recruitment to sites of DNA damage via interaction with the Nbs1 C-terminus (Berkovich et al., 2007; Falck et al., 2005; You et al., 2005), as this enables its retention at sites of DNA damage. While S1981 was the first described ATM autophosphorylation site, several others have now been described and also contribute to ATM activation and the ability of ATM to propagate effective damage response signals (Kozlov et al., 2011; Kozlov et al., 2006). ATM, like ATR, preferentially phosphorylates Ser and Thr residues with Gln in the +1 position (Kim et al., 1999; O'Neill et al., 2000). These SQ/TQ motifs are present on many putative substrates that have also been identified as damage-induced ATM/ATR targets via large-scale proteomics screens (Matsuoka et al., 2007). Histone H2AX is one target of ATM and phosphorylation on H2AX S139 (γH2AX) is detectable soon after induction of DNA damage on the chromatin surrounding the break (Burma et al., 2001; Rogakou et al., 1998) **(Figure 1-8A)**. These signals can extend up to several megabases from the site of damage (Bekker-Jensen et al., 2006; Rogakou et al., 1999) and serve to mark the damaged chromatin region. Mdc1 localizes to sites of DNA damage by virtue of its BRCT domains, which bind the S139 phosphosite on γH2AX with high affinity (Stucki et al., 2005). As the full name of Mdc1 (mediator of DNA damage checkpoint 1) indicates, Mdc1 is required for ATM-, Chk2-, and Chk1- mediated induction of cell cycle checkpoints, most notably at the intra-S and G2/M checkpoints (Lou et al., 2003; Stewart et al., 2003). Functionally,

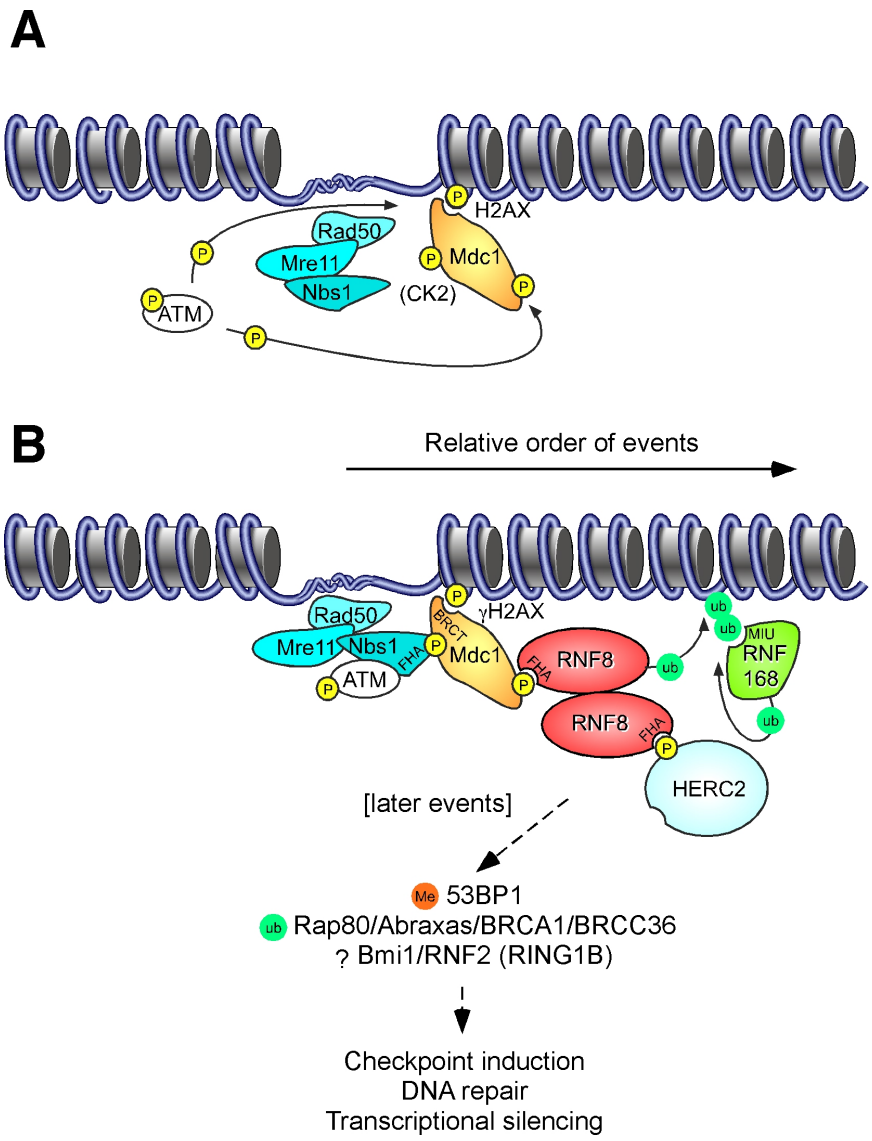

Figure 1-8. Post translational modifications and protein protein interactions in the DNA damage response. A. A DSB is detected by the MRN complex, which results in ATM activation. ATM is autophosphorylated and then phosphorylates a large number of substrates, including H2AX and Mdc1. Mdc1 also contains a constitutively phosphorylated region catalyzed by the CK2 kinase. **B.** A cascade of PTM-dependent interactions via structured protein-interaction domains. Mdc1 binds γH2AX by virtue of its BRCT domains. Nbs1 binds phospho-Mdc1 by virtue of its FHA domains. RNF8 binds phospho-Mdc1 and phospho-HERC2 by virtue of its FHA domains. Ubiquitin chains catalyzed by RNF8 serve as binding sites for the MIU domains of RNF168. RNF8 and RNF168 dependent events include 53BP1 recruitment via diMe H4K20. The Rap80/Abraxas/ BRCA1/BRCC36 complex is recruited through UIM domains on Rap80, and downstream Bmi1/RNF2 ubiquitin ligase complex is recruited in an RNF8 dependent manner, although the precise mechanism by which it is recruited is still unclear. These events facilitate effector functions, some of which are listed.

Mdc1 serves as a large scaffolding protein and is required for recruitment of almost every DDR protein to sites of DNA damage **(Figure 1-8B)**. Phosphosites on Mdc1 directly bind two FHA domain proteins. The first of these is Nbs1, which through its FHA domain binds the constitutively phosphorylated residues at Mdc1 N-terminal SDTD repeats (Chapman and Jackson, 2008; Spycher et al., 2008). The second FHA domain protein is RNF8, a RING domain E3 ubiquitin ligase recently found to function in the DDR, and which bridges the upstream phosphorylation events with downstream ubiquitin-based signaling events.

Ubiquitin dependent interactions at sites of DNA damage

The identification of RNF8 and another E3 ubiquitin ligase, RNF168, as DDR proteins has highlighted the importance of ubiquitin-based signaling events in this pathway. The FHA domain of RNF8 binds ATM-catalyzed phospho-TQXF motifs on Mdc1, and upon recruitment RNF8 ubiquitylates proteins, including histones H2A and H2AX, on the chromatin surrounding the break (Huen et al., 2007; Kolas et al., 2007; Mailand et al., 2007). The accumulation of ubiquitin conjugates at sites of damage can be visualized using a conjugated ubiquitin antibody, FK2 (Mailand et al., 2007). These ubiquitin marks have been implicated in at least two functions. First, the ubiquitin chains serve as a binding site for motifs interacting with ubiquitin (MIUs) and ubiquitin interacting motifs (UIMs) of other DDR proteins, including RNF168 (Doil et al., 2009; Stewart et al., 2009) and Rap80 of the Rap80/Abraxas/BRCA1/BRCC36 complex (Sobhian et al., 2007; Wang and Elledge,

2007). Second, deposition of ubH2A on the chromatin surrounding the break has been implicated in regulating transcriptional silencing at the break, as described in more detail below (Shanbhag et al., 2010).

Recently the RNF2(RING1B)/Bmi1 E3 ligase complex, which has canonically mediated polycomb silencing through ubiquitylation of H2A (Wang et al., 2004) , has also been described to localize to sites of DNA damage and promote DNA repair (Chagraoui et al., 2011; Ginjala et al., 2011; Ismail et al., 2010). It is as yet unclear whether this recruitment is RNF8 dependent, as both RNF8- dependent and – independent mechanisms have been described. A HECT domain E3 ligase, HERC2, has recently been identified as a DDR protein. It is recruited sites of DNA damage via phosphorylation dependent interaction with the RNF8 FHA domain (Bekker-Jensen et al., 2010). The apparent paradox of the RNF8 FHA domain simultaneously binding phosphosites on Mdc1 and HERC2 can be resolved by observations that RNF8 can oligomerize, potentially providing a 2X or more RNF8 FHA domain stoichiometry along the damaged chromatin (Bekker-Jensen et al., 2010). While the targets of these novel DDR E3 ligases have not yet been identified, they do contribute to accumulation of conjugated ubiquitin at sites of DNA damage. These observations suggest that the RNF8 dependent accumulation of conjugated ubiquitin reflects both the ability of RNF8 to catalyze ubiquitin chains as well as recruit other ubiquitin ligases to the site of DNA damage **(Figure 1-8B)**.

RNF8 and RNF168 in the DNA damage response

RNF8 and RNF168 are integral to the execution of a successful DNA damage response. RNF8 null mice are defective for class-switch recombination and meiotic recombination (Santos et al., 2010), consistent with the role of the DDR in facilitating these processes. More recently, RNF168 null mice have been generated and they are also deficient for class-switch recombination and spermatogenesis, are radiosensitive, and display increased genomic instability that can synergize with p53 to promote tumor formation (Bohgaki et al., 2011).

Two patients containing mutations in the RNF168 gene have been identified. The first is heterozygous for two nonsense mutations, yielding one RNF168 copy deleted of the two MIU domains, and one copy containing the RING and first MIU (Stewart et al., 2007). The second is homozygous for nonsense mutations yielding no functional RNF168 protein (Devgan et al., 2011). Among other features, these patients exhibited immunodeficiencies, predisposition to cancer, and cellular radiosensitivity, which are similar to features of ataxia-telangeitasia disorder (A-T), found in patients lacking functional ATM (Chun and Gatti, 2004). Interestingly, the severity of disease correlated with the status of RNF168 protein in the patients. The patient lacking any functional RNF168 exhibited more symptoms similar to A-T than the patient containing some functional RNF168, who exhibited some but not all of the characteristics (Devgan et al., 2011). Cells from both patients were radiosensitive and defective for 53BP1 recruitment to IRIF, and combined with the clinical

manifestations of the genetic diseases, these observations highlight the importance of ubiquitin-dependent DDR signaling in the maintenance of genomic integrity.

As described above, RNF8 and RNF168 function as DDR proteins that promote ubiquitin-based signaling events at DSBs. Both are RING domain E3 ligases that contain protein-interacting motifs to localize to their substrates at sites of DNA damage. RNF8 contains an N-terminal FHA domain, which as described above binds pThr residues, and a C-terminal RING domain **(Figure 1-9A)**. RNF168 contains an N-terminal RING domain and C-terminal MIU domains, which facilitate its ability to bind ubiquitin chains **(Figure 1-9B)**.

The substrates of RNF8 and RNF168 described to date are the histones H2A and H2AX (Doil et al., 2009; Huen et al., 2007; Mailand et al., 2007; Stewart et al., 2009). RNF8 can conjugate ubiquitin to H2A (ubH2A) *in vitro* and RNF8 knockdown leads to a partial loss of ubH2A levels in cells (Mailand et al., 2007). RNF8 is also required for H2AX ubiquitylation following DNA damage (Huen et al., 2007). MEFs from RNF8 null mice exhibit a marked decrease in ubH2A levels as well as ubH2B levels (Wu et al., 2009), indicating that RNF8 may also play a role in regulating ubH2B. Biochemically, RNF8 has been shown to function with the E2 enzyme Ubc13, catalyzing primarily K63 linked chains (Plans et al., 2006). The synergy between RNF8 and Ubc13 has also been demonstrated *in vivo*, as RNF8 and Ubc13 co-purify from cell lysates (Plans et al., 2006) and knockdown of either RNF8 or Ubc13 abolishes the accumulation of conjugated ubiquitin at sites of DNA damage (Huen et al., 2007). This accumulation is dependent on both the FHA and RING

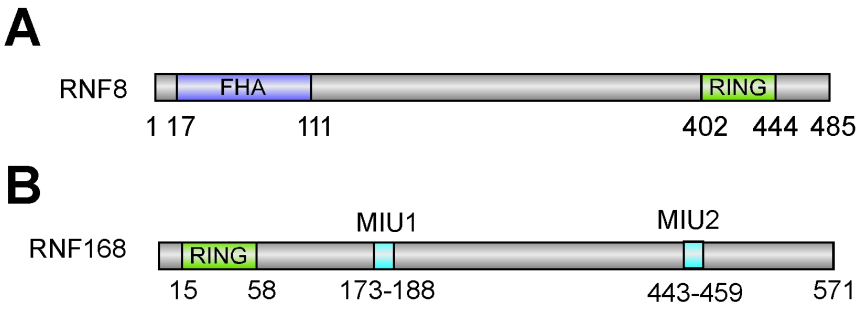

Figure 1-9. Domain organization of the DDR RING domain E3 ligases RNF8 and RNF168. **A.** RNF8 contains a pThr-binding FHA domain at its N terminus and RING domain at its C-terminus. **B.** RNF168 contains the RING domain at its N-terminus and two ubiquitin binding MIU (motifs interacting with ubiquitin) domains. Numbers represent amino acid positions.

domains of RNF8 (Mailand et al., 2007), and linkage specific antibodies have demonstrated the accumulation of predominantly K63-linked chains at DSBs (Doil et al., 2009; Shanbhag et al., 2010). RNF168 also uses Ubc13 to catalyze K63-linked ubiquitin chains at DSBs, and RNF168 knockdown results in loss of ubH2A after induction of DNA damage (Doil et al., 2009).

RNF8 appears to promote a predominantly di-ubiquitylated form of H2AX after DNA damage (Huen et al., 2007). It was proposed that a di-ub form of H2A and H2AX may function differently from monoubiquitylated H2A (Panier and Durocher, 2009), which has canonically been shown to function in transcriptional silencing (Wang et al., 2004). However, more recent work has demonstrated that transcription is silenced at the site of a DSB (Shanbhag et al., 2010). The transcriptional silencing is at least partially dependent on RNF8 and RNF168, and the combined knockdown of both ligases impairs transcriptional silencing at the site of the break more than either ligase alone. Furthermore, the transcriptional silencing correlated strongly with accumulation of ubH2A at the DSB, but not necessarily total K63-linked ubiquitylation. Thus it appears that DDR-induced K63-linked ubiquitin chains at a DSB serve as a binding platform for DDR proteins, while the subset of ubH2A serves to repress transcription at the site of the break. These observations also highlight the likelihood that other proteins are ubiquitylated at sites of DNA damage, either by RNF8 and RNF168 or other ubiquitin ligases, and many studies are currently aimed at identifying the relevant substrates.

Viruses and the DNA damage response

Viruses have a complex relationship with the DDR. The DDR has been shown to be detrimental to some viruses and is inactivated during infection, while other viruses harness DDR mechanisms to promote infection (Lilley et al., 2007). Infection by many viruses initiates ATM- and ATR- mediated signaling cascades (Weitzman et al., 2010), likely due to the sensing of viral genomes that the DDR recognizes as aberrant DNA structures. Two examples where the DDR is inactivated and where it is harnessed are in Ad and HSV-1, respectively.

In the case of Ad, the DDR can recognize the double stranded ends of the viral genome and ligate them into longer-than-unit-length concatemers (Weiden and Ginsberg, 1994) that are too large to be packaged. As a countermeasure, the virus encodes three regulatory proteins, E1B55K, E4orf3, and E4orf6, to impair MRN complex and prevent activation of ATM- and ATR- dependent signaling pathways (Carson et al., 2003; Stracker et al., 2002). E1B55K and E4orf6 hijack a cullin 5-based ubiquitin ligase complex (Querido et al., 2001) to direct MRN for degradation, and the E4orf3 protein can mislocalize MRN into aggregated nuclear structures, sequestering them from access to the viral DNA present in viral replication centers (Stracker et al., 2002). Thus during a WT Ad infection, the DDR is not activated and the viral genomes remain as unit-length molecules that are packaged into the virion.

In contrast to the detrimental effects of MRN to Ad infection, HSV-1 appears to benefit from aspects of DDR signaling during infection. WT HSV-1 infection activates ATM- mediated signaling cascades during infection, characterized by

autophosphorylation of ATM, Nbs1, and Chk2 (Lilley et al., 2005; Shirata et al., 2005; Wilkinson and Weller, 2004). DDR proteins are then recruited into viral replication centers (Lilley et al., 2005; Shirata et al., 2005; Taylor and Knipe, 2004; Wilkinson and Weller, 2004). Here, they appear to serve a beneficial function, as HSV-1 infection in the absence of functional ATM or Mre11 yields fewer viral progeny (Lilley et al., 2005). It is as yet unclear exactly what function the activated DDR proteins serve at viral replication centers, although it is possible that viral recombination and genome processing are facilitated by cellular DNA processing and repair enzymes activated through the DDR (Wilkinson and Weller, 2003). While the ATM signaling pathway is activated during HSV-1 infection, the ATR- and DNA-PK-coordinated branches of the DDR are inactivated (Lees-Miller et al., 1996; Mohni et al., 2010; Parkinson et al., 1999). Thus it appears that HSV-1 can selectively target and manipulate DDR pathways in distinct ways in order to facilitate its replication. Work described in this thesis highlights the complexity of HSV-1 interaction with the DDR and uncovers a novel aspect of the DDR that is detrimental to HSV-1 infection.

Thesis overview

The work presented in this Dissertation focuses on the interaction between the cellular DDR and HSV-1, the interface of which we demonstrate occurs through the phosphorylation- and ubiquitylation- dependent events on both the viral and cellular fronts. The consequences of these interactions for both the virus and host cell are explored, highlighting implications for the HSV-1 life cycle. Work in Chapter 2

reveals that phosphorylation- and ubiquitin- dependent DDR events can recognize and repress incoming HSV-1 genomes, and that HSV-1 inactivates the DDR via ICP0 to relieve this transcriptional repression. In uncovering the mechanism behind this inactivation, we identify RNF8 and RNF168 as novel degradation targets of ICP0 and new players in intrinsic antiviral defenses. This work also highlights the ability of ICP0 to affect novel epigenetic marks, and suggests this may contribute to its transcriptional transactivation functions and roles in reactivation from latency. Work in Chapter 3 reveals the mechanism by which ICP0 targets RNF8 for degradation and highlights the ability of ICP0 to mimic cellular phosphorylation marks to target the RNF8 FHA domain. In addition, evidence is presented demonstrating that ICP0 has the potential to target other FHA domain proteins through mimicking phosphorylation marks. In Chapter 4, an assay to identify novel substrates of ICP0 is presented, with preliminary data mapping the proteins and pathways interacting with ICP0 that may represent ICP0 substrates for future study. Combined, these studies reveal that the cell is able to deploy the DDR not only to recognize DNA damage, but also to recognize incoming HSV-1 genomes. The cell attempts to silence these genomes, with important implications for the transition of HSV-1 between its lytic and latent states and the mechanisms by which ICP0 promotes infection.

Chapter 2. HSV-1 ICP0 degrades RNF8 and RNF168 to prevent DNA damage response-mediated recognition and repression of viral genomes.

Background

The HSV-1 genome is extensively processed during both the lytic and latent phases of the viral life cycle. Incoming HSV-1 genomes are double-stranded, linear molecules, which have been observed by electron micrograph and biochemical studies to assume circular forms and complex branched structures upon infection (Friedmann et al., 1977; Garber et al., 1993; Poffenberger and Roizman, 1985; Strang and Stow, 2005). Generation of these forms does not necessarily require the synthesis of viral proteins or the onset of viral replication (Garber et al., 1993; Strang and Stow, 2005), indicating that cellular proteins can fulfill this role. The replicated genome exists as longer than unit-length concatemers that are cleaved before packaging (Jacob et al., 1979; Severini et al., 1994), and DSB-dependent recombination events result in inversion of the U_S and U_L subunits, giving rise to the four different isomers of the genome (Delius and Clements, 1976; Hayward et al., 1975; Sarisky and Weber, 1994). Combined, these observations suggest that cellular DNA repair and processing enzymes are able to recognize and manipulate the viral genome during infection.

Consistent with this hypothesis, lytic HSV-1 infection induces ATM autophosphorylation and ATM dependent phosphorylation of Nbs1, p53, and Chk2 (Lilley et al., 2005; Shirata et al., 2005; Wilkinson and Weller, 2004). DNA repair proteins including Mre11 and Nbs1 associate with viral replication centers, as assessed

by co-localization or biochemical association with the viral ssDNA binding protein ICP8 (Lilley et al., 2005; Taylor and Knipe, 2004). These DDR proteins appear to perform a beneficial role, as HSV-1 replication and progeny production are decreased in the absence of functional ATM and Mre11 (Lilley et al., 2005).

Other arms of the DNA damage response, including those spearheaded by ATR and DNA-PKcs, are inactivated during HSV-1 infection. DNA-PKcs is degraded by ICP0, (Parkinson et al., 1999) and both DNA-PKcs and Ku70 are detrimental to HSV-1 infection (Parkinson et al., 1999; Taylor and Knipe, 2004). While Ku70 is recruited to viral replication centers, it is likely that its inability to complex with DNA-PKcs, which is degraded, inhibits its function during infection. ATR and ATRIP are recruited to viral replication centers, but ATR signaling is inhibited (Mohni et al., 2010). Thus it appears that ATM-dependent signaling events are beneficial to HSV-1 infection while ATR- and DNA-PKcs- dependent events are inhibitory.

Research over the last several years has revealed new players in the DNA damage response, many of which function downstream of MRN/ATM sensing and induction of γH2AX (see Chapter 1 for detailed explanation). Roles for ubiquitylation have been elucidated with the discovery of two cellular E3 ubiquitin ligases, RNF8 and RNF168, functioning in the pathway (Doil et al., 2009; Huen et al., 2007; Kolas et al., 2007; Mailand et al., 2007; Stewart et al., 2009; Wang and Elledge, 2007). RNF8 and RNF168 bridge early DDR phosphorylation signals with subsequent ubiquitin-based signaling events. The RNF8 FHA domain binds DDR-induced and ATM-

catalyzed phospho-TQXF motifs on Mdc1, a protein recruited soon after induction of a DDR and which serves as a primary platform for the recruitment of downstream repair factors. RNF8 then ubiquitylates proteins at the site of the break, including histones H2A and H2AX, and these ubiquitin chains in turn serve as a recruiting platform for the ubiquitin-binding domains of RNF168. RNF8- and RNF168-mediated ubiquitylation of H2A also appears to regulate DDR-induced transcriptional silencing at the site of the break (Shanbhag et al., 2010). 53BP1, a downstream mediator protein, is recruited to sites of damage dependent on Mdc1, RNF8, and RNF168 (Bekker-Jensen et al., 2005; Doil et al., 2009; Huen et al., 2007; Kolas et al., 2007; Mailand et al., 2007; Stewart et al., 2009). It is recruited via its Tudor domains, which bind di-methyl groups on H4K20 that are catalyzed by the histone methyltransferase MMSET (Botuyan et al., 2006; Pei et al., 2011; Sanders et al., 2004).

In order to study the contribution of these events to infection, we dissected the propagation of DNA damage signals at the earliest stages of HSV-1 infection, when viral genomes have just entered the cell and immediate-early genes are beginning to be expressed. We sought to more directly determine whether DNA damage response proteins can recognize incoming, un-replicated genomes and compared the signaling events to those that occur after induction of a DNA damage response, focusing on the phosphorylation and ubiquitin-dependent events. We demonstrate that proteins functioning during the early stages of the DDR, including ATM and H2AX, are phosphorylated and recruited to sites associated with incoming viral genomes. The

signaling events at these sites are orchestrated in the same sequence as observed after damage to cellular DNA. However, we noted a distinct point in the pathway where DDR proteins were no longer recruited to sites associated with incoming viral genomes, and found that this was dependent on the viral E3 ubiquitin ligase ICP0. Using these observations, we were able to map the point in the pathway where recruitment events were prevented, and identified RNF8 and RNF168 as new degradation targets of ICP0. ICP0-mediated RNF8 and RNF168 degradation correlated with loss of ubH2A and ubH2AX levels. In contrast to the beneficial function of ATM and Mre11 during infection, experiments elucidating the effect of RNF8 and RNF168 on infection demonstrated that these proteins are repressive to viral transcription and progeny production. These observations indicate that, rather than an absolute activation or inactivation of the pathway, HSV-1 dissects the ATM-spearheaded branch of the DDR via ICP0, potentially to promote the beneficial aspects while inhibiting the detrimental ones. These observations also highlight the importance of the ubiquitin pathway, as it is used by the cell to repress the virus and used by the virus to counteract those repression events.

Results

DNA damage response proteins are recruited to sites associated with incoming HSV-1 genomes during infection

To investigate the effects of incoming HSV-1 genomes on localization of DNA damage proteins, we used a previously described assay to visualize cell nuclei at the

earliest stages of infection (Everett and Murray, 2005; Everett et al., 2004). In this assay, cells are infected at low multiplicity (MOI) so that directional viral spread through developing plaques can be analyzed. This directionality, combined with the fact that incoming viruses often congregate near the microtubule organizing center, means that nuclei of cells at the edge of plaques frequently display an asymmetric arc of incoming viral genomes **(Figure 2-1)**. Human foreskin fibroblasts (HFFs) were infected with WT HSV-1 at low MOI, fixed 24 hours post-infection and processed for immunofluorescence. We detected sites of incoming viral genomes by visualizing the viral ICP4 protein, which binds viral DNA and has been previously shown to co-localize with viral genomes in this assay (Everett and Murray, 2005). In mock-infected cells there was minimal γH2AX staining and the DNA damage checkpoint mediators Mdc1 and 53BP1 were diffusely nuclear. Upon infection with WT HSV-1, we observed activation of the cellular DDR as measured by phosphorylation of H2AX (γH2AX) and relocalization of γH2AX and Mdc1 in distinct asymmetric arcs in close proximity to incoming viral genomes **(Figure 2-2A)**. In contrast, 53BP1, which is recruited in an Mdc1-dependent manner, remained diffusely nuclear in HSV-1 infected cells and did not relocalize to sites associated with incoming viral genomes.

Other cellular proteins known to recognize incoming HSV-1 genomes include PML and associated PML body components such as hDaxx, ATRX, and Sp100 (Everett and Murray, 2005; Everett et al., 2004; Lukashchuk and Everett, 2010). In these cases, recruitment is prevented by ICP0, which degrades PML and disrupts PML bodies (Everett et al., 1998a; Everett and Maul, 1994; Maul and Everett, 1994). We

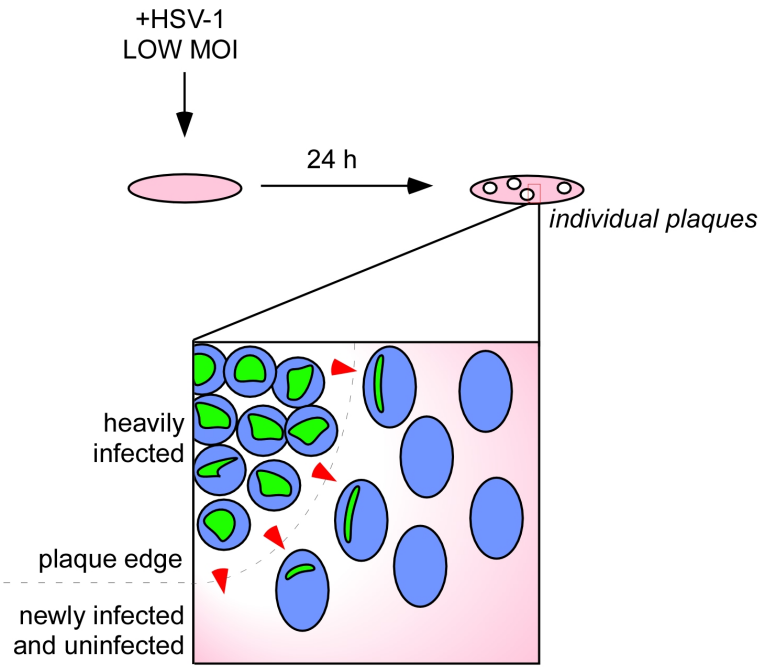

Figure 2-1. Schematic of a plaque edge experiment. Monolayers of cells are infected with HSV-1 at very low MOI, such that at 24 h post-infection separated plaques are visible. The plaque itself contains heavily infected cells (nuclei are in blue), and as viral progeny escape, they travel outward (red arrows). The nuclei of newly infected cells at the plaque edge (grey dashed line) are often infected asymmetrically as viruses approach from the plaque. After fixing the cells, viral genomes can be visualized using an antibody to the viral ICP4 protein (green), which localizes to the viral DNA.

asked whether ICP0 played a similar role in preventing 53BP1 recruitment to incoming viral genomes. To address this question we infected HFFs with HSV-1 lacking the ICP0 gene (ΔICP0) and found that in this case, 53BP1 was recruited to sites associated with incoming viral genomes **(Figure 2-2A, right panel)**. These observations are quantified in **Figure 2-2B,** and together indicate that ICP0 is required to prevent 53BP1 localization to sites of incoming HSV-1 genomes during infection, while it does not affect recruitment of upstream proteins such as γH2AX and Mdc1.

ICP0 prevents accumulation of DNA repair proteins at irradiation-induced foci

ICP0 is sufficient to disrupt PML bodies outside the context of infection (Everett and Maul, 1994) and we hypothesized that ICP0 might similarly disrupt recruitment of DDR proteins to sites of DNA damage outside the context of infection. To test this hypothesis, we assessed the impact of ICP0 on the ability of DNA repair proteins to localize to sites of damage induced by exposure to ionizing radiation (IR). HeLa cells were transfected with ICP0, irradiated 24 h post-transfection, and fixed and processed for immunfluorescence 1 h post-IR. We observed that Mdc1 was recruited to irradiation-induced foci (IRIF) both in the presence and absence of ICP0 **(Figures 2-3A and 2-3C)**, while 53BP1 remained diffusely nuclear when ICP0 was present **(Figures 2-3B and 2-3D)**. Thus it appears that ICP0 is both necessary and sufficient to disrupt the cellular DDR, either in response to DNA from incoming viral genomes during infection or in response to DNA damage induced by IR. Moreover, ICP0

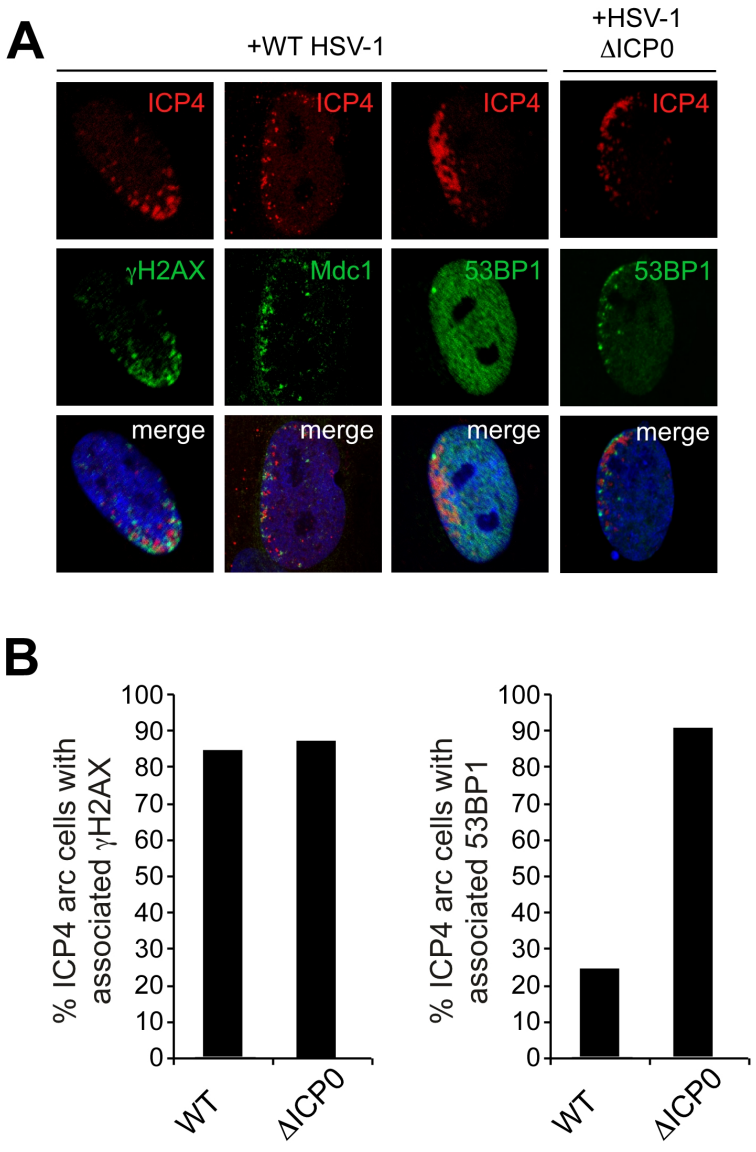

Figure 2-2. DNA repair proteins accumulate at sites associated with incoming genomes. **A.** HFF cells were infected with WT or ICP0-null (ΔICP0) HSV-1 at MOI=0.1, fixed at 24 hpi, and stained for ICP4. Localization of γH2AX, Mdc1, and 53BP1 was assessed in asymmetrically infected cells at edges of plaques. Nuclei were counterstained with DAPI. **B.** Localization was quantified by counting 100 asymmetrically infected cells at edges of plaques.

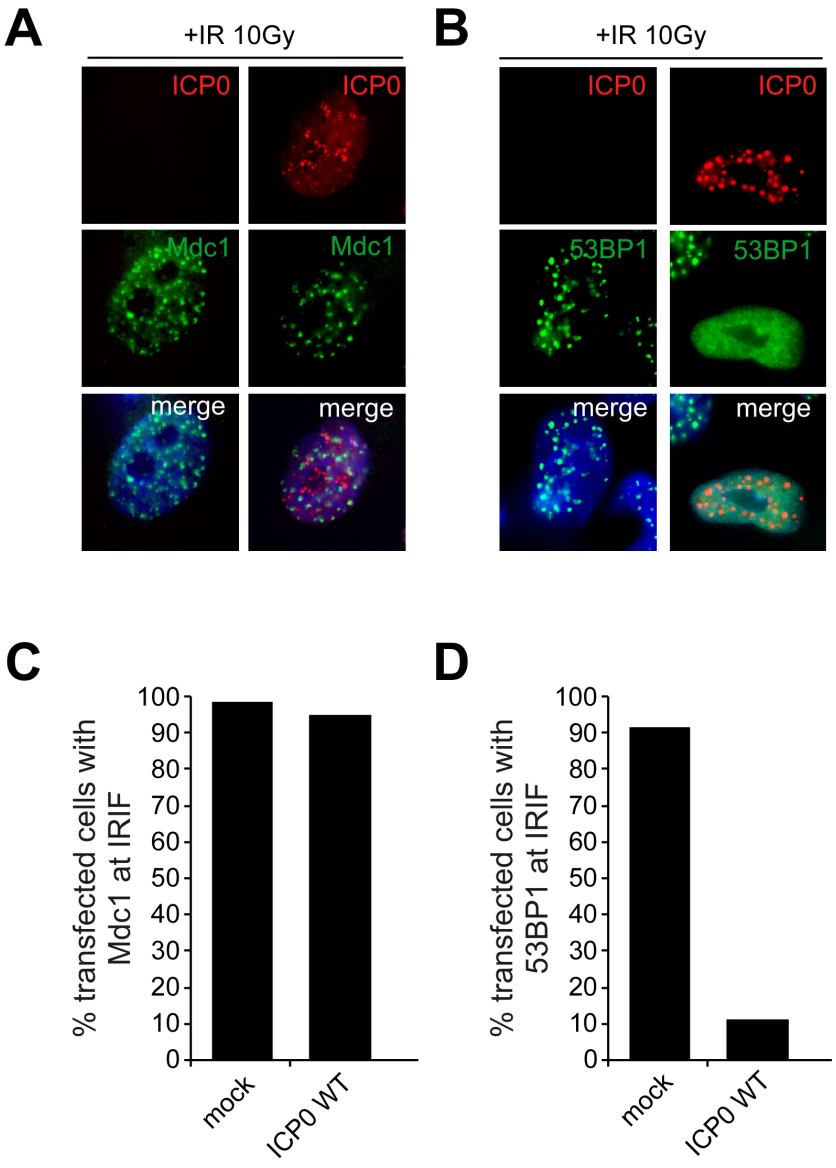

Figure 2-3. ICP0 disrupts IRIF formation after exposure to ionizing radiation (IR). A. ICP0 blocks IRIF formation downstream of Mdc1. HeLa cells were transfected with an ICP0 expression plasmid for 16 h, exposed to 10 Gy IR, fixed 1 h post-IR, and stained for Mdc1 and ICP0. **B.** Cells were prepared as in A and stained for ICP0 and 53BP1. **C.** 200 ICP0 expressing cells were assessed for localization of Mdc1 at IRIF. **D.** 200 ICP0 expressing cells were assessed for localization of 53BP1 at IRIF.

blocks the DDR pathway at the same point in both systems – before 53BP1 recruitment, but after Mdc1 recruitment.

To distinguish whether the observed diffusely nuclear 53BP1 staining reflected a dynamic or static pool of 53BP1, we performed Fluorescence Recovery After Photobleaching (FRAP) analysis of GFP-53BP1 before and after IR, and in the presence or absence of ICP0. In these experiments, U2OS cells stably expressing GFP-53BP1 (Bekker-Jensen et al., 2005) were transfected with ICP0 or a RING-deleted mutant (ΔRING). In non-irradiated cells, GFP-53BP1 was diffusely nuclear **(Figure 2-4A, top panel)** and highly mobile **(Figure 2-4B, left panel)** in both control cells and in cells expressing ICP0. After exposure to 10 Gy IR, GFP-53BP1 readily relocated to IRIF **(Figure 2-4A, bottom panel)** and FRAP analysis at these sites confirmed that 53BP1 was retained there **(Figure 2-4B, right panel)**. In contrast, GFP-53BP1 was diffusely nuclear in cells expressing ICP0 and displayed kinetics similar to non-irradiated cells. We also determined that the loss of GFP-53BP1 retention was dependent on the RING domain of ICP0, as a ΔRING mutant of ICP0 displayed GFP-53BP1 localization and kinetics similar to control cells, both before and after IR **(Figures 2-4A and 2-4B)**.

Loss of RNF8, RNF168, and ubH2A during HSV-1 infection

As described above, two RING domain E3 ubiquitin ligases, RNF8 and RNF168, have recently been shown to function in the DNA damage response, coordinating phosphorylation- and ubiquitnation- dependent events occurring between

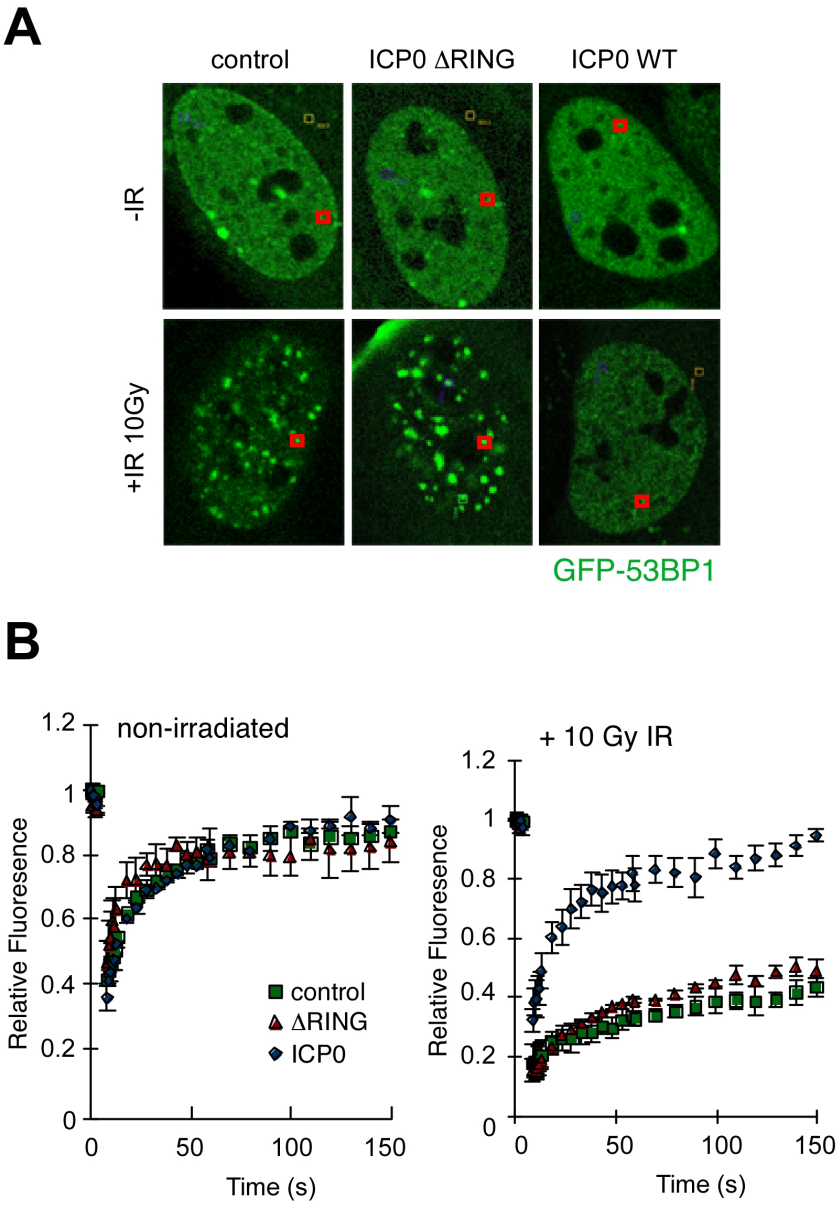

Figure 2-4. ICP0 prevents the IR-induced retention of 53BP1 at IRIF. U2OS cells stably expressing GFP-53BP1 were transfected with WT or ΔRING ICP0. 16 h post-transfection, cells were subject to 10 Gy IR and analyzed 15 min post-IR. **A.** Pre-bleach image indicating 53BP1 localization after IR and a sample region chosen for FRAP analysis (red box). **B.** FRAP analysis of GFP-53BP1. Adjusted fluorescence intensity is shown as a fraction of the pre-bleach intensity. Data points reflect the average of three independent experiments measuring FRAP of 10 foci in each experiment, and error bars represent SEM of the three experiments.

Mdc1 and 53BP1 recruitment to sites of DNA damage. ICP0 appeared to block 53BP1 recruitment to sites of incoming genomes and IRIF, dependent specifically on the RING domain, but 53BP1 levels themselves appeared unaffected by ICP0 (C. Lilley, unpublished observations). It was possible that the loss of 53BP1 recruitment actually reflected ICP0 targeting of RNF8 or RNF168. We therefore examined the total protein levels of RNF8, RNF168, and H2A during a timecourse of HSV-1 infection. HeLa cells were infected with WT or ΔICP0 HSV-1 at MOI=3, harvested between 0.5 and 8 h post-infection, and protein levels analyzed by SDS-PAGE and immunoblotting. DNA-PKcs, a known ICP0 degradation target, was used as a control for ICP0-mediated degradation events. We observed a decrease in the levels of RNF8 and RNF168 during WT HSV-1 infection but not ΔICP0 infection, and not during WT HSV-1 infection where proteasome inhibitors had been added **(Figure 2-5)**. This was accompanied by a concomitant, ICP0-dependent loss of ubiquitylated H2A as measured by a total H2A antibody, which recognizes a higher molecular weight form corresponding to ubH2A. Total H2A levels were unchanged in all cases, indicating that loss of ubH2A was not due to a general loss of H2A. We also found that previously described H2A ubiquitin ligases, including 2A-HUB and RNF2, remained at constant levels throughout WT HSV-1 and ΔICP0 infection **(Figure 2-5)**. Thus loss of ubH2A is not due to loss of these other H2A ubiquitin ligases. Combined, these observations indicate that RNF8 and RNF168 are degraded by HSV-1 in an ICP0 dependent manner, suggesting this loss contributes to ICP0-dependent loss of ubH2A during infection.

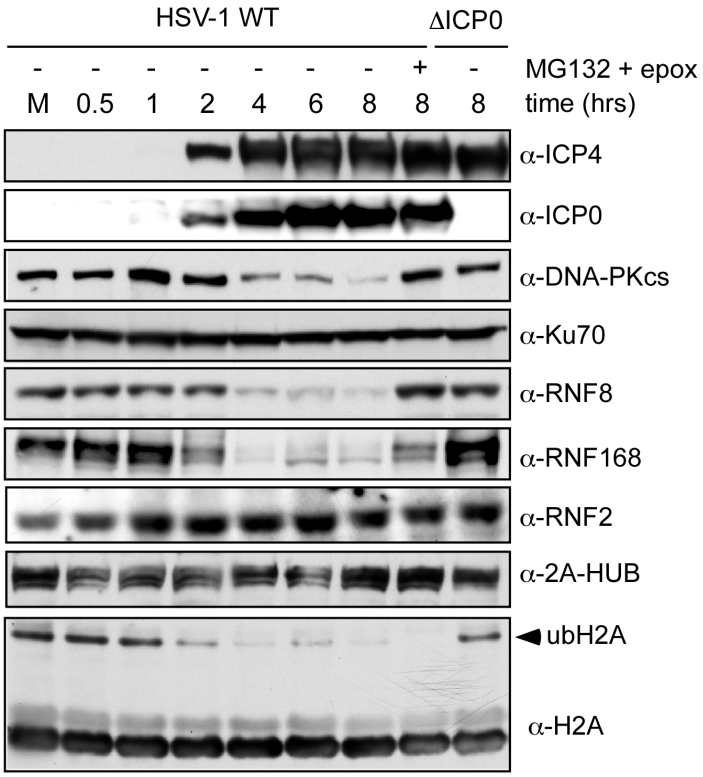

Figure 2-5. Loss of RNF8, RNF168, and ubH2A during WT HSV-1 infection. A. HeLa cells were infected with WT or ΔICP0 at MOI=3 and collected at the indicated timepoints. Protein levels were analyzed by SDS-PAGE and immunoblotting. Where indicated, proteasome inhibitors (MG132, 10 μM and epoxomycin, 1 μM) were added 2 h post-infection. The loss of ubH2A in the presence of proteasome inhibitors likely reflects the sequestration of poly-ubiquitin chains in the cytoplasm, depleting the nuclear supply.

ICP0 is sufficient to degrade RNF8 and RNF168 and induce loss of ubH2A and ubH2AX

To determine if ICP0 was sufficient to induce degradation of RNF8 and RNF168 outside the context of infection, we co-transfected ICP0 with Flag-RNF8 or HA-RNF168 and measured protein levels 24 h post-transfection by SDS-PAGE and immunoblotting. Both Flag-RNF8 and HA-RNF168 were degraded in the presence of ICP0, but not in the presence of ICP0 ΔRING **(Figures 2-6A and 2-6B)**.

To measure ICP0-induced loss of ubH2A and ubH2AX in cells, we used 6xHis-tagged ubiquitin (His-ub) to purify and analyze His-ub conjugated proteins from cells in the presence and absence of ICP0. 293T cells were co-transfected with His-ub and ICP0 or empty vector and harvested 24 h post-transfection. His-ub conjugated proteins were purified over Ni-NTA resin under denaturing conditions, and analyzed via SDS-PAGE and immunoblotting. As a positive control, we measured ubiquitylation of ICP0, which we observed to be heavily autoubiquitylated this experiment. We observed a decrease in ubiquitylated H2A and H2AX in the presence of ICP0 **(Figure 2-7A)**, even though total H2A and H2AX levels remained constant.

To examine whether the ICP0 RING domain was required to induce loss of ubH2A, we repeated the above experiment using two ICP0 mutants, one deleted of the RING domain (ΔRING) and one mutated at the two catalytic cysteines (C116G/C156A). We observed that, whereas WT ICP0 was heavily autoubiquitylated, the ICP0 RING mutants were not **(Figure 2-7B)**. Furthermore, the RING mutants were less able to induce loss of ubH2A. Combined, these observations

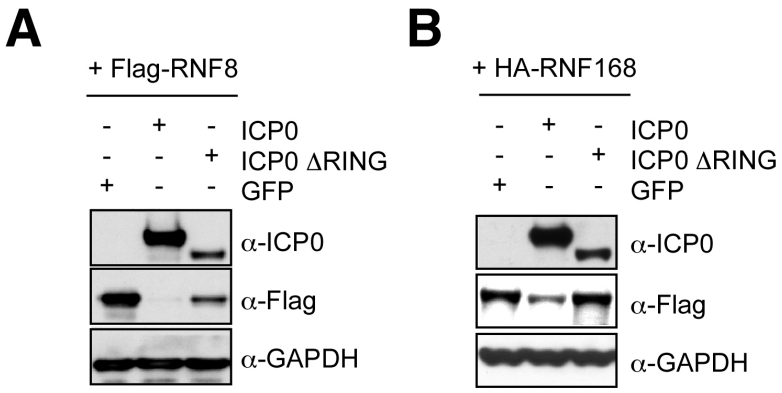

Figure 2-6. ICP0 is sufficient to degrade RNF8 and RNF168. A. HeLa cells were co-transfected with ICP0 or the ΔRING mutant in 3X excess of Flag-RNF8, harvested 24 h post-transfection, and protein levels were analyzed by SDS-PAGE and immunoblotting. **B.** HeLa cells were co-transfected with ICP0 or the ΔRING mutant in 3X excess of HA-RNF168, and processed as in **(A)**.

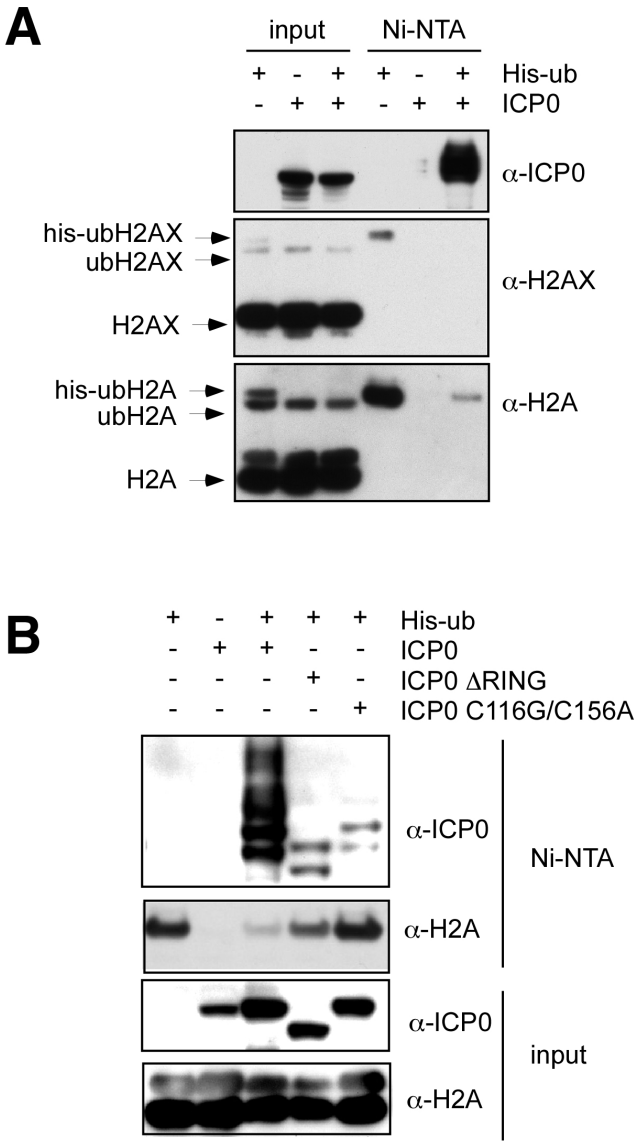

Figure 2-7. ICP0 expression induces loss of ubiquitylated forms of H2A and H2AX. A. 293T cells were co-transfected with His-ub in the presence or absence of ICP0, lysed 24h post tranfection, and His-ub conjugated proteins were purified using Ni-NTA resin under denaturing conditions. Input (5%) and eluted proteins were analyzed by SDS-PAGE and immunoblotting. **B.** 293T cells were transfected with WT ICP0, or catalytic mutants thereof, and His-ub. Samples were purified and analyzed as in **(A).**

indicate that ICP0 is sufficient to induce loss of RNF8, RNF168, ubH2A, and ubH2AX outside the context of infection, and that this is dependent on the RING domain of ICP0.

ICP0-mediated disruption of the DNA damage response occurs through targeting of RNF8 and RNF168

To address whether ICP0-mediated degradation of RNF8 and RNF168 was responsible for the block to IRIF, we examined the ability of 53BP1 to be recruited to IRIF in the presence of ICP0 when both Flag-RNF8 and Flag-RNF168 were overexpressed in cells. In this way we aimed to saturate the RNF8 and RNF168 levels such that there would be protein available in the cell even as they were being degraded by ICP0. HeLa cells were co-transfected with eGFP-ICP0 and excess amounts of Flag-RNF8 and Flag-RNF168. As controls, we over-expressed RING mutants of RNF8 or RNF168. 24 h post-transfection, cells were irradiated and 1 h post-IR were fixed and processed for immunofluorescence. We observed that the combined over-expression of RNF8 and RNF168 was sufficient to rescue the ICP0-induced block of 53BP1 recruitment to IRIF **(Figure 2-8A and 2-8B)**. Importantly, neither ligase alone nor one WT ligase combined with one catalytically inactive ligase was sufficient. This experiment demonstrates that degradation of both RNF8 and RNF168 by ICP0 is directly responsible for the ICP0-induced block to IRIF.

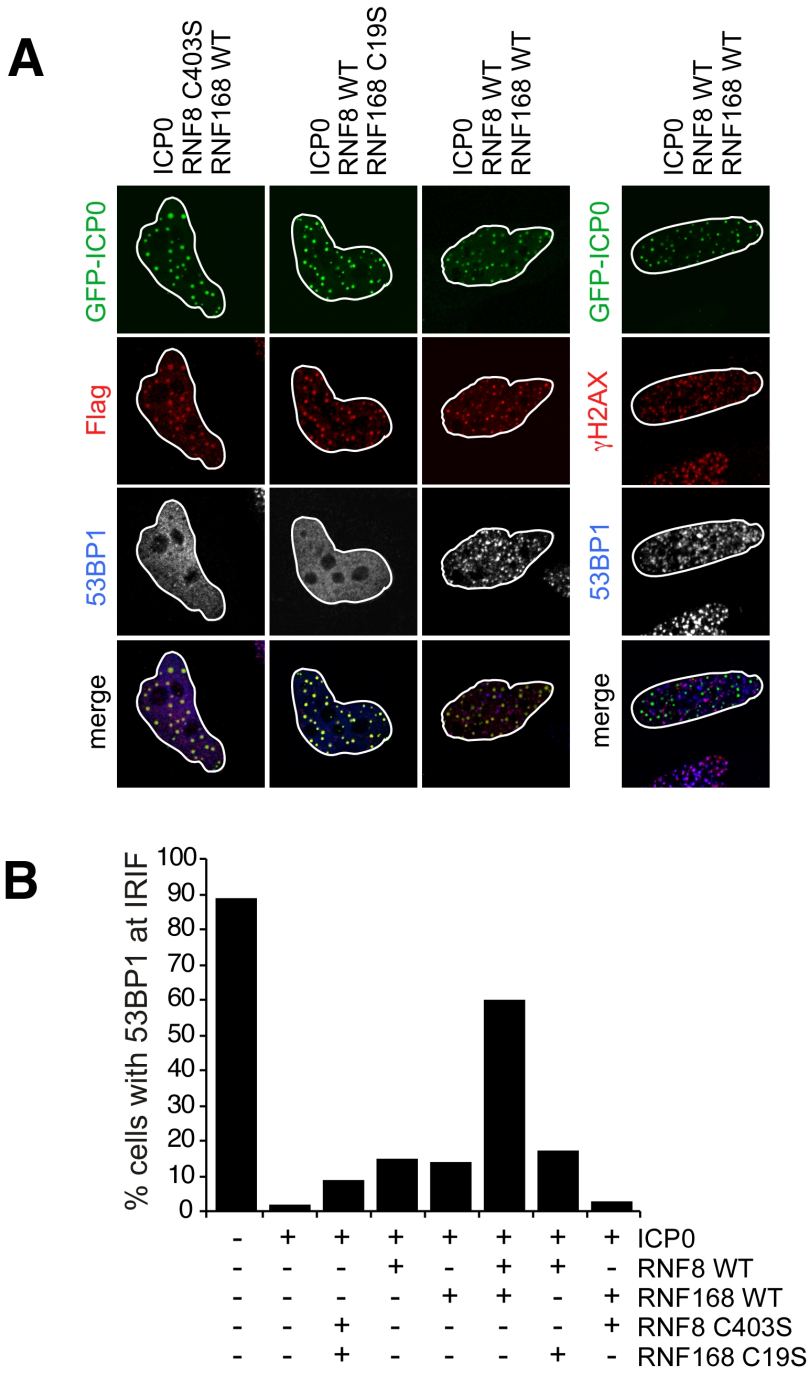

Figure 2-8. Rescue of the ICP0-induced block to IRIF. A. HeLa cells were transfected with GFP-ICP0 in the presence of WT or catalytically inactive Flag-RNF8 or Flag-RNF168, irradiated 24 h post-transfection, fixed 1 h post-IR, and processed for immunofluorescence. **B.** Transfected cells (200) from **(A)** were scored for presence or absence of 53BP1 at IRIF.

RNF8 and RNF168 are required for accumulation of conjugated ubiquitin and 53BP1 at incoming viral genomes

While RNF8 and RNF168 are required for 53BP1 recruitment to IRIF, their relevance to the DDR-mediated recognition of incoming HSV-1 genomes had not been addressed. To analyze the requirement for RNF8, we constructed a HepaRG cell line expressing a short hairpin RNA targeting RNF8, infected these cells with WT and ΔICP0 HSV-1, and analyzed recruitment of 53BP1 to incoming viral genomes. In cells expressing a scrambled shRNA sequence (shNeg), 53BP1 was recruited to incoming viral genomes during ΔICP0 infection but not during WT HSV-1 infection. In contrast, 53BP1 recruitment was prevented during both ΔICP0 and WT HSV-1 infection in cells expressing shRNF8 **(Figure 2-9A)**. To analyze whether RNF168 was required for 53BP1 recruitment to sites associated with incoming genomes, we used cells derived from a patient who has a biallelic mutation in RNF168 (RIDDLE cells, (Stewart et al., 2009)) and RIDDLE cells complemented with a cDNA expressing HA-tagged RNF168. We observed that 53BP1 was recruited to incoming viral genomes during ΔICP0 infection but not during WT HSV-1 infection in the presence of HA-RNF168. In contrast, we did not observe 53BP1 recruitment to sites associated with incoming genomes during WT or ΔICP0 infection in the RIDDLE cells, which lack functional RNF168 **(Figure 2-9B)**. These experiments demonstrate that 53BP1 recruitment to sites associated with incoming viral genomes is dependent on RNF8 and RNF168, similar to the requirements at IRIF.

Accumulation of conjugated ubiquitin at sites of DNA damage is dependent on RNF8 and RNF168 and can be visualized using immunofluorescence using antibodies against conjugated ubiquitin chains (FK2). We repeated the experiments described above and analyzed the ability of conjugated ubiquitin to accumulate at sites associated with incoming viral genomes using the FK2 antibodies. We observed that conjugated ubiquitin accumulated at sites associated with incoming viral genomes in normal cells, but failed to accumulate in cells deficient in either RNF8 or RNF168 **(Figures 2-10A and 2-10B)**. Combined, these observations demonstrate that the series of events orchestrated by RNF8 and RNF168 are the same in response to DNA damage and incoming HSV-1 genomes.

RNF8 and RNF168 pose barriers to infection that are overcome by ICP0

While accumulation of cellular factors at sites associated with incoming HSV-1 genomes has been linked to restricting the invading virus (Everett et al., 2008; Lukashchuk and Everett, 2010), it has also been previously demonstrated that proteins functioning in the early stages of the DDR, such as ATM and Mre11, are beneficial to HSV-1 infection (Lilley et al., 2005). We hypothesized that a dissection of the pathway might be necessary in order to promote activation and recruitment of upstream DDR proteins, which are favorable, while preventing the subsequent downstream events, which could be detrimental. In this scenario we would predict that RNF8 and/or RNF168 would be restrictive to infection. To test this hypothesis, we assessed the ability of WT or ΔICP0 HSV-1 to form plaques on cells deficient for

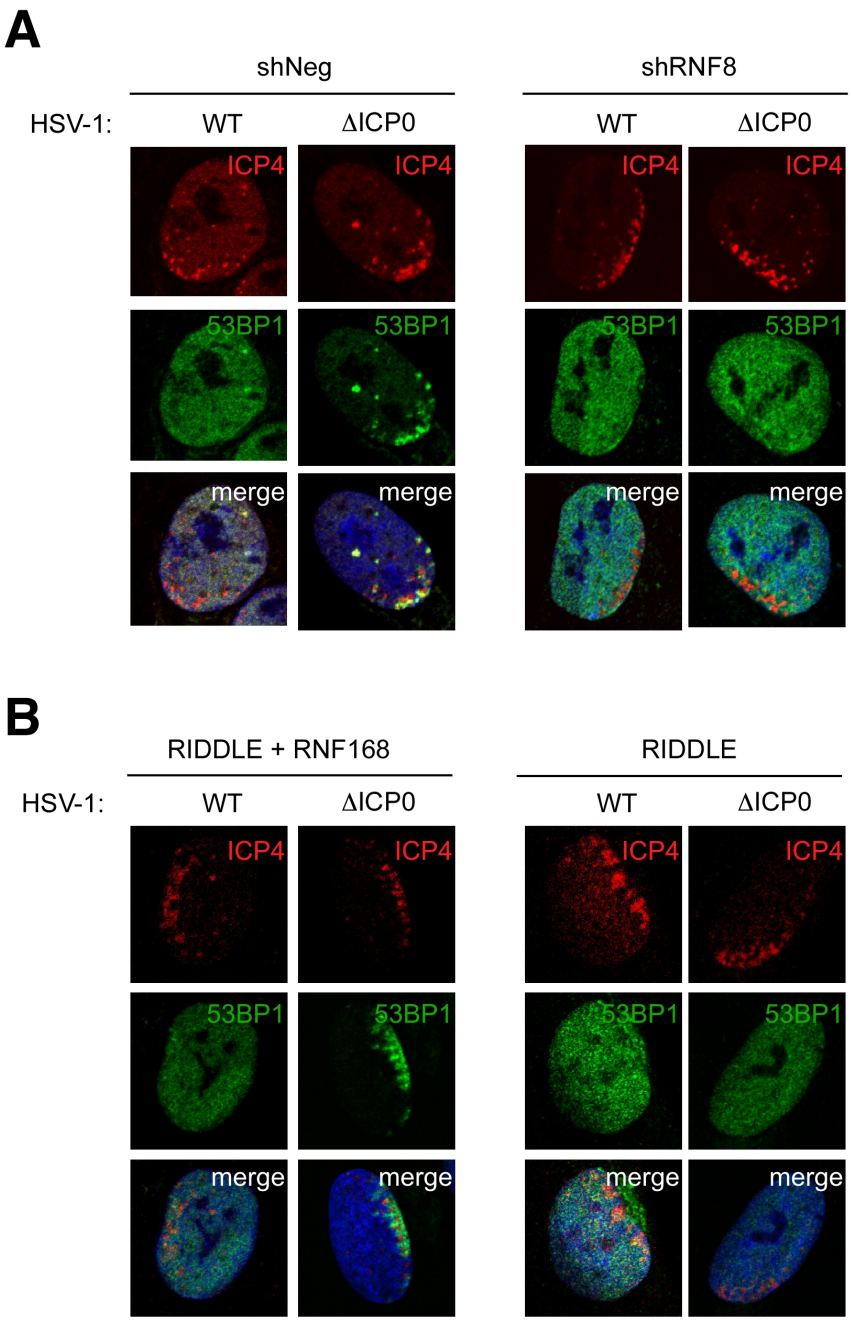

Figure 2-9. RNF8 and RNF168 are required for 53BP1 recruitment to sites associated with incoming viral genomes. A. Control HepaRG cells or cells in which RNF8 had been depleted using shRNA were infected with WT HSV-1 at MOI=0.001 or ΔICP0 virus at MOI=0.1 for 1 h. Cells were fixed at 24 hpi, stained for ICP4, and 53BP1 localization was assessed in asymmetrically infected cells. **B.** RIDDLE cells or RIDDLE cells expressing HA-tagged RNF168 were infected and analyzed as in **(A)**.

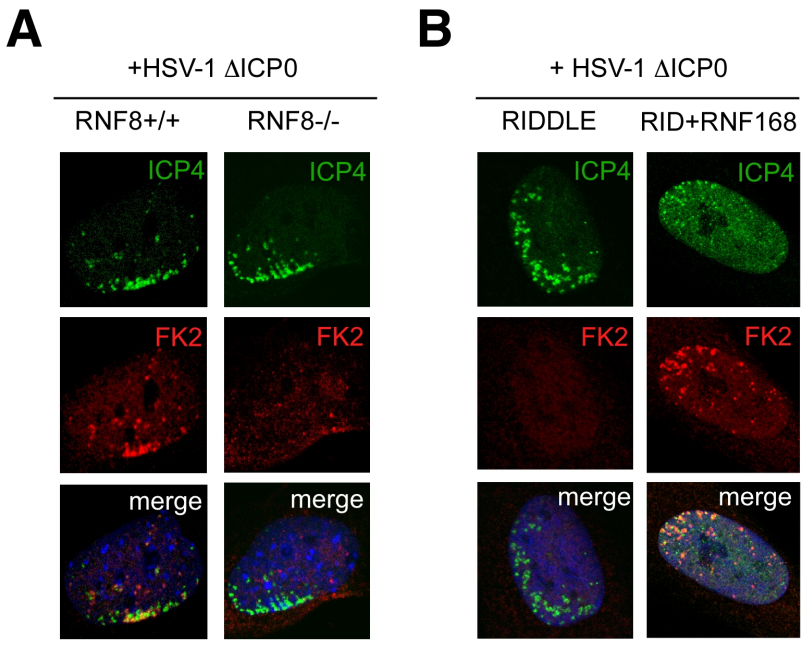

Figure 2-10. RNF8 and RNF168 are required for the generation of conjugated ubiquitin at sites associated with incoming genomes. A. RNF8 -/- MEFs or matched control MEFs were infected with ICP0-null HSV-1 at MOI=0.1 for 1 h. Cells were fixed at 24 hpi, stained for ICP4, and localization of conjugated ubiquitin (FK2) was assessed in asymmetrically infected cells. **B.** RIDDLE cells or RIDDLE cells expressing HA-tagged RNF168 were infected and analyzed as in **(A)**.

H2AX, RNF8, or RNF168 and compared them to matched controls complemented with the wild-type proteins. In the case of H2AX, we observed that both WT and ΔICP0 were approximately 10-fold more likely to form plaques in the presence of H2AX **(Figure 2-11).** These observations indicate that H2AX, like other proteins functioning at the early stages of the DDR, is beneficial for HSV-1 replication. We then performed the same experiment using cells deficient in RNF8 or RNF168. In both cases, the probability of WT virus to form plaques was no different in the presence or absence of either of these proteins. However, ΔICP0 HSV-1 was approximately 4-fold less likely to form plaques in the presence of RNF8 or RNF168 **(Figures 2-12A and 2-12B)**. These observations establish RNF8 and RNF168 as repressive factors to HSV-1 infection that are overcome by ICP0.

RNF8 represses early transcription events during HSV-1 infection

Our immunofluorescence data indicate that in the absence of ICP0, RNF8- and RNF168- dependent ubiquitylation events accumulate at the vicinity of incoming viral genomes. RNF8 has been shown to ubiquitylate histone H2A at sites of DNA damage, and these ubiquitylation events can repress transcription at the site of the break. We hypothesized that the restrictive function of RNF8 could be to repress viral transcription in a manner similar to that observed at sites of DNA damage. To address this possibility, we compared the transcriptional competence of viral genomes in the presence and absence of RNF8. RNF8-/- MEFs transduced with empty retrovirus or complemented with retrovirus encoding human WT RNF8 were infected with WT or

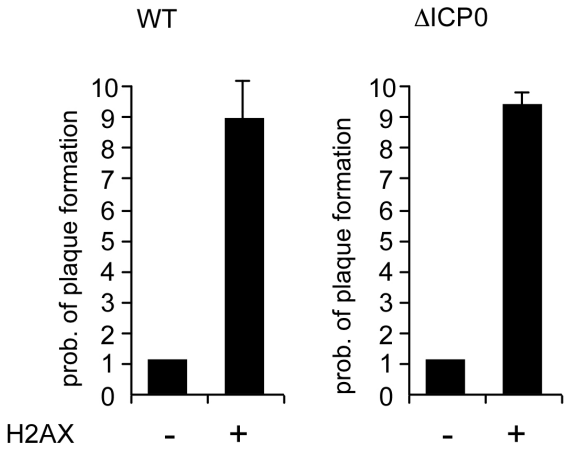

Figure 2-11. H2AX is beneficial to HSV-1 infection. H2AX-/- MEFs or matched controls were infected with WT or ΔICP0 HSV-1 and analyzed 48 h post-infection. Relative probabilities of plaque formation were calculated by counting the numbers of plaques on the different cell lines at each separate dilution of virus. Infections were carried out at least in duplicate and the experiment was repeated four times. Data are represented as mean +/- SEM.

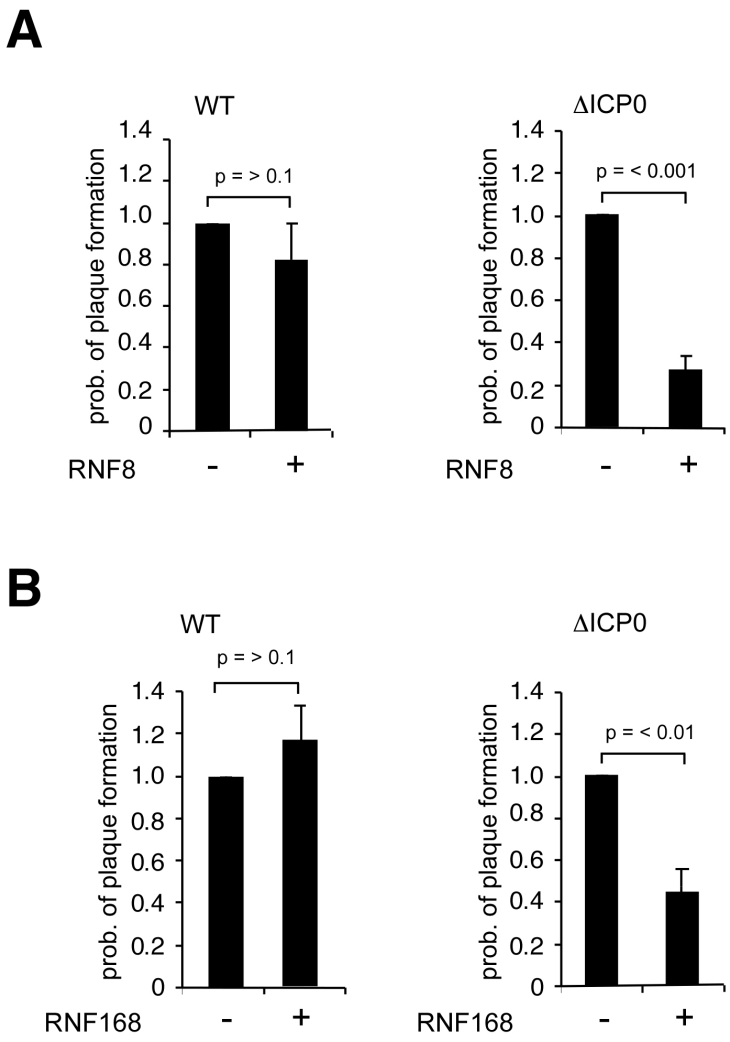

Figure 2-12. RNF8 and RNF168 pose barriers to infection that are overcome by ICP0. **A.** RNF8-/- MEFs (RNF8 -) or RNF8-/- MEFs reconstituted with RNF8 (RNF8 +) were infected with WT or ΔICP0 HSV-1 at low MOI and analyzed 48 h post-infection. Relative probabilities of plaque formation were calculated by counting the numbers of plaques on the different cell lines at each separate dilution of virus. Infections were carried out at least in duplicate and the experiment was repeated four times. Values are expressed as the relative number of plaques in complemented vs. depleted cell lines for each virus at a given dilution. Data are represented as mean +/- SEM. **B.** RIDDLE cells (RNF168 -) or RIDDLE cells complemented with HA-RNF168 (RNF168 +) were infected and analyzed as in **(A)**.

ΔICP0 HSV-1 at MOI=0.01 and harvested 2 and 5 hpi. RNA was isolated and reverse transcribed, and cDNA levels were measured via qPCR using primers targeted to the viral immediate-early ICP27 transcript. We confirmed that input viral DNA was similar in all infections and analyzed the data by comparing transcription in the presence of RNF8 to transcription in the absence of RNF8. We observed that both WT and ΔICP0 virus were transcriptionally repressed in the presence of RNF8 **(Figure 2-13)**. This repression was more significant in the absence of ICP0. We also observed that repression decreased over time during WT but not ΔICP0 infection, presumably as a consequence of ICP0-mediated RNF8 degradation. These data indicate that RNF8 is transcriptionally repressive to HSV-1 genomes and suggest an explanation as to why HSV-1 forms plaques less efficiently in the presence of RNF8 and/or RNF168.

Discussion

Four concepts are highlighted as a result of these studies. First is the finding that the cell is able to deploy the DDR not only to recognize damage to the host genome, but also to recognize and restrict incoming HSV-1 genomes. Second is the very specific dissection of the DDR by HSV-1, in which early events are activated upon infection while downstream events are blocked by ICP0- mediated degradation of RNF8 and RNF168. Third, these findings highlight the possibility that ubH2A is a novel epigenetic mark deposited on viral genomes, that may be countered by ICP0. Fourth, it appears that the cell uses ubiquitin-based mechanisms to attempt to repress

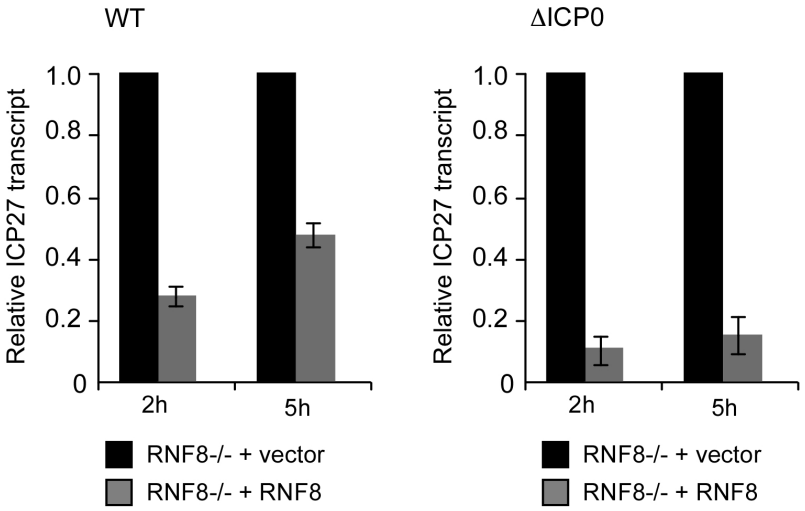

Figure 2-13. RNF8 represses viral transcription. RNF8-/- MEFs expressing RNF8 or empty vector were infected with WT or ΔICP0 HSV-1 at MOI=0.01. ICP27 transcripts were detected at 2 and 5 hpi and normalized to a cellular control. Data were analyzed by comparing transcription in the presence of RNF8 to transcription in the absence of RNF8 and therefore represent fold repression by RNF8 for each virus. Experiments were performed in duplicate and averaged. Results are representative of three independent experiments and the error is one standard deviation of the duplicate samples.

an incoming viral genome, and the virus responds via ubiquitin-based mechanisms: it encodes a ubiquitin ligase to target the restrictive cellular ubiquitin ligases for degradation. This convergence highlights the importance of the ubiquitin-proteasome system both for the host and the pathogen as they compete for control of host cell resources **(Figure 2-14)**.

As mentioned in Chapter 1, the ability of cells to redirect pre-existing resources to restrict an incoming viral infection constitutes an intracellular mechanism of defense recently described as intrinsic antiviral defense (Bieniasz, 2004). A characteristic of these defenses is that they are often overcome by virally encoded factors that have evolved to counteract them. In these regards, RNF8 and RNF168 can be considered a part of the intrinsic antiviral defense. They are constitutively expressed cellular factors that we demonstrate are restrictive to infection and counteracted by ICP0, which targets them for degradation. While other intrinsic antiviral defenses include receptor interference to prevent viral entry (Fv1) or targeting viral genomes for disabling levels of hypermutation or degradation (APOBEC3G) (reviewed in (Bieniasz, 2004)), RNF8 and RNF168 may contribute to a novel mechanism of intrinsic antiviral defense as they appear to affect transcriptional competence of the viral genome.

Our data indicate that viral transcription is repressed in the presence of RNF8 and that this is at least partially overcome in the presence of ICP0. Given the described roles of RNF8 and RNF168 as E3 ubiqutin ligases for H2A and H2AX, the ICP0-induced loss of ubH2A and ubH2AX, and the role of ubH2A in transcriptional

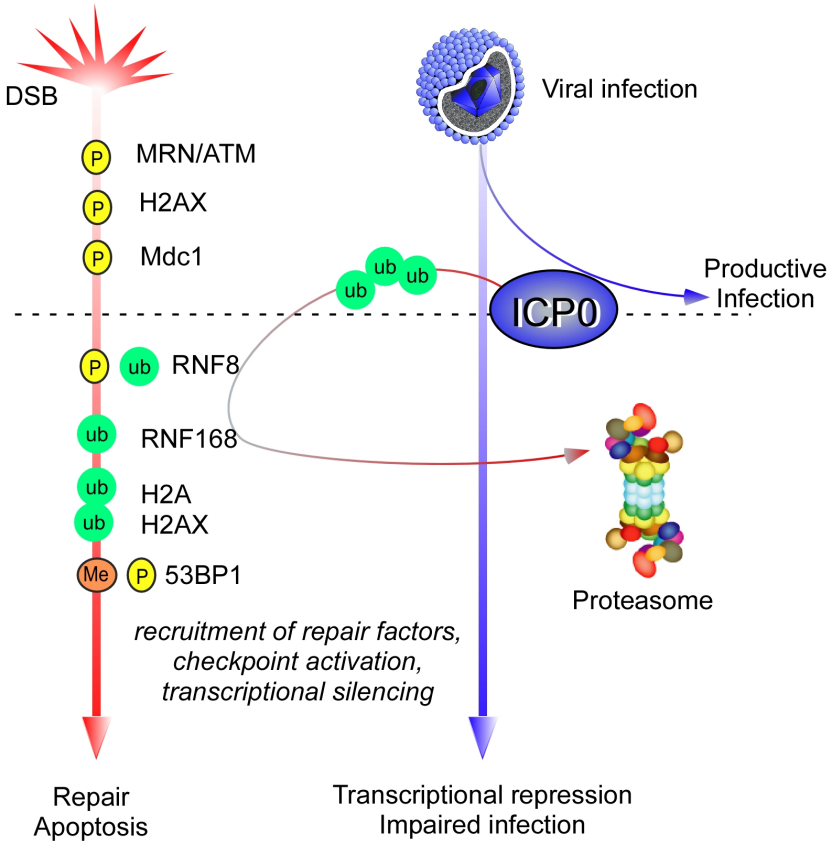

Figure 2-14. The DNA damage response is an intrinsic antiviral defense counteracted by ICP0. The series of signaling events occurring at the site of a DSB or at sites associated with incoming viral genomes are parallel and are similarly disrupted by ICP0-mediated degradation of RNF8 and RNF168. Thus ICP0-mediated dissection of the DDR can allow for potentially beneficial, DDR-facilitated genome processing events to occur while avoiding downstream consequences such as transcriptional repression of the genome. (*Proteasome image from http://plantsubq.genomics.purdue.edu*)

silencing (Shanbhag et al., 2010; Wang et al., 2004), an attractive hypothesis is that RNF8- and RNF168- mediated deposition of ubH2A on the viral genome would enable the cell to transcriptionally repress the viral genome. The added benefit of using DDR-activated H2A and H2AX ubiquitin ligases is that the same DNA-structure recognition motifs used to locate DNA damage events in the cell can be used to recognize double-stranded, linear viral genomes resembling ends of a double-stranded break as they enter the nucleus.

Our current data indicate that the DDR is recruited toward and activated at nuclear sites associated with incoming viral genomes, but the partially distinct immunofluorescence signals between ICP4 and DDR proteins leave open the possibility that these DDR events are converging on cellular chromatin at the vicinity of viral genomes, and not on the viral genomes themselves. More sensitive biochemical studies, such as chromatin immunoprecipitation of the viral genome, would be necessary to determine if DDR proteins are in fact deposited on incoming viral genomes. If the DDR instead converges on chromatin surrounding incoming viral genomes, an interesting question to address would be if and how accumulation on the cellular chromatin could affect the transcriptional dynamics of the nearby viral genomes.

It is clearly emerging that the DDR has a complex, multifaceted relationship with HSV-1. This is particularly highlighted by the very specific dissection of the DDR by ICP0, allowing upstream events such as phosphorylation and recruitment of ATM and H2AX to occur while preventing downstream events. While it is unclear

exactly how the upstream proteins are contributing to viral infection, it is possible that they promote processing or recombination of genomic and replicative intermediates that have been previously observed during HSV-1 infection (Wilkinson and Weller, 2003). Interestingly, while Mdc1 is recruited to IRIF in the presence of ICP0, we noted that its retention at IRIF appeared slightly impaired in the presence of ICP0, as assessed by FRAP analysis **(Appendix Figure A-1)**. It is possible that inhibiting the downstream DDR events may impair a feedback loop that signals for sustained Mdc1 retention. Supporting these observations, we have found that the intensity of γH2AX signals at IRIF decreases over time in the presence of ICP0, even though recruitment can clearly be observed (C. Lilley, unpublished observations). As γH2AX serves as a binding site for Mdc1, the decrease in the γH2AX signal may explain the decreased retention of Mdc1 at IRIF. Further studies will be needed to determine the causal events underlying these observations. Recently, ubH2B has also been shown to accumulate at sites of DNA damage and contribute to the DDR (Moyal et al., 2011). Interestingly, we did note a loss of ubH2B during HSV-1 infection, but this was not ICP0-dependent **(Appendix Figure A-2)**. Thus while the loss of ubH2B may contribute to HSV-1 infection, the effects of ICP0 on the DDR are not occurring through loss of ubH2B.

Many viruses encode E3 ubiquitin ligases or proteins that are able to redirect cellular ubiquitin ligase complexes in order to target cellular proteins for degradation. What is most interesting here is that the targeted proteins are themselves ubiquitin ligases, and the ultimate mechanism of intrinsic antiviral defense in this case may be

the use of ubH2A in order to silence the viral genome. Thus the ubiquitin pathway is harnessed both by the virus and cell as they compete to gain control of host cell resources.

ICP0 has long been known to be a promiscuous transcriptional transactivator of many viral and cellular promoters, but has never been shown to be able to bind DNA. Instead, its E3 ubiquitin ligase activity is most crucial to this ability. In the context of the findings presented here, it may be more accurate to describe the effect of ICP0 as a de-repression rather than a transactivation, and this would also explain the seemingly broad, sequence-independent effect it has on a variety of exogenous and endogenous promoters. Further work will be required to determine if ubH2A is deposited on the viral genome upon HSV-1 infection, and whether ubH2A is directly responsible for transcriptional silencing of the viral genome in the absence of ICP0. As described in more detail in Chapter 1, latent genomes exist in an episomal state and are bound in a chromatin-like structure, epigenetic marks on the viral genome change as the virus switches between lytic and latent infections, and ICP0 can contribute to these changes (Placek and Berger, 2010). Accumulation of ubH2A on viral genomes, particularly during reactivation and in the presence and absence of ICP0, should be investigated. The ability of ICP0 to regulate ubH2A deposition on the viral genome may constitute an important mechanism by which ICP0 is able to promote lytic infection and reactivation from latency.

Materials and Methods

Cell lines

Vero, U20S, HEK-293T, IMR90, and HEK-293 cells were purchased from the American Tissue Culture Collection. MEFs from RNF8-/- knockout mice and matched wild-type controls were obtained from R. Hakem (Li et al., 2010) or J. Chen (Minter-Dykhouse et al., 2008) and for some experiments RNF8-/- MEFs complemented with human RNF8 were used. U20S cells expressing GFP-53BP1 were from J. Bartek and J. Lukas (Bekker-Jensen et al., 2005). RNF8 knockdown HepaRG cells were generated by introduction of a targeting sequence 5' ACATGAAGCCGTTATGAAT 3' as previously described (Mailand et al., 2007) using pLKO based vectors. Human foreskin fibroblasts (HFFs), obtained from the University of California Medical Center, were kindly provided by D. Spector. Cells were maintained in Dulbecco modified Eagle's medium (DMEM) containing 100 U/m of penicillin and 100 μg/ml of streptomycin, supplemented with 10% fetal bovine serum (FBS) and selection antibiotics as appropriate. Cells were grown at 37^{o}C in a humidified atmosphere containing 5% CO_2. HepaRG hepatocyte cells (Gripon et al., 2002) were grown in William's medium E supplemented with 2 mM glutamine, 5 μg/ml insulin, and 0.5 μM hydrocortisone. H2AX-/- MEFs were obtained from A. Nussenzweig (Celeste et al., 2002).

Viruses and infections

The WT HSV-1 strain was 17 *syn*+ and the matched ICP0 deletion mutant was *dl*1403, which expresses the first 105 amino acids of ICP0, followed by a frame shift of 56 amino acids and a premature STOP codon (Stow and Stow, 1986). Viruses were grown on Vero cells and titered on U20S cells, in which ICP0 is not required for efficient plaque formation. Infections were performed on monolayers of cells in DMEM with 0% FBS. After 1 h at 37^{o}C, virus was removed and media containing 10% FBS was added. For plaque edge experiments, this media was supplemented with 1% human serum to limit spread of the virus. For plaque assays, 24 well dishes were infected with 3-fold dilutions of WT or ΔICP0 HSV-1. After adsorption, the cells were overlaid with medium containing 10% FBS and 1% human serum. Plaques were stained with crystal violet 24-36 h post-infection. For complementation of RNF-/- MEFs, retroviruses were prepared and infections performed as previously described (Carson et al., 2003).

Plasmids and transfections

Expression vectors for WT and mutant ICP0 were from S. Silverstein or previously described (Everett et al., 1999b). The ΔRING version of ICP0 was FXE, which lacks amino acids 106-149. Flag-RNF8 was from J. Chen and J. Lukas. 6xHis-ubiquitin expression plasmid was from T. Hunter. For complementation of RNF8-/- MEFs, RNF8 WT was cloned into pLPC (Serrano et al., 1997) between *EcoRI* and *XhoI* restriction sites. Mammalian cells were transfected with Lipofectamine 2000

(Invitrogen) or polyethylenimine (PEI, Polysciences Inc.) according to the manufacturer's protocol.

Antibodies

Primary antibodies were purchased from Bethyl (PML), Santa Cruz (53BP1, Ku70), Millipore/Upstate (H2AX S139, H2AX, FK2, H2A, ubH2A, ubH2B), Abcam (RNF20 and RNF40), Medimabs (H2B), Cell Signaling (H2AX), Research Diagnostics Inc. (GAPDH), Covance (HA), Transduction Laboratories (DNA-PKcs), and Sigma (Flag). Rabbit antisera to Mdc1 were from J. Chen. The 58S monoclonal antibody to ICP4 was generated from an ATCC hybridoma cell line (Showalter et al., 1981). All secondary antibodies were from Jackson Laboratories or Invitrogen.

Immunoblotting and immunofluorescence

For immunoblotting, infected or transfected cells were collected and lysates prepared by resuspending the pellet in lysis buffer (PBS containing 0.25% Triton X-100, 0.1% SDS, 1% NP-40, protease inhibitors (Roche), 1mM PMSF, and the phosphatase inhibitors 20 mM NaF, 1 mM Na_3VO_4, and β-glycerophosphate). Lysates were incubated for 30 min on ice and cleared by centrifugation at 14,000 rpm at 4^{o}C, and protein concentration was measured by Lowry (BioRad). Chromatin associated proteins were isolated by extracting the insoluble pellet with 0.1 M HCl for 30 min on ice. Proteins were separated by electrophoresis using polyacrylamide gels (Invitrogen) and transferred to Hybond ECL membranes (Amersham), blocked in 5%

milk in PBS-T, and subject to immunoblotting using the indicated antibodies diluted in PBS containing 3% BSA. HRP-conjugated secondary antibodies (Jackson Laboratories) were used to detect the primary antibodies and visualized using Western Lightning Plus ECL (Perkin-Elmer) exposed on CL-X Posure Film (Thermo Scientific). For immunofluorescence, cells were washed in PBS, fixed in 4% paraformaldehyde in PBS, and extracted in 0.5% Triton-X in PBS. Primary antibodies were diluted in PBS containing 3% BSA and Alexa-fluor conjugated secondary antibodies (488, 564, or 647, Jackson Laboratories) were diluted 1:2000 in PBS containing 3% BSA. Nuclei were visualized using DAPI. Confocal images were acquired using a Leica TCS SP2 microscope.

Purification and analysis of 6xHis-ub conjugated proteins from cell lysates

A total of 5 X 10^6 293T cells were transfected with 10 μg of 6xHis-ub plus 10 μg GFP, ICP0, or mutants thereof. Cells were collected 24 h post-transfection and processed for immunoblotting (inputs) or purification over nickel-nitriloacetic acid (Ni-NTA) beads (Qiagen). For purification, cell pellets were lysed in 6 ml guanidinium lysis buffer (6 M guanidinium-HCl, 0.1 M Na_2HPO_4-NaH_2PO_4, 10 mM Tris-HCl (pH=8.0), 10 mM β-mercaptoethanol) and incubated with 75 μl Ni-NTA beads at 25°C for 4 h or 4°C overnight. Beads were washed once in guanidinium lysis buffer and then in urea wash buffer (8 M urea, 0.1 M Na_2HPO_4–NaH_2PO_4, 10 mM Tris–HCl (pH=8.0), 10 mM β-mercaptoethanol), and washed twice with buffer C (8 M urea, 0.1 M Na_2HPO_4–NaH_2PO_4, 10 mM Tris–HCl (pH=6.3), 10 mM β-

mercaptoethanol) containing 0.2% and then 0.1% Triton X-100. Proteins were eluted from beads by boiling in NuPAGE LDS sample buffer (Invitrogen), separated by SDS-PAGE, and visualized via immunoblotting.

qPCR

2 X 10^6 cells were infected with WT or ΔICP0 virus at MOI=0.01 and harvested at 2 and 5 h post-infection. 75% of the cell pellet was used for RNA isolation (RNeasy, Qiagen) and 25% for DNA extraction (DNeasy, Qiagen). 1 μg RNA was reverse transcribed using SuperScriptIII (Invitrogen) and Oligo dT in a 20 μl reaction. qPCR was run in triplicate with 3 μl cDNA or 100 ng genomic DNA using SYBR Green PCR master mix (ABI) on an ABI 7900 HT system. ICP27 transcript was detected using primers GCATCCTTCGTGTTTGTCATT (F) and GCATCTTCTCTCCGACCCCG (R) (Liang et al., 2009) and normalized to endogenous RPLPO transcript detected using primers CTGGAAGTCCAACTACTTCC (F) and TGCTGCATCTGCTTGGAGCC (R).

FRAP analysis

U2OS cells stably expressing GFP-53BP1 (Bekker-Jensen et al., 2005) were grown on glass bottom 35 mm dishes with 14 mm glass microwells (MatTeK Corp). Before imaging, cells were supplemented with fresh phenol-red free medium with 10% FBS and 10 μM HEPES. Images were acquired using a Leica TCS SP2 confocal microscope. After acquisition of five pre-bleach images, a defined region of interest

(ROI) of 1 μM square was bleached five times by the 488-nm argon laser set to 100% transmission. Post-bleach images were acquired at 1-, 5-, and 10-s intervals for a total of 125 s at 10% transmission. The adjusted fluorescence intensity at each timepoint is represented as the fraction of the pre-bleach intensity at the ROI.

Acknowledgements

I am grateful to Caroline Lilley who has been a wonderful mentor and who has guided many of these studies. She is responsible for all images of protein recruitment to sites associated with incoming viral genomes and viral growth assays, and made the initial observations characterizing ICP0-mediated disruption of the DDR. Many of the experiments presented in this chapter are the results of our joint efforts. We thank J. Chen, A. Nussenzweig, J. Lukas, J. Bartek, D. Spector, Y. Shiloh, D. Durocher, G. Stewart, S. Silverstein, S. Weller, M. Rosenfeld, H. Koseki, J. Wilson, T. Hunter, R. Greenberg, C. Preston, E. Hendrickson and R. Hakem for generous gifts of reagents. We thank Quan Zhu for help with lentivirus shRNA constructs.

Some material in this chapter is reprinted in part as it appears in Lilley CE, Chaurushiya MS, Boutell C, Landry S, Suh J, Panier S, Everett RD, Stewart GS, Durocher D, and Weitzman MD, A viral E3 ligase targets RNF8 and RNF168 to control histone ubiquitylation and DNA damage responses, EMBO J. 2010 29:943-955, and is reprinted by permission from Nature publishing group, copyright 2010, Macmillan Publishers Ltd. Some material from this chapter is reprinted in part as it appears in Lilley CE, Chaurushiya MS, Boutell C, Everett RD, and Weitzman MD,

The Intrinsic Antiviral Defense to Incoming HSV-1 Genomes Includes Specific DNA Repair Proteins and is Counteracted by the Viral Protein ICP0, PLoS Pathogens 2011, 7(6): e1002084, and is reprinted by permission from the authors under the terms of the Creative Commons Public License. The dissertation author was a researcher and author on these papers.

Chapter 3. HSV-1 ICP0 mimics a cellular phosphorylation mark to target cellular FHA domain proteins

Background

A wide variety of viruses encode E3 ubiquitin ligases to promote viral infection, although in many cases the mechanisms by which these enzymes converge on their substrates are unknown. In the previous Chapter we identified novel degradation targets of the HSV-1 encoded E3 ubiquitin ligase ICP0: the cellular ubiquitin ligases RNF8 and RNF168. We next sought to understand how these proteins were targeted, and in this Chapter we identify the binding interface between ICP0 and RNF8.

Cellular protein-protein interactions are orchestrated through a variety of structured domains that can bind to each other or to short linear motifs. Short linear motifs can be induced by phosphorylation events and bound by phospho-binding domains (Pawson and Scott, 1997; Ren et al., 2008). For example, fork-head associated (FHA) domains bind pThr (Durocher et al., 1999), BRCA C-terminal (BRCT) domains bind pSer (Yu et al., 2003a), and Src homology 2 (SH2) domains bind pTyr (Songyang et al., 1993). Structural variation within these domain families results specific preferences for the context in which the phosphorylated residue is presented, and thus short linear motifs that are differentiated by only a few amino acids can recruit distinct members of the same phospho-binding family (Durocher et al., 2000; Rodriguez et al., 2003). As described in more detail in Chapters 1 and 2, the

cellular DNA damage response relies heavily on these interactions to regulate many pathways including DNA processing and repair, cell cycle, and transcription. Because short linear motifs are usually less than ten amino acids in length, the generation of one may require only the introduction of a point mutation, rendering this system highly susceptible to hijacking by rapidly evolving viruses (Davey et al., 2011).

Here we identify a short linear motif encoded by ICP0 that mimics those found on Mdc1, in order to bind RNF8 via the RNF8 FHA domain. We demonstrate that this interaction is direct, that it is required for the ICP0-mediated ubiquitylation and degradation of RNF8, and that it occurs through phosphorylated T67 on ICP0 *in vitro* and in cells. Biochemical studies identify CK1 as the cellular kinase catalyzing this phosphorylation and facilitating interaction with RNF8. Construction of HSV-1 virus containing the ICP0 T67A mutation reveals that this residue is required for targeting RNF8 in the context of infection and important to counter cellular attempts to repress transcription from the viral genome. Finally, we demonstrate through mass spectrometry studies that the pT67 region of ICP0 can target other cellular FHA domain containing proteins, and highlight the possibility that this viral hijacking of a cellular short linear motif contains a unique flexibility required for the potential to target structurally diverse FHA domains. These studies highlight the possibility that other viral ubiquitin ligases and regulatory proteins may mimic cellular short linear motifs and phosphosites in order to insert themselves into key cellular pathways.

Results

ICP0 associates with RNF8 in cells

We previously observed that RNF8 and RNF168 were degraded during HSV-1 infection in an ICP0- and proteasome- dependent manner and that ICP0 was sufficient to induce degradation of both RNF8 and RNF168 outside the context of infection, indicating they are direct substrates of ICP0. We next asked whether these proteins could interact with ICP0 in cells, and focused on RNF8 to initiate these studies.

ICP0 localizes to PML bodies in the nucleus, where it induces co-localization of conjugated ubiquitin (Everett, 2000a) and degrades PML and associated PML body components (Everett et al., 1998a; Everett et al., 2004). We wanted to determine whether ICP0 affected the localization of RNF8, which in the absence of DNA damage is normally diffusely nuclear. HeLa cells were co-transfected with Flag-RNF8 and eGFP-ICP0 ΔRING, fixed 16 h post-transfection, and visualized using α-Flag immunofluorescence and GFP fluorescence. We observed that Flag-RNF8 readily re-localized to ICP0 foci upon ICP0 expression **(Figure 3-1A)**, indicating that ICP0 interacts with RNF8 in cells. To test the interaction biochemically, we constructed a mammalian expression plasmid encoding a TAP-tagged ICP0 (TAP-ICP0), which contained streptavidin-binding peptide and calmodulin-binding peptide sequences at the amino terminus of ICP0. As a control, we fused the TAP sequence to mRFP. TAP-ICP0 or TAP-mRFP was co-transfected with Flag-RNF8 into 293T cells, harvested 24 h post-transfection, and lysates were prepared. We used Streptavidin Sepharose to pull down TAP-ICP0 or TAP-mRFP from lysates and analyzed co-

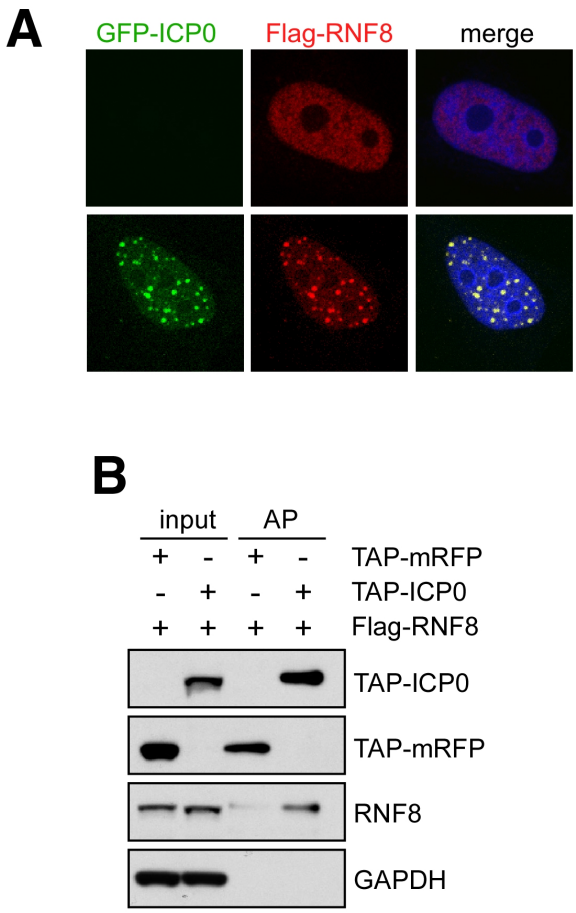

Figure 3-1. ICP0 associates with RNF8 in cells. A. ICP0 co-localizes with RNF8. Flag-RNF8 and eGFP-ICP0 ΔRING were co-transfected into HeLa cells, fixed 24 h post transfection, and processed for immunofluorescence. **B.** RNF8 co-purifies with ICP0. TAP-ICP0 or TAP-mRFP was co-transfected into 293T cells with Flag-RNF8 and harvested 24 h post-transfection. Lysates were affinity purified (AP) using Streptavidin Sepharose beads. Precipitated proteins were analyzed via SDS-PAGE and immunoblotting.

purifying proteins via SDS-PAGE and immunoblotting. We observed that Flag-RNF8 co-purified with TAP-ICP0 but not TAP-mRFP **(Figure 3-1B)**. Combined, the immunofluorescence and affinity purification experiments indicate that ICP0 and RNF8 associate, either indirectly or directly, in cells.

The FHA domain of RNF8 is required for targeting by ICP0

The FHA domain of RNF8 is located at the N terminus, while the C terminus encodes its RING domain. In order to determine the regions required for RNF8 interaction with ICP0, we constructed Flag-tagged fragments of RNF8 comprising these different functional domains **(Figure 3-2)** and tested whether they were recruited to ICP0 foci. HeLa cells were transfected with Flag-RNF8 fragments in the presence or absence of eGFP-ICP0 ΔRING (to prevent ICP0-mediated degradation) and protein localization was assessed via α-Flag immunofluorescence and GFP autofluorescence. All of the RNF8 fragments were diffusely nuclear in the absence of eGFP-ICP0 ΔRING **(Figure 3-3A)**. Upon co-transfection with eGFP-ICP0 ΔRING, WT Flag-RNF8 and Flag-F3 were recruited to ICP0 foci while Flag-F1 and Flag-F2 remained diffusely nuclear **(Figure 3-3B)**. Both Flag-F1 and Flag-F2 lacked the FHA domain, indicating that localization to ICP0 foci could be coordinated through the RNF8 FHA domain. Supporting these observations, introduction of an inactivating point mutation in the FHA domain, R42A, was sufficient to abolish RNF8 recruitment to ICP0 foci **(Figure 3-3B)**.

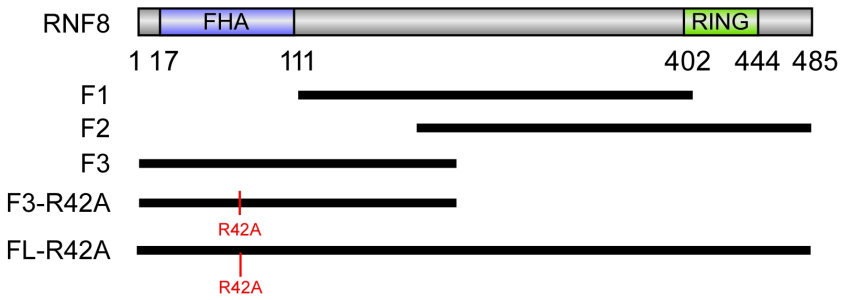

Figure 3-2. Functional domains of RNF8 and fragments generated for analysis. All fragments contain an N-terminal Flag tag.

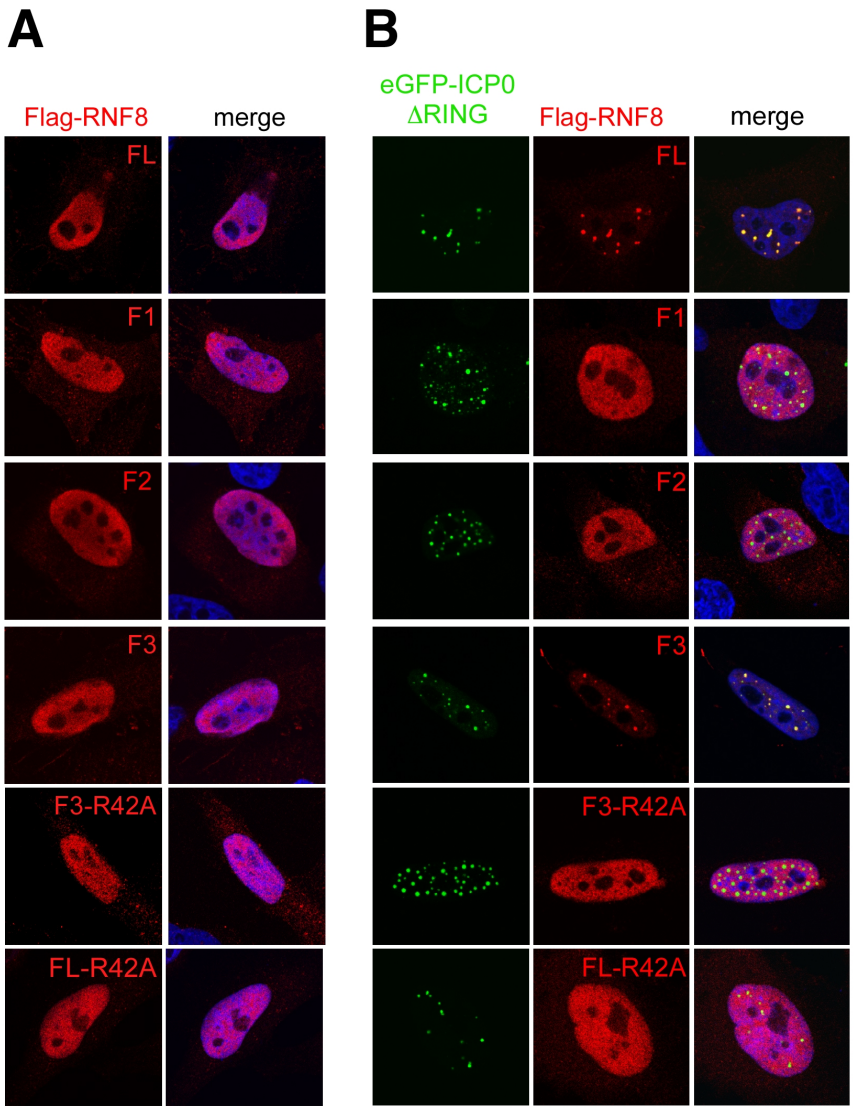

Figure 3-3. The RNF8 FHA domain is required for co-localization with ICP0. HeLa cells were co-transfected with Flag-RNF8 fragments in the presence or absence of eGFP-ICP0 ΔRING, fixed 24 h post transfection, and localization assessed via immunofluorescence. **A.** All fragments are diffusely nuclear in the absence of ICP0. **B.** Fragments lacking the FHA domain cannot localize to ICP0 foci.

We next sought to determine whether the FHA domain of RNF8 was required for RNF8 degradation during HSV-1 infection. To test this, we transfected WT RNF8 or the R42A mutant into HeLa cells and infected cells with WT HSV-1 at MOI=3 24 h post transfection. Cells were harvested 8 h post infection and protein levels were analyzed by SDS-PAGE and immunoblotting. We found that WT Flag-RNF8 was degraded during infection but that the R42A mutant was resistant to degradation **(Figure 3-4A)**. Furthermore, all Flag-RNF8 fragments lacking the FHA domain were resistant to degradation during infection **(Figure 3-4B)**. Supporting these observations, ICP0 ubiquitylated recombinant His-Flag-RNF8 R42A protein *in vitro* much less efficiently than WT His-Flag-RNF8 **(Figure 3-4C)**. Combined, these observations lead us to conclude that ICP0 targets RNF8 for ubiquitylation and degradation via interaction with the FHA domain of RNF8.

ICP0 phosphorylation is required for interaction with the RNF8 FHA domain

FHA domains have been well described as phospho-threonine binding motifs (Durocher and Jackson, 2002), and ICP0 has been shown to be a heavily phosphorylated protein (Davido et al., 2005). Because the ICP0-RNF8 interaction requires the FHA domain of RNF8, we hypothesized that the interaction was phosphorylation dependent. To address this possibility, recombinant GST-RNF8-FHA protein and the R42A mutant were purified from *E. coli* **(Figure 3-5A)** and used in GST pulldown assays. ICP0 was transfected into 293T cells and lysates prepared for GST pulldown. We observed that GST-RNF8-FHA but not the R42A mutant was

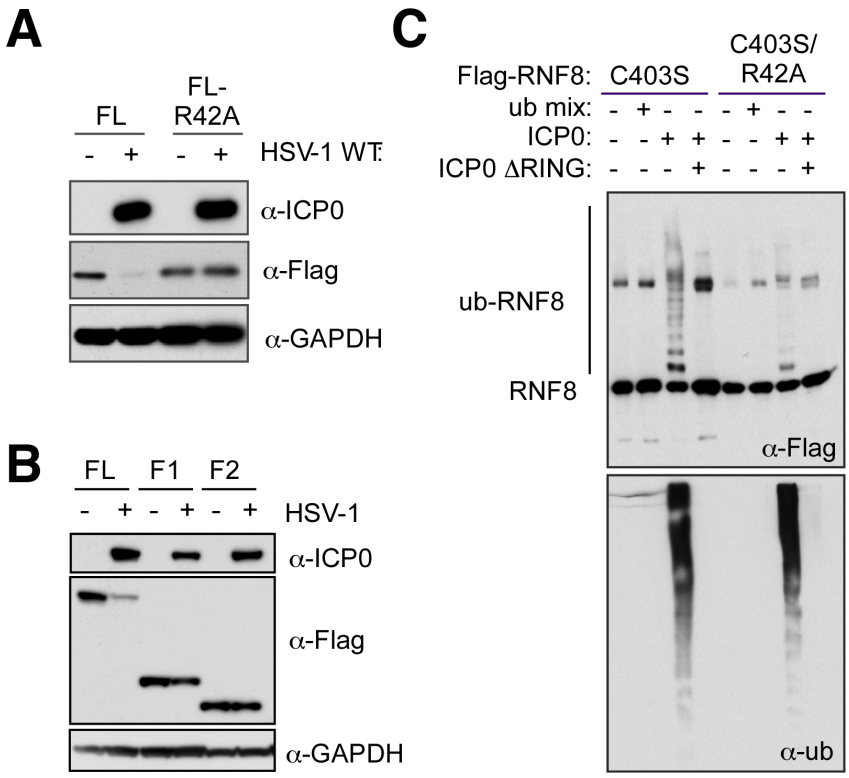

Figure 3-4. The RNF8 FHA domain is required for its ubiquitylation and degradation by ICP0. A. Full-length RNF8 and the R42A mutant were co-transfected into HeLa cells with 3X excess eGFP-ICP0, harvested 24 h post transfection, and protein levels analyzed via SDS-PAGE and immunoblotting. **B.** FHA domain mutants are resistant to ICP0-mediated degradation. RNF8 fragments were transfected and analyzed as in (A). **C.** ICP0 ubiquitylates RNF8 R42A less efficiently *in vitro*. Catalytically inactive (C403S) His-Flag-RNF8 or C403S/R42A proteins were purified from *E. coli* and used in *in vitro* ubiquitylation assays with recombinant ICP0 purified from a baculovirus system. Reaction products were analyzed for RNF8 ubiquitylation (top panel) and ubiquitin conjugation (bottom panel) via SDS-PAGE and immunoblotting.

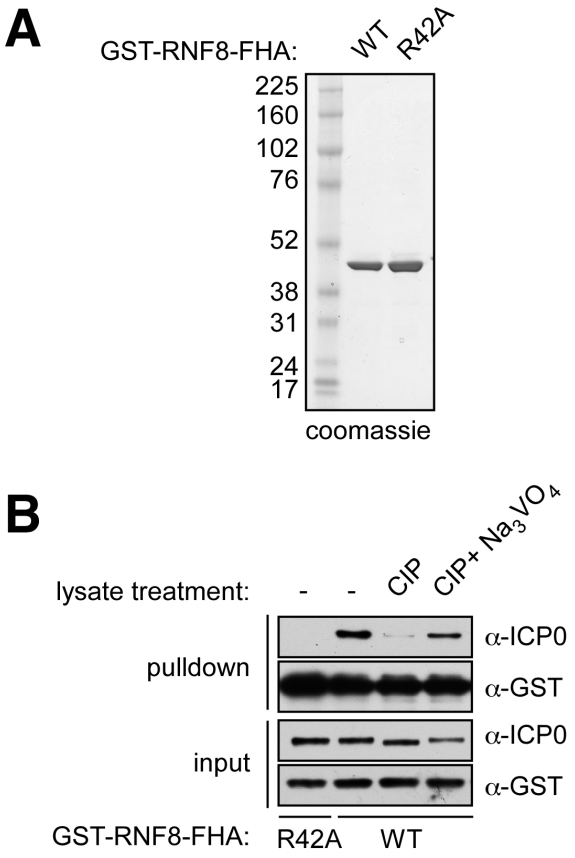

Figure 3-5. ICP0 interaction with the RNF8 FHA domain is phosphorylation dependent. **A.** Recombinant GST-RNF8-FHA or R42A mutant proteins were purified from E. coli and analyzed by SDS-PAGE and coomassie staining. **B.** ICP0 was transfected into 293T cells and harvested 24 h post transfection. Cells were lysed in GST lysis buffer and, where indicated, treated with CIP or CIP plus phosphatase inhibitors for 30 min at 30^{o}C. Lysates were then incubated with the indicated recombinant protein and glutathione sepharose beads. Precipitated proteins were analyzed by SDS-PAGE and immunoblotting.

able to retrieve ICP0 from lysates **(Figure 3-5B)**. To determine if the interaction was phosphorylation dependent, we treated lysates with alkaline phosphatase (CIP) prior to GST pulldown. GST-RNF8-FHA was unable to retrieve ICP0 from lysates after CIP treatment and this was rescued when sodium orthovanadate (Na_3VO_4), a phosphatase inhibitor, was included **(Figure 3-5B)**. We also observed increased migration of ICP0 after phosphatase treatment, consistent with generation of a dephosphorylated form of the protein. These data demonstrate that the FHA domain of RNF8 is sufficient to interact with ICP0 in a phosphorylation dependent manner.

ICP0 T67 is required for interaction with the RNF8 FHA domain

In order to identify the phosphorylated residue on ICP0 that mediates the interaction with the FHA domain of RNF8, we scanned the ICP0 amino acid sequence for Thr residues conforming to the RNF8 FHA binding consensus motif. Peptide mapping studies have revealed that the FHA domain of RNF8 has a preference for phospho-Thr with Phe or Tyr in the +3 position (Huen et al., 2007). ICP0 contains only one such consensus motif, at amino acids 67-70: TELF **(Figure 3-6A)**. This sequence is well conserved in other strains of HSV-1 and in ICP0 of HSV-2, which shares 61% identity with the HSV-1 ICP0 sequence. We generated a T67A mutant of eGFP-ICP0 and tested its ability to interact with RNF8 using GST pulldown assays as described above. GST-RNF8-FHA retrieved WT but not T67A eGFP-ICP0 from cell lysates **(Figure 3-6B)**. We next examined the sub-cellular localization of eGFP-ICP0 T67A via immunofluorescence in HeLa cells as described above. Both eGFP-ICP0

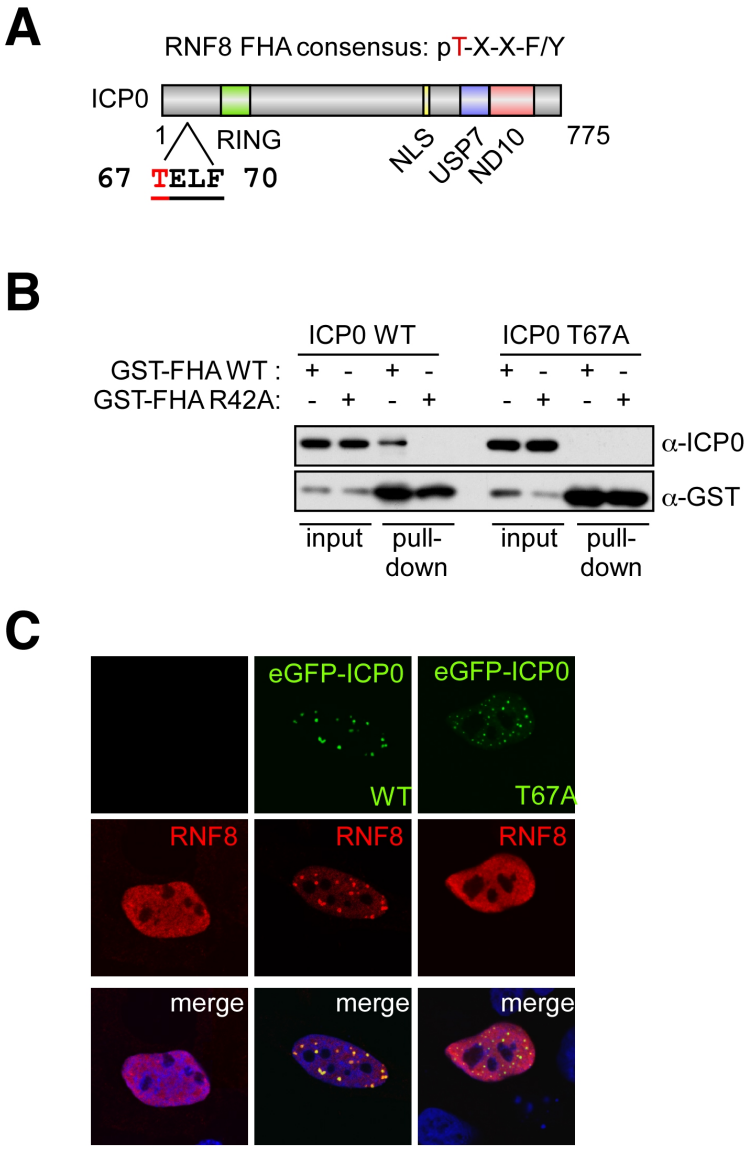

Figure 3-6. ICP0 T67 is required for interaction with the RNF8 FHA domain. A. Schematic of ICP0 domain organization with RNF8 consensus motif. **B.** eGFP-ICP0 or the T67A mutant were transfected into 293T cells and harvested 24 h post transfection. Lysates were incubated with GST-RNF8-FHA or the R42A mutant and Glutathione Sepharose beads, and precipitated proteins were analyzed via SDS-PAGE and immunoblotting. **C.** HeLa cells were co-transfected with Flag-RNF8 and eGFP-ICP0 or the T67A mutant, fixed 24 h post transfection, and processed for immunofluorescence.

and the T67A mutant localized to discrete foci, indicating that the T67A mutation did not alter normal ICP0 localization. In the presence of eGFP-ICP0, Flag-RNF8 was re-localized to ICP0 foci while in the presence of the T67A mutant, Flag-RNF8 remained diffusely nuclear **(Figure 3-6C)**. Together, the immunofluorescence and GST pulldown experiments indicate that ICP0 T67 is required for interaction with the RNF8 FHA domain.

To determine whether the ICP0 T67A mutation affected the ability of ICP0 to degrade RNF8 or RNF168, we co-transfected eGFP-ICP0 or the T67A mutant with Flag-RNF8 or HA-RNF168 into 293T cells and analyzed protein levels 24 h post transfection via SDS-PAGE and immunoblotting. We observed that WT eGFP-ICP0 but not T67A expression resulted in loss of Flag-RNF8 levels **(Figure 3-7A)**. In contrast, both WT eGFP-ICP0 and the T67A mutant were able to degrade HA-RNF168 **(Figure 3-7B)**.

We have previously shown that ICP0 expression blocks 53BP1 recruitment to IRIF due to ICP0-mediated degradation of RNF8 and RNF168 (Weitzman et al., 2010). We thus analyzed the ability of ICP0 T67A to block 53BP1 recruitment to IRIF. We transfected HeLa cells with eGFP-ICP0 or the T67A mutant, exposed cells to 10 Gy IR, and fixed and processed cells for immunofluorescence 1 h post IR. We observed that 53BP1 recruitment to sites of DNA damage was blocked by both WT eGFP-ICP0 and eGFP-ICP0-T67A **(Figure 3-7C)**. This block is likely due to the T67A mutant retaining the ability to degrade RNF168, which is also required for 53BP1 recruitment.

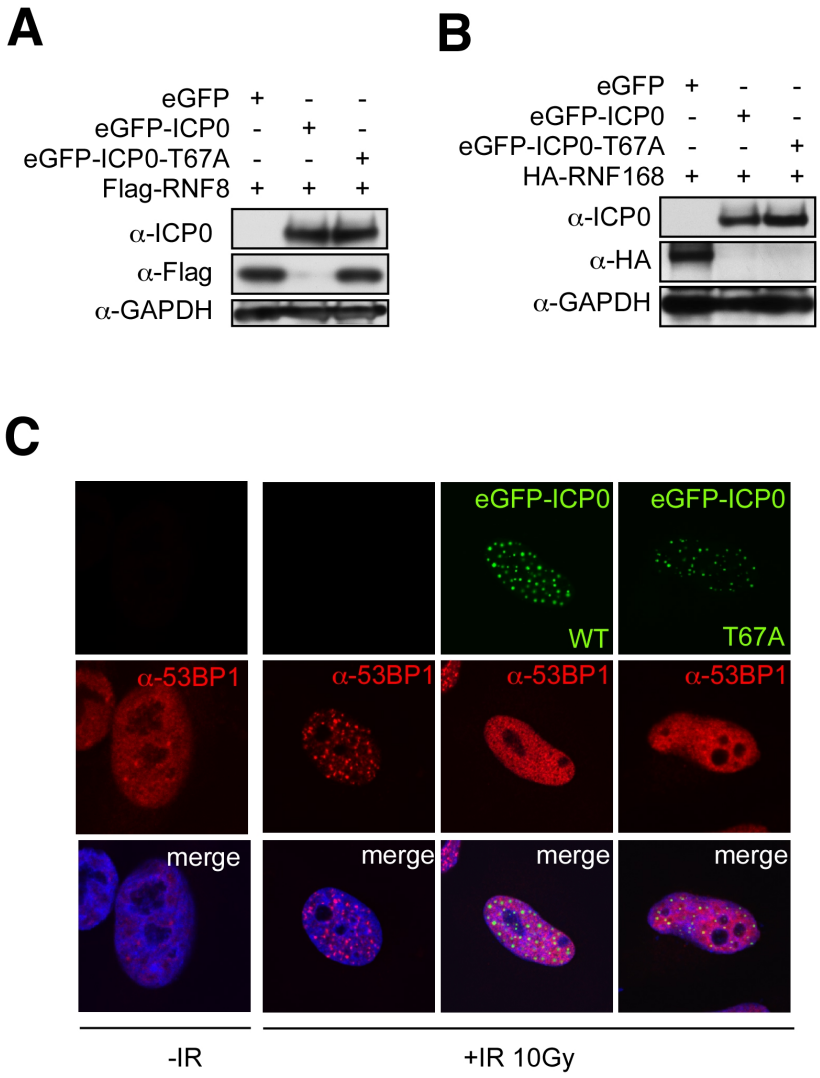

Figure 3-7. ICP0 T67 targets RNF8 and not RNF168. A. ICP0 T67A cannot degrade RNF8. HeLa cells were co-transfected with eGFP-ICP0 or the T67A mutant in 3X excess of Flag-RNF8, harvested 24 h post transfection, and protein levels assessed via SDS-PAGE and immunoblotting. **B.** ICP0 T67A does degrade RNF168. HeLa cells were co-transfected with eGFP-ICP0 or the T67A mutant in 3X excess of HA-RNF168 and processed as in (A). **C.** eGFP-ICP0 blocks 53BP1 recruitment to IRIF. HeLa cells were transfected with eGFP-ICP0 or the T67A mutant, irradiated (10 Gy) 24 h post transfection, and fixed and processed for immunofluorescence 1 h post IR.

Combined, these observations indicate that ICP0 T67A targets RNF8 but not RNF168 for degradation, demonstrating the mechanisms of ICP0-mediated degradation of RNF8 and RNF168 are distinct.

Phosphorylation of ICP0 T67 is necessary and sufficient to directly bind the RNF8 FHA domain

To investigate whether phosphorylation of ICP0 T67 directly mediates the RNF8-ICP0 interaction, we purified the untagged RNF8 FHA domain from *E. coli* **(Figure 3-8A)** and used isothermal calorimetry to measure the binding affinity of synthetic ICP0 peptides to the FHA domain. A peptide containing phosphorylated T67 bound the RNF8 FHA domain **(Figure 3-8B)**, whereas an unphosphorylated peptide of the same sequence did not **(Figure 3-8C)**. The interaction was prevented when the FHA domain contained the R42A mutation **(Figure 3-8D)**. We measured the dissociation constant to be 816 nM, which is comparable to those observed for the TQXF motifs in Mdc1 (3.1 μM to 11.7 μM) (Huen et al., 2007). Thus we concluded that phosphorylation of T67 was both sufficient and necessary for interaction with the RNF8 FHA domain.

ICP0 T67 is phosphorylated in cells

Our observations thus far point to a direct interaction between the RNF8 FHA domain and ICP0 pT67. To demonstrate that ICP0 T67 is indeed phosphorylated in cells and identify kinases mediating this phosphorylation, we generated antibodies

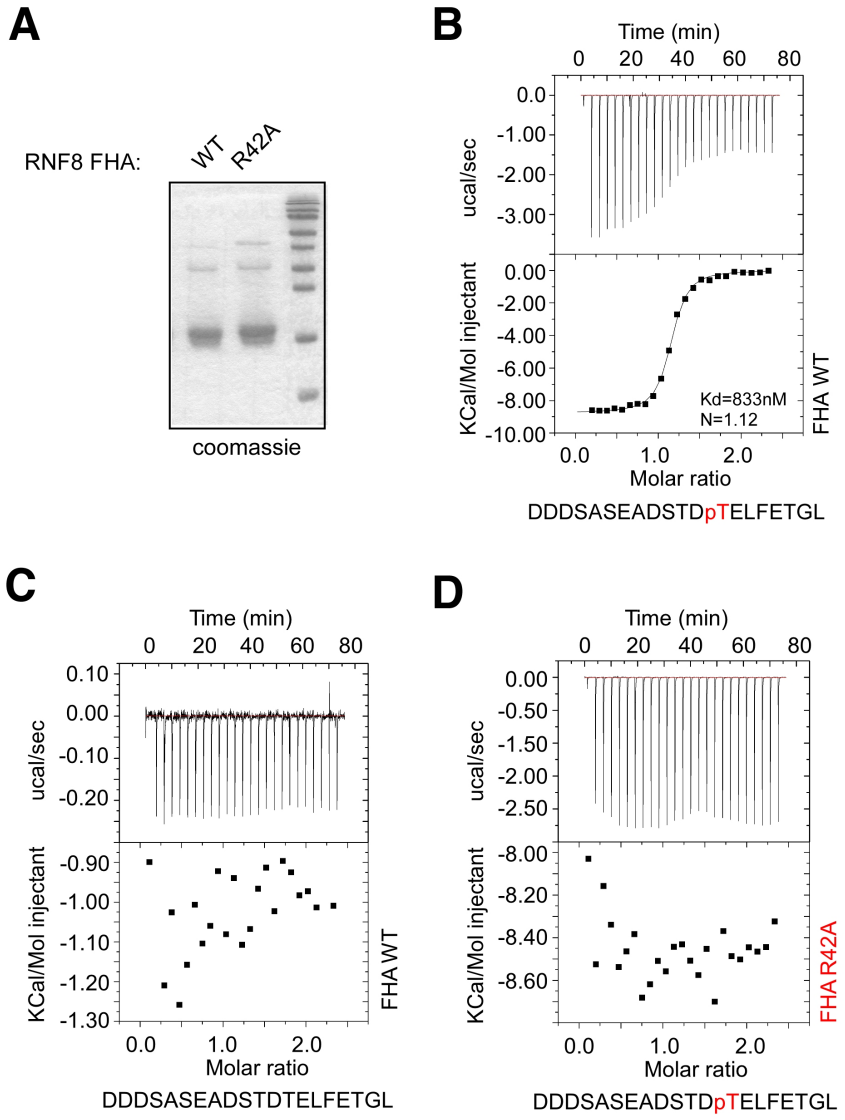

Figure 3-8. Phosphorylated ICP0 T67 is necessary and sufficient to bind directly to the RNF8 FHA domain. A. The untagged RNF8 FHA domain and R42A mutant were purified from E. coli and analyzed by SDS-PAGE and coomassie staining. **B.** Peptides comprising the ICP0 T67 region were synthesized and binding of the peptides to RNF8 FHA domain were analyzed by isothermal calorimetry. Phosphorylation of T67 was sufficient to bind the RNF8 FHA domain. **C.** Unphosphorylated T67 peptide did not bind the FHA domain. **D.** Phosphorylated T67 peptide could not bind the RNF8 FHA R42A mutant.

specific for the phosphorylated T67 residue of ICP0. We synthesized a peptide containing the pT67 region of ICP0, which was used to immunize rabbits and generate antibodies recognizing pT67. Antibodies specific for pT67 were purified from rabbit sera by first passing the sera over beads conjugated to nonphosphorylated T67 peptide, eliminating T67 region antibodies not specific for T67 phosphorylation. The flowthrough was then passed over a pT67 peptide column and bound antibodies were eluted **(Appendix Figure A-3)**. To test whether this purified fraction was specific for pT67, peptides were spotted onto nitrocellulose membranes and subject to immunoblotting using antibodies purified over both columns (α-pT67), or antibodies purified over unphosphorylated T67 peptide (α-T67 total). The α-T67 total antibodies recognized both unphosphorylated and T67 phosphorylated peptide while the α-pT67 antibodies only recognized the phosphorylated peptide **(Figure 3-9A)**.

We next used these antibodies to determine whether ICP0 was phosphorylated at T67 in cells. eGFP-ICP0 or the T67A mutant were transfected into 293T cells and immunoprecipitated using α-GFP antibodies. The α-pT67 antibodies recognized WT eGFP-ICP0 protein but failed to recognize the T67A mutant **(Figure 3-9B)**. Combined, these observations indicate that ICP0 is phosphorylated on T67 in cells.

CK1 phosphorylates ICP0 T67 to facilitate interaction with RNF8

Bioinformatic analysis of the ICP0 T67A region indicated the presence of high probability consensus sites for the cellular CK2 and CK1 kinases, which phosphorylate Ser and Thr residues in acidic regions. To determine whether these

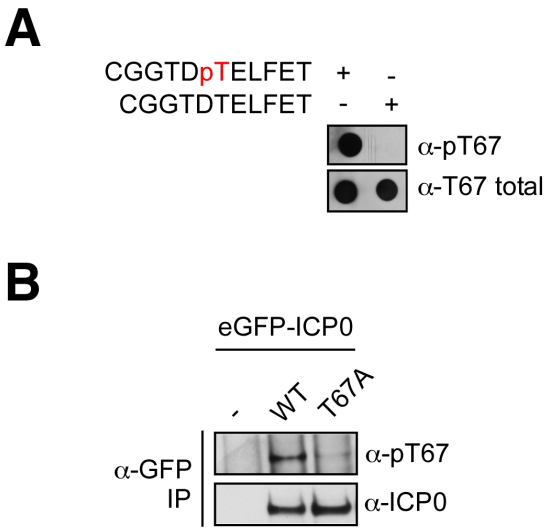

Figure 3-9. ICP0 T67 is phosphorylated in cells. A. α-pT67 antibodies were purified from rabbits immunized with the ICP0 pT67 peptide. Sera were purified over unphosphorylated T67 peptide columns to eliminate antibodies that were not phosphorylation-specific. The flowthrough was then purified over pT67 peptide columns. Antibodies eluted from the unphosphorylated column (a-T67 total) recognized both phosphorylated and unphosphorylated T67 peptide. Antibodies eluted from the pT67 column recognized only the pT67 peptide. **B.** ICP0 is phosphorylated at T67 in cells. eGFP-ICP0 or the T67A mutant were transfected into 293T cells, harvested 24 h post transfection, and immunoprecipitated using a-GFP antibodies. Immunoprecipitated proteins were analyzed by SDS-PAGE and immunoblotting.

kinases could catalyze phosphorylation of T67 *in vitro* we expressed and purified GST-ICP0 containing the N-terminal 241 amino acids (GST-241) from *E. coli*. We also purified mutants at several predicted phosphorylation sites, including T67A, S58/60/64A, and S36/37/39A. We incubated recombinant, purified rat CK1 (δ isoform) or human CK2α/β holoenzyme with purified GST-241 or the T67A mutant in the presence of ATP and analyzed the reaction products via SDS-PAGE and immunoblotting. We observed that CK1 but not CK2 could phosphorylate GST-241 at T67. The GST-241-T67A mutant was not phosphorylated by either CK1 or CK2, providing further evidence that the phosphorylation was specifically on T67 **(Figure 3-10A)**.

While CK1 can phosphorylate Ser and Thr residues in acidic regions, there exists a distinct preference for a priming phosphorylation in the -3 position of the targeted residue (Flotow et al., 1990; Flotow and Roach, 1991). ICP0 encodes three Ser residues directly upstream of T67: S58 (-8), S60 (-6), and S64 (-3), and these are conserved in ICP0 from HSV-2. We analyzed whether mutation of these residues affected the ability of CK1 to phosphorylate ICP0 T67. *In vitro* phosphorylation reactions were carried out as described above, using GST-241 and T67A or S58/60/64A mutants and analyzed at 5 min intervals between 0 and 20 min. We observed robust CK1-mediated T67 phosphorylation on GST-241 but not the T67A or S58/60/64A mutants **(Figure 3-10B)**. To test the relevance of these observations on RNF8 interaction, we first examined whether CK1-mediated phosphorylation of GST-241 facilitated interaction with Flag-RNF8 expressed in lysates. Flag-RNF8 or the

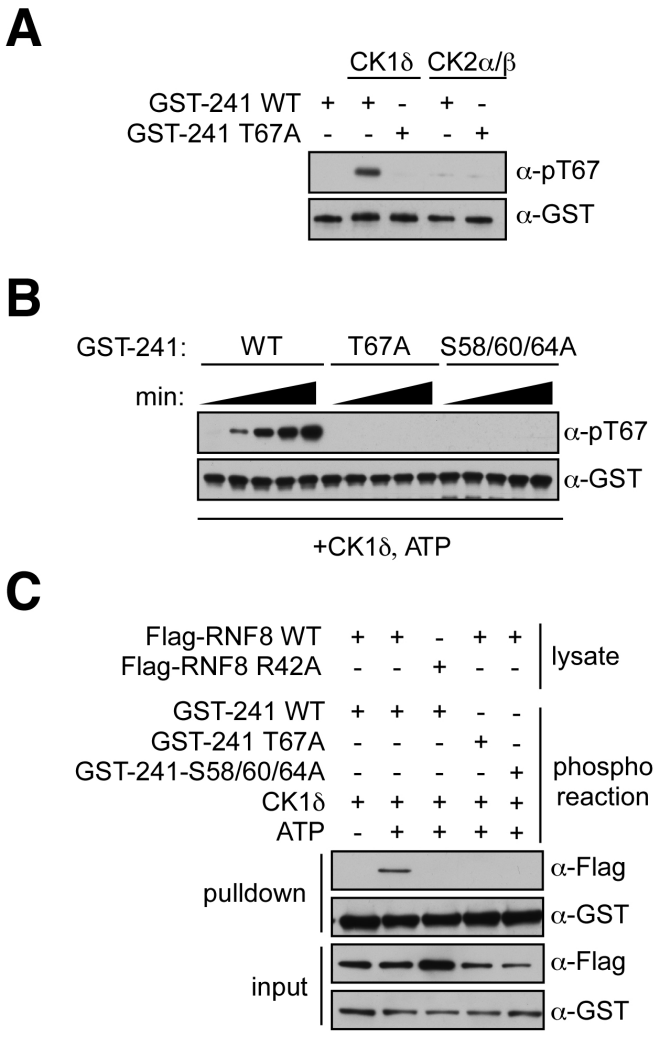

Figure 3-10. The cellular CK1 kinase can phosphorylate ICP0 T67. **A.** CK1 but not CK2 phosphorylates ICP0 T67. GST-241 or the T67A mutant were phosphorylated *in vitro* with recombinant rat CK1δ or CK2α/β holoenzyme. Reaction products were analyzed via SDS-PAGE and immunoblotting. **B.** Upstream Ser residues are required for CK1 phosphorylation of T67. GST-241 or the indicated mutants were phosphorylated in vitro by CK1δ. Reactions were quenched at 5 min intervals from 0 to 20 minutes and analyzed by SDS-PAGE and immunoblotting. **C.** CK1 phosphorylation facilitates RNF8 interaction with ICP0. Flag-RNF8 or the R42A mutant were transfected into 293T cells, harvested 24 h post transfection, and used in GST-pulldown assays. GST-241 or the indicated mutants were phosphorylated in vitro with CK1 before pulldown.

R42A mutant were transfected into 293T cells and harvested 24 h post transfection. Lysates were incubated with GST-241 or the T67A mutant and Glutathione Sepharose beads, and precipitated proteins were analyzed via SDS-PAGE and immunoblotting. The unphosphorylated GST-241 protein was unable to retrieve Flag-RNF8 from lysates but did interact after phosphorylation by CK1, and this was dependent on RNF8 R42. We also observed that GST-241-T67A and S58/60/64A mutants could not retrieve WT Flag-RNF8 from lysates even after phosphorylation by CK1 **(Figure 3-10C)**. Combined, these observations indicate that the upstream Ser residues in the ICP0 T67 region contribute to CK1-mediated phosphorylation of ICP0 T67. In these experiments it is likely that CK1 is catalyzing its own priming phosphorylation *in vitro*, though bioinformatic analysis indicates that these Ser residues are much higher probability CK2 consensus sites. Consistent with these observations, both CK1 and CK2 appear to be able to catalyze phosphorylation at S58, S60, and/or S64 *in vitro* **(Figures 3-11A and 3-11B)**.

ICP0 S64 is required for T67 phosphorylation

Given that S64 is located in the -3 position of T67, we hypothesized that this was the specific residue required for priming T67 phosphorylation in cells. To test this, we used mammalian expression plasmids encoding the first 241 amino acids of ICP0 fused to a nuclear localization signal (ICP0-nls241) and generated T67A and S64A mutants via site-directed mutagenesis. WT, T67A, or S64A constructs were transfected into 293T cells and phosphorylation of T67 was analyzed via SDS-PAGE

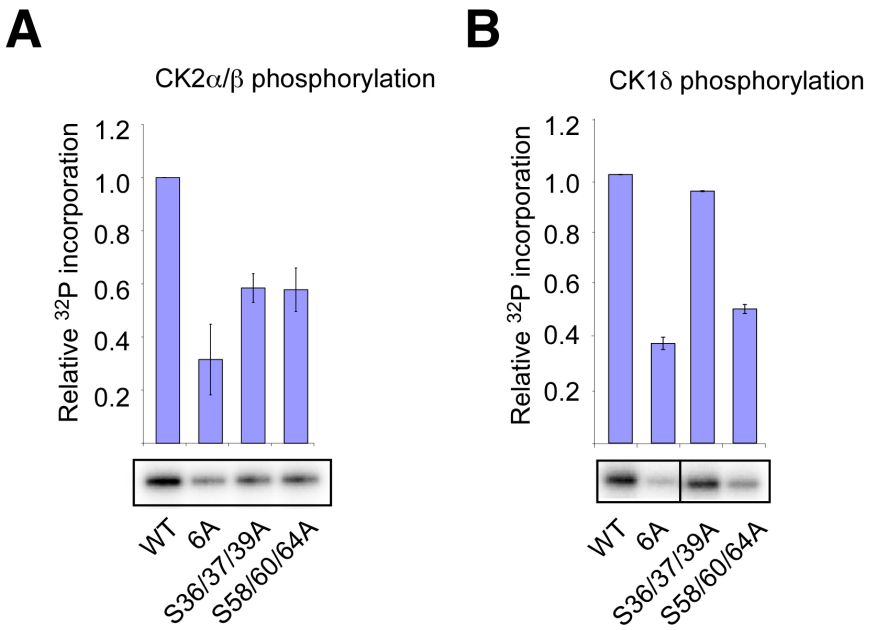

Figure 3-11. CK2 and CK1 can phosphorylate S58, S60, and/or S64. A. Recombinant GST-241 protein or mutants thereof were incubated with CK2α/β holoenzyme and γ^{32}P-ATP. Reaction products were separated by SDS-PAGE and exposed on a phosphorimager. Signal intensities were quantified using MultiGauge v. 3.1. Values are represented as signal intensities relative to WT, and error is SEM of three independent experiments. **B.** Recombinant GST-241 protein or mutants thereof were incubated with CK1δ and γ^{32}P-ATP. Reaction products were analyzed as in **(A)**. Dividing lines indicates non-adjacent lanes of the same gel, exposure, and image.

and immunoblotting. We observed phosphorylation of WT ICP0-nls241 but not the T67A or S64A mutants **(Figure 3-12A)**.

We next used GST-pulldown assays with S58A, S60A, and S64A mutants of ICP0-nls241 in order to dissect the individual contributions of these Ser residues to the RNF8-ICP0 interaction. We expressed ICP0-nls241 or mutants thereof in 293T cells and harvested cells 24 h post infection. Lysates were prepared and incubated with purified recombinant GST-RNF8-FHA protein or R42A mutant protein. We observed that GST-RNF8-FHA was able to retrieve ICP0-nls241 WT, S58A, and S60A from lysates whereas T67A and S64A mutants did not interact **(Figure 3-12B)**. We thus conclude that ICP0 S64 is required as a priming phosphorylation site for CK1-mediated phosphorylation of T67 in cells, whereas S58 and S60 are dispensible.

Relevance of the ICP0 T67A mutation during HSV-1 infection

To determine the role of ICP0 T67 during HSV-1 infection, we constructed HSV-1 virus containing the T67A mutation in ICP0. We used an ICP0-deleted mutant of HSV-1 strain KOS which encodes LacZ under control of the ICP0 promoter at the ICP0 locus (7134, (Cai and Schaffer, 1989), denoted here as ΔICP0). We generated a T67A mutation in ICP0 in a plasmid encoding flanking regions of the ICP0 locus and recombined this plasmid into HSV-1 by co-transfecting the plasmid with purified HSV-1 ΔICP0 DNA into U2OS cells. As a control, we recombined WT ICP0 into the ΔICP0 virus. Recombined viruses were identified as clear plaques when stained with X-gal, isolated, and purified. Presence of ICP0 and the T67A mutation was confirmed

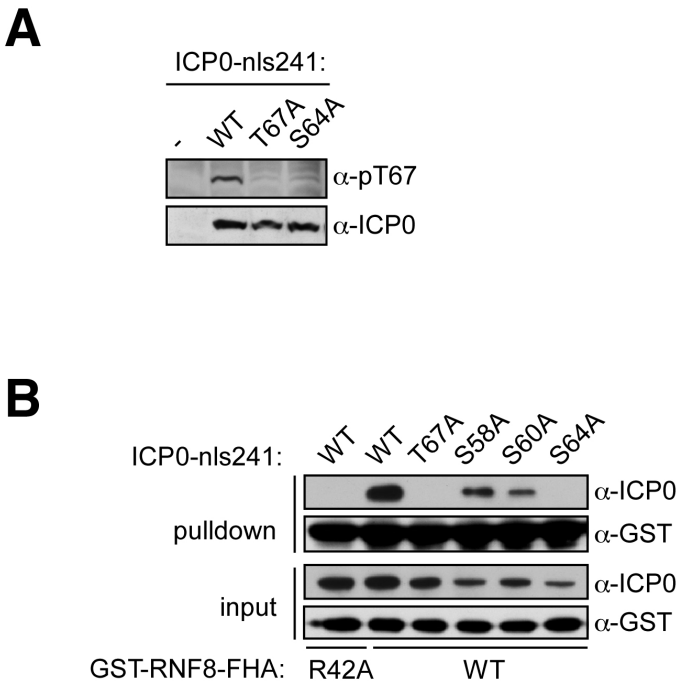

Figure 3-12. S64 is required for T67 phosphorylation in cells. A. S64 is required for T67 phosphorylation in cells. ICP0 nls241 or the indicated mutants were tranfected into 293T cells, harvested 24 h post transfection, and analyzed by SDS-PAGE and immunoblotting. **B**. ICP0 S64 is required for ICP0 interaction with RNF8. ICP0 nls241 or the indicated mutants were transfected into 293T cells, harvested 24 h post transfection and used in GST pulldown assays with GST-RNF8-FHA. Precipitated proteins were analyzed via SDS-PAGE and immunoblotting.

by purifying the DNA synthesized during infection, amplifying the ICP0 T67 region of the viral genome via PCR, and sequencing the PCR product.

We tested the ability of this virus to degrade previously identified targets of ICP0. HeLa cells were infected with WT, ΔICP0, or T67A HSV-1 at MOI=3 and collected at 2 h intervals from 0 to 8 h post-infection. We observed decreased expression of ICP0 targets including DNA-PKcs, RNF168, and RNF8 over the course of WT HSV-1 infection. During infection with T67A virus, RNF8 levels were comparable to infection with ΔICP0 virus, while DNA-PKcs and RNF168 were still degraded **(Figure 3-13A)**. These observations indicate that T67 is required to target RNF8 for degradation during HSV-1 infection, while the other substrates tested in this experiment are targeted via different mechanisms.

As demonstrated in Chapter 2, we have observed that early transcription events during HSV-1 infection are repressed by RNF8. We examined whether the ICP0 T67A virus, which does not degrade RNF8 during infection, was transcriptionally repressed during early stages of infection as compared to WT HSV-1. HFFs were infected with WT, T67A, or ΔICP0 HSV-1 and harvested at 2, 4, and 6, h post infection. RNA was isolated, reverse transcribed, and transcript levels were measured using qPCR with primers targeted to the ICP27 transcript. We observed that at 2 hpi there was no significant difference between transcript levels in WT and T67A virus, but transcription from the ΔICP0 virus was repressed approximately 10-fold. At 4 and 6 hpi, transcripts of the T67A virus steadily decreased compared to WT virus **(Figure 3-13B)**. This pattern mirrored that of the ΔICP0 virus, which also became more

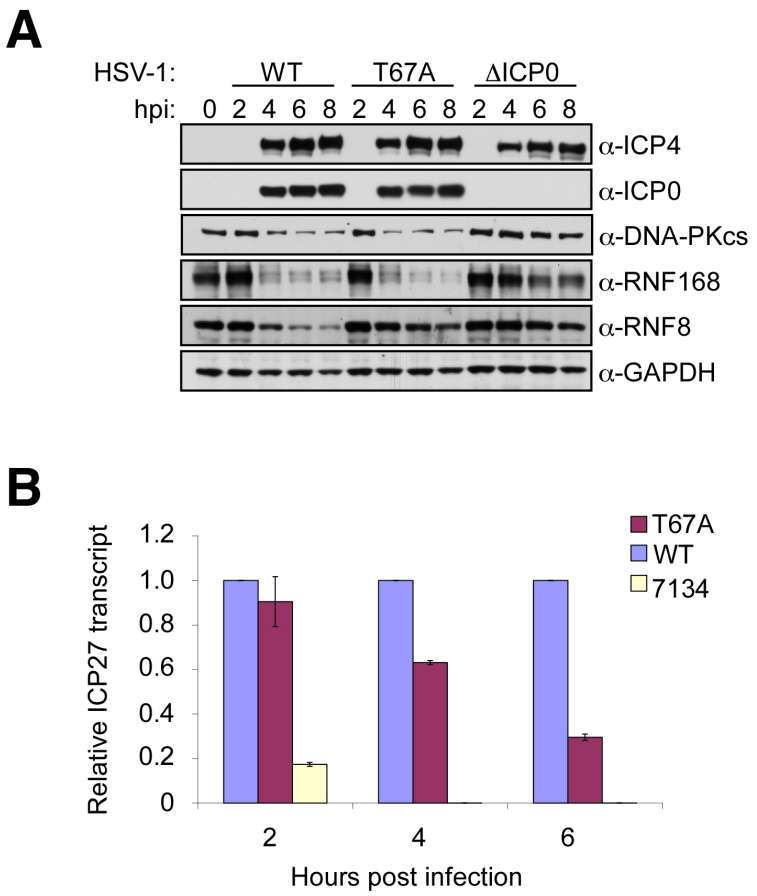

Figure 3-13. Analysis of HSV-1 virus containing the ICP0 T67A mutation. A. HSV-1 ICP0 T67A virus does not degrade RNF8 during infection. WT and mutant versions of HSV-1 strain KOS were used to infect HeLa cells at MOI=3. Cells were harvested at the indicated timepoints and protein levels were analyzed by SDS-PAGE and immunoblotting. **B.** HFF cells were infected with WT, T67A, or ΔICP0 (7134) versions of HSV-1 strain KOS at MOI=0.01 and harvested at the indicated timepoints. RNA was isolated, reverse transcribed, and quantified via qPCR with primers targeted to the immediate early ICP27 transcript.

repressed over the timecourse though to a greater extent. We anticipate that this repression is due to the inability of ICP0 T67A to target RNF8 for degradation, although the contribution of other repressive cellular factors targeted though ICP0 pT67 cannot be ruled out.

ICP0 T67 can bind other cellular FHA domain proteins

In order to determine whether ICP0 pT67 can indeed target other FHA-domain containing proteins, we synthesized biotinylated peptides comprising the T67 region of ICP0. We used unphosphorylated peptide or peptides phosphorylated at T67 (pT67), S64 (pS64), or S64 and T67 (pS64/pT67) to precipitate cellular proteins from 293T lysates via Streptavidin Sepharose beads, and co-purifying proteins were analyzed via SDS-PAGE and silver staining. The pT67 and pTS64/pT64 peptide pulldowns contained unique bands at approximately 60 kDa and 102 kDa **(Figure 3-14A)**. We analyzed proteins co-purifying with unphosphorylated and pT67/S64 peptides via mass spectrometry analysis and identified several hundred proteins that co-purified uniquely with pT67/S64. Among these were three FHA domain proteins: Chk2, Nbs1, and FOXK2 **(Figure 3-14B)**. To dissect the individual contributions of pS64 and pT67 to the interactions, as well as confirm the mass spectrometry results, we repeated the peptide pulldowns and analyzed precipitated proteins by SDS-PAGE and immunoblotting. In all cases, the unphosphorylated and pS64 peptides did not pull down the FHA domain proteins, whereas pT67 and pS64/p67 peptides did **(Figure S-14C)**. The absolute dependence on pT67 suggests that FHA domains are

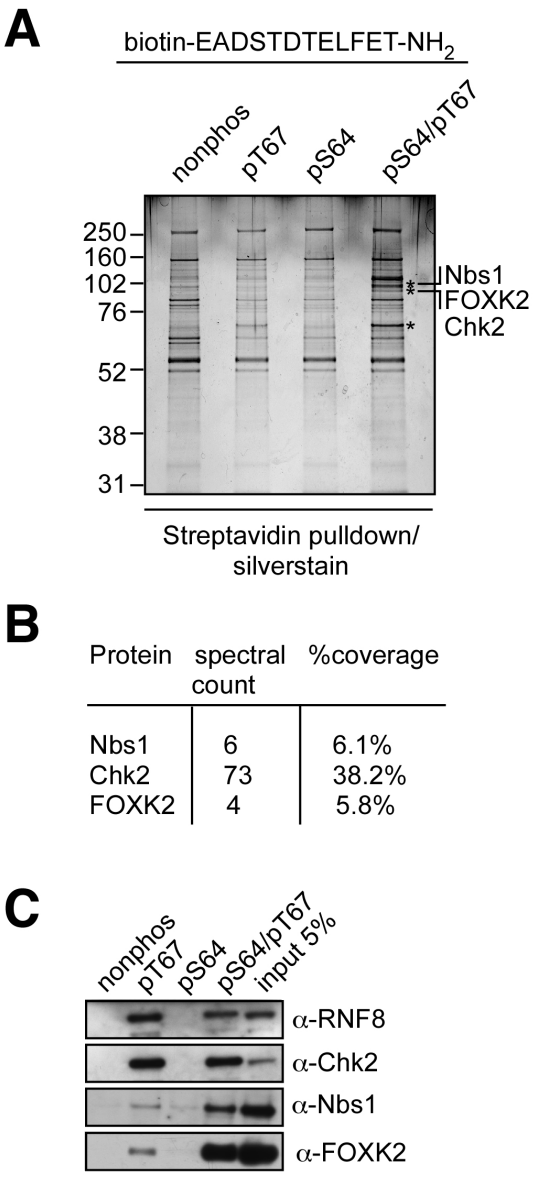

Figure 3-14. ICP0 pT67 can interact with other cellular FHA domain proteins. A. The indicated ICP0 peptides were biotinylated and used to precipitate proteins from 293T lysates via streptavidin sepharose beads. Purifications were analyzed via SDS-PAGE and silver staining. **B.** Co-purifying proteins were identified by mass spectrometry. Three FHA domain proteins identified are listed with number of spectra observed. **C.** Mass spectrometry results were confirmed by SDS-PAGE and immunoblotting.

mediating interaction with these proteins. The ability of ICP0 to interact with such diverse FHA domains may be because it encodes a hybrid sequence, containing elements characteristic of Nbs1, FOXK2, and RNF8 FHA consensus regions (**Figure 3-15**; see discussion for more details). Thus HSV-1 encoding the ICP0 pT67 region may be a generalized strategy to target FHA domains functioning in pathways relevant to the viral life cycle.

Discussion

The studies described here demonstrate that ICP0 has evolved a short linear motif, STD(p)TELF, to mimic a cellular phosphosite normally catalyzed on Mdc1 by ATM after DNA damage. ICP0 uses this motif to induce phosphorylation via the cellular CK1 kinase, bind the RNF8 FHA domain, and redirect it for ubiquitylation and proteasome-mediated degradation. We demonstrate that phosphorylation of ICP0 T67 is necessary and sufficient to bind directly to the RNF8 FHA domain both *in vitro* and in cells, and that this targeting mechanism is distinct from ICP0-mediated degradation of RNF168 and other previously described substrates. The significance of this targeting is highlighted by reduced viral transcription from HSV-1 containing the T67A mutation in ICP0, which cannot induce RNF8 degradation during infection. These observations indicate that ICP0 pT67 functions to counteract cellular attempts to repress transcription from the viral genome. Furthermore, it appears that ICP0 can bind other FHA domain proteins via pT67, implicating this targeting mechanism as a

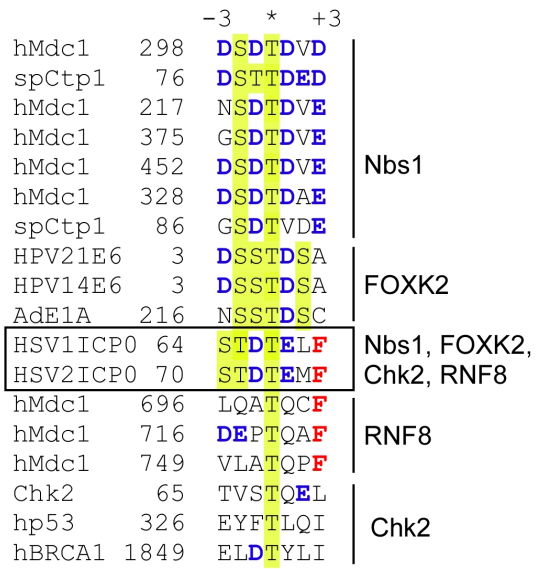

Figure 3-15. The short linear motif encoded by ICP0 contains sequences characteristic of other FHA domain consensus sequences. Sequence alignment of the pT-3 to pT+3 positions of sequences previously shown to bind FHA domains of the indicated proteins (right column), either *in vitro* or *in vivo*. pThr is indicated by an asterisk. Acidic amino acids are in blue, Ser and Thr highlighted in yellow, and Phe conforming to the RNF8 FHA consensus is in red. HSV-1 and HSV-2 ICP0 sequences are boxed and share characteristics of Nbs1, FOXK2, and RNF8 FHA consensus sequences.

broader viral strategy to modulate cellular pathways at key regulatory nodes **(summarized in Figure 3-16)**.

While ICP0 mimics Mdc1-like short linear motifs conforming to the RNF8 FHA binding consensus, it is interesting to note that the subtle differences between the Mdc1 and ICP0 sequences lead to distinct phosphorylation mechanisms. Specifically, the presence of Glu instead of Gln at pT+1 and the presence of Ser at pT-3 lead to loss of the ATM phosphoryation site (TQ) and induction of a CK1 site (pSXXT) for ICP0 T67. A key difference between ATM and CK1 is that while ATM normally exists as an inactive dimer in cells (Bakkenist and Kastan, 2003), CK1 is a constitutively active kinase and therefore is available to be recruited by ICP0 upon protein synthesis, without the requirement for upstream signaling events. While it has been demonstrated that ATM is activated upon lytic HSV-1 infection, this activation requires the formation of pre-replicative sites or the onset of viral replication (Lilley et al., 2005; Wilkinson and Weller, 2004). ICP0 is most important during the earliest stages of infection, before the onset of viral replication, at a time when ATM may not be fully activated.

The second reason that ICP0 may have evolved the presence of Glu instead of Gln at pT+1 is that this more closely conforms to the consensus sequences recognized by the Nbs1 and FOXK2 FHA domains, which appear to recognize similar consensus sequences **(Figure 3-15)**. The Nbs1 FHA domain binding sites on Mdc1 and *S. pombe* (sp) Ctp1 contain a conserved Asp at pT+1, and in the case of spCtp1, structural data support the primary involvement of this residue in the interaction

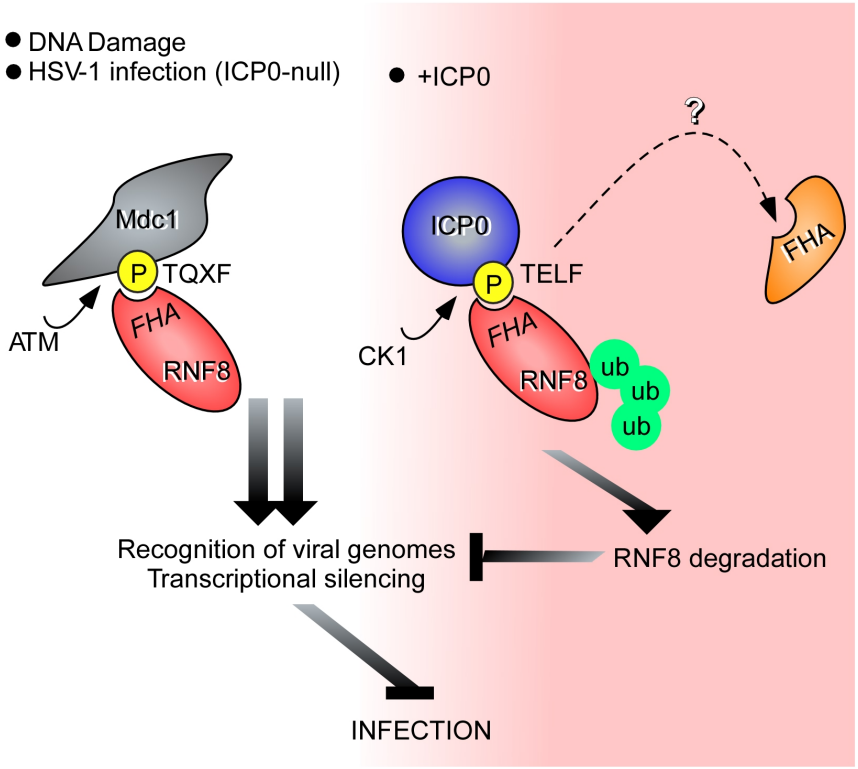

Figure 3-16. ICP0 mimicking of cellular phosphosites targets cellular FHA domain proteins, promoting viral infection. The parallels between RNF8-Mdc1 interaction during the DNA damage response (or as induced upon HSV-1 infection in the absence of ICP0) and RNF8-ICP0 interaction during HSV-1 infection are shown, highlighting and comparing the short linear motifs on both Mdc1 and ICP0. These motifs use distinct mechanisms to catalyze phosphorylation, but are both able to use the induced phosphorylation to target RNF8. Also depicted are consequences for the virus and the possibility that ICP0 can use this mimicking to target other cellular pathways coordinated by FHA domain proteins.

(Williams et al., 2009). The recent observation that FOXK2, a forkhead transcription factor, binds Ad E1A and HPV E6 proteins (Komorek et al., 2010) indicates that it might be a common target among DNA viruses. The sequences on the viral proteins that are involved in binding the FOXK2 FHA domain possess Asp at pT+1 as well **(Figure 3-15)**.

Chk2 was by far the most abundant protein in the pT67 and pS64/pT67 pulldowns, yet compared to Nbs1, RNF8, and FOXK2, its FHA recognition sequence is the most distinct and bears little resemblance to the sequence encoded by ICP0 **(Figure 3-15)**. These observations suggest either the interaction is not mediated through the FHA domain of Chk2 or that the Chk2 FHA consensus may be more flexible than previously observed. Though Nbs1 levels appear constant during HSV-1 infection indicating Nbs1 is not an ICP0 degradation target (Lilley et al., 2005), we have observed Nbs1 to interact with the full-length ICP0 protein and increased ubiquitylation of Nbs1 in the presence of ICP0 (see Chapter 4). It is possible that ICP0-mediated, non-degradative ubiquitylation may affect protein function in this case. Future studies will be needed to fully elucidate the binding interfaces involved in these interactions as well as the potential contribution of these interactions to HSV-1 infection.

Though the studies presented here did not address the mechanism of RNF168 targeting by ICP0, our data indicate that it is clearly not targeted through pT67, consistent with the fact that RNF168 does not contain FHA or other phospho-binding domains. RNF168 loss in the presence of ICP0 does not appear to be an indirect

consequence of the RNF8 degradation, as RNF168 levels do not change in RNF8 knockdown cells. Thus ICP0 likely directly targets RNF168 for degradation. Interactions between two RING domain E3 ligases can be orchestrated through RING-RING interactions, as has been described in the case of BARD/BRCA (Brzovic et al., 2001) and Bmi1/RING1b (Buchwald et al., 2006). However, we have not been able to detect an interaction using purified GST-ICP0-241, which includes the RING domain, and RNF168 in GST-pulldown assays. It is also possible that, like RNF8, post-translational modifications of ICP0 or RNF168 are required. RNF168 contains two MIU domains and ICP0 is heavily autoubiquitylated in cells. Thus the interaction may be mediated through RNF168 MIU recognition of ubiquitin chains on ICP0. Conversely, ICP0 has recently been described to bind SUMO via several SIM-like sequences, and SUMOylation of RNF168 may play a role.

Viruses have compact genomes and must maximize the number of functions that can be executed by a protein through a minimal number of residues. Short linear motifs therefore provide an ideal strategy for viruses as they are encoded by few amino acids and can be generated via the induction of point mutations. Cellular proteins commonly employ short linear motifs to mediate protein-protein interactions, often via post-translational modifications. These motifs can act as binding sites to nucleate signaling and regulatory networks. These critical points of interaction make the networks vulnerable to viral proteins that aim to inactivate or subvert intrinsic host defense systems. Our data reveal a novel example of motif mimicry by a viral ubiquitin ligase to target substrates through a recognition motif prevalent amongst

DDR proteins. Since many viruses intersect with the cellular DDR machinery, there are likely to be other conserved examples of viral proteins that have evolved to exploit the phospho-dependent interactions that are a cornerstone of this signaling cascade. This creative targeting mechanism provides a combinatorial strategy for viral factors to target numerous cellular proteins as the virus hijacks fundamental cellular processes.

Materials and Methods

Plasmids and Transfections

RNF8 fragments and mutants were generated by PCR amplification of RNF8 from pcDNA4/TO-Flag-RNF8 (Mailand et al., 2007) or Quikchange mutagenesis (Stratagene) of RNF8 and inserted into pcDNA3.1(+) using the *Xho1* restriction site. To construct TAP-ICP0 the CMV promoter and a TAP tag consisting of a calmodulin-binding peptide and streptavidin-binding peptide were excised from pNTAP (Stratagene) using *AseI* and *BglI* and inserted into pEGFP-ICP0 between the same sites. mRFP was excised from pcDNA3.1(+) and inserted into pNTAP using *EcoRI*. For bacterial expression, RNF8 WT or C403S were excised from pcDNA4/TO and cloned into pET28a between *EcoRI* and *XhoI*. His-MBP-RNF8-FHA was from M. Yaffe and the R42A mutant was generated by Quikchange mutagenesis (Stratagene). Plasmids encoding eGFP-ICP0, ICP0-nls241, and GST-ICP0-241 were from R. Everett and C. Boutell (Boutell et al., 2002) and all point mutants thereof were generated via Quikchange mutagenesis (Stratagene). HA-RNF168 and GST-RNF8-

FHA plasmids were from D. Durocher. Transfections were performed as described in Chapter 2.

Antibodies

Primary antibodies were purchased from Cell Signaling Technologies (GST), Clontech (GFP), and as described in the Methods section of Chapter 2. The RNF8 antibody was from J. Lukas and RNF168 antibody was from D. Durocher. Phosphorylated T67 antibodies were generated using a peptide (CGGTDpTELFET-NH_2) synthesized at the Salk Peptide Synthesis Core and KLH conjugated and injected at Pocono Rabbit Farm and Laboratory. Purification columns were prepared by coupling the peptides, via N-terminal cysteine residues, to Sulfolink resin (Pierce) according to the manufacturer's protocol. Rabbit sera were diluted 1:3 in 1X PBS, purified over an unphosphorylated T67 peptide column to eliminate antibodies specific for the unphosphorylated form of the peptide, and the flowthrough was then purified over the phosphorylated T67 peptide column. Antibodies were eluted using 0.1 M Glycine, pH=2.5, and neutralized in 1 M Na_2HPO_4, pH=9. All secondary antibodies were from Jackson Laboratories. Immunofluorescence and immunoblotting were performed by standard methods.

Viruses and infections

Mutant HSV-1 encoding ICP0 with the T67A mutation was created by recombination into the ICP0 null virus 7134 (Cai and Schaffer, 1989), which encodes

lacZ in place of the ICP0 coding sequence. Infectious 7134 viral DNA was co-transfected via calcium phosphate into U2OS cells with linearized WT or T67A ICP0 in a shuttle plasmid containing genomic sequences flanking ICP0 (p111, (Everett, 1987)) to facilitate homologous recombination. 5 days post transfection, cells were harvested, freeze-thawed, and samples were plated on HFFF cells. Two days post-plating, plaques were stained with X-Gal (5-bromo-4-chloro-3-indolyl-β-d-galactopyranoside). ICP0-containing recombinants were identified as clear plaques, isolated and plaque purified until no blue plaques were detectable. Viral DNA was extracted from pure plaque isolates, and incorporation of the T67A mutation into the viral genome was confirmed by PCR amplification and sequencing of the ICP0 T67 region. Viruses were propagated, titered, and used for infections as described in Chapter 2.

GST pulldowns

ICP0 or RNF8 and mutants thereof were expressed in 293T cells and harvested 24h post-transfection. Cells were lysed in GST lysis buffer (20 mM Tris-HCl (pH 8.0), 200 mM NaCl, 1x protease inhibitors (Roche), 2 mM PMSF, and 0.5% NP-40). 500 μg lysate was incubated with 10μg GST-RNF8-FHA or GST-ICP0-241 and mutants thereof, and 20 μl Glutathione-Sepharose (Clontech) in 500 μl total volume for 2 h at 4^{o}C. Where indicated, 100 U CIP and/or 200 mM sodium orthovanadate was added to the lysate and incubated for 30 min at 30^{o}C prior to pulldown. For *in vitro* phosphorylation of GST-ICP0-241 before pulldown, 10 μg protein was incubated

with 1000 U rat CK1δ (NEB) for 30min at 30°C in a 20 μl reaction containing 50 mM Tris pH 7.5, 10 mM $MgCl_2$ and 5 mM DTT, with or without ATP (10mM). The entire phosphorylation reaction was added to the pulldown. Proteins were eluted in 2X SDS-PAGE loading dye, boiled, and analyzed via SDS-PAGE and immunoblotting.

Isothermal Calorimetry

RNF8-FHA WT and R42A proteins were buffer matched over a NAP-5 column (GE Healthcare) into ITC buffer (25 mM Tris-HCl pH 8.0, 200 mM NaCl). Peptides (DDDSASEADSTDTELFETGL or DDDSASEADSTDpTELFETGL) were synthesized at the Hartwell Center at St. Jude Children's Research Hospital. 0.4 μl of peptide solutions (1.2 mM in ITC buffer) were injected into a sample cell containing 0.1 mM RNF8-FHA domain. Measurements were performed on a Microcal ITC200 and binding isotherms were plotted and analyzed using Origin (v7.0).

***In vitro* ubiquitylation**

Human ubiquitin-activating enzyme (E1) and full-length ICP0 were purified as previously described (Boutell et al., 2002). Ubiquitin was purchased from Sigma. Clones expressing recombinant UbcH5a, RNF8-C403S (lacking E3 ligase activity), or RNF8-C403S/R42A were expressed in BL21 and purified by nickel affinity chromatography. *In vitro* ubiquitylation assays were performed in the presence of 50 ng of purified RNF8 in 1x reaction buffer (10 mM Tris–HCl pH 7.0, 10 mM $MgCl_2$, 1 mM dithiothreitol and 5 mM ATP) with 20 ng of E1, 50 ng of E2, 2.5 ug of ubiquitin,

and 50 ng of purified ICP0. Reactions were carried out in a final volume of 10 μl for 1 h at 37°C and terminated by the addition of SDS–PAGE boiling mix buffer containing 8 M urea and 100 mM DTT. The reaction products were analyzed by SDS-PAGE and immunoblotting.

qPCR

All qPCR experiments measuring ICP27 transcription during HSV-1 infection were performed essentially as described in Chapter 2, except HFF cells were used instead of RNF8-/- MEFs.

Affinity purifications

Cells were lysed 24 h post transfection in 500 μl IP buffer (50 mM Tris 7.5, 150 mM NaCl, 1 mM EDTA, 1%NP-40, 2 mM PMSF, 0.5 mM idoacetimide, 0.5 mM NEM, and protease inhibitors). 100 μg protein was incubated with 40 μl Streptavidin–Sepharose beads (GE Healthcare) in 500 μl IP buffer overnight at 4°C. Beads were washed 3 × in IP Buffer and boiled in SDS loading dye. Purified proteins were analysed by immunoblotting.

Peptide pulldowns

Biotinlyated peptides (nonphos: biotin-EADSTDTELFET-NH_2; pT67: biotin-EADSTDpTELFET-NH2; pS64: biotin-EADpSTDTELFET-NH_2; pT67/pS64: biotin-EADpSTDpTELFET-NH_2) were synthesized and conjugated at the Salk Institute

Peptide Synthesis Core. 10 μg peptide was incubated with 60 μl Streptavidin-Sepharose beads (GE Healthcare) and 5 mg cell lysate (20 mM Tris-HCl (pH 8.0), 200 mM NaCl, 1X protease inhibitors (Roche), 2 mM PMSF, and 0.5% NP-40), and rotated for 2 h at 4^{o}C. Beads and precipitated proteins were washed 3X in lysis buffer, boiled in 2X SDS loading dye, separated by SDS-PAGE, and visualized by silver staining. For mass spectrometry analysis, bead-bound proteins were directly denatured, reduced, and digested in trypsin.

Mass spectrometry

Samples were first denatured in 8M urea and then reduced and alkylated with 10 mM Tris(2-carboxyethyl)phosphine hydrochloride and 55 mM iodoacetamide respectively. Samples were then digested over-night with trypsin (Promega) according to the manufacturer's specifications. The protein digests were pressure-loaded onto a 250 micron i.d. fused silica capillary (Polymicro Technologies) column with a Kasil frit packed with 3 cm of 5 micron Partisphere strong cation exchange (SCX) resin (Whatman) and 3 cm of 5 micron C18 resin (Phenomenex). After desalting, this bi-phasic column was connected to a 100 micron i.d. fused silica capillary (Polymicro Technologies) analytical column with a 5 micron pulled-tip, packed with 10 cm of 5 micron C18 resin (Phenomenex). The MudPIT column was placed inline with an 1100 quaternary HPLC pump (Agilent Technologies) and the eluted peptides were electrosprayed directly into an LTQ mass spectrometer (Thermo Scientific). The buffer solutions used were 5% acetonitrile/0.1% formic acid (buffer

A), 80% acetonitrile/0.1% formic acid (buffer B) and 500 mM ammonium acetate/5% acetonitrile/0.1% formic acid (buffer C). A six step MudPIT was run with salt pulses of 0%, 20%, 40%, 70% and 100% buffer C and 90% buffer C/10% buffer B. The 120 minute elution gradient had the following profile: 15% buffer B beginning at 10 minutes to 55% buffer B at 90 minutes to 100% buffer B from 100 minutes to 110 minutes. A cycle consisted of one full scan mass spectrum (400-1600 m/z) followed by five data-dependent collision induced dissociation (CID) MS/MS spectra. Application of mass spectrometer scan functions and HPLC solvent gradients were controlled by the Xcalibur data system (Thermo Scientific). MS/MS spectra were extracted using RawXtract (version 1.9.9) (McDonald et al., 2004). MS/MS spectra were searched with the Sequest algorithm (Eng et al., 1994) against a human International Protein Index (IPI) database concatenated to a decoy database in which the sequence for each entry in the original database was reversed (Peng et al., 2003). The Sequest search was performed using no enzyme specificity and a static modification of cysteine due to carboxyamidomethylation (57.02146). Sequest search results were assembled and filtered using the DTASelect (version 2.0) algorithm (Tabb et al., 2002), requiring peptides to be at least half tryptic and a minimum of two peptides per protein identification. The protein identification false positive rate was below two percent for each sample.

Acknowledgements

I thank Caroline Lilley for her input in many aspects of this project, as well as all of her efforts in the construction, purification, and characterization of the ICP0 T67A virus, which required several attempts and various strategies to successfully make. She also generated bacterial expression constructs encoding His-Flag-RNF8 used for *in vitro* ubiquitylation assays. Simina Ticau generated the Flag-RNF8 constructs for localization analysis. I am grateful for the advice and resources provided by Brenda Schulman at St. Jude Children's Research Hospital in Memphis, TN. I purified RNF8 FHA domains and measured protein binding via ITC using their facilities and equipment. Aaron Aslanian analyzed peptide pulldowns by mass spectrometry and Chris Boutell performed *in vitro* ubiqutination reactions. I also thank Jill Meisenhelder for advice and help with *in vitro* phosphorylation reactions and peptide design and synthesis to generate α-pT67 antibodies. We thank J. Chen, D. Durocher, M. Yaffe, and R. Everett for generous gifts of reagents, and the Weitzman lab for providing insightful discussion and input on this project.

The data from this Chapter have been submitted for publication for material as it may appear in Mol. Cell 2011, Viral E3 ubiquitin-mediated degradation of a cellular E3: viral mimicry of a cellular phosphorylation mark to target cellular FHA domain proteins, M.S. Chaurushiya, C.E. Lilley, A. Aslanian, S. Ticau, J. Meisenhelder, C. Boutell, J.R. Yates III, B.A. Schulman, T. Hunter, and M.D. Weitzman. The dissertation author was the primary researcher and author of this paper.

Chapter 4. Identification of cellular proteins and pathways targeted by HSV-1 ICP0.

Background

ICP0 targets diverse substrates for ubiquitylation and degradation. In addition to RNF8 and RNF168, ICP0 has been shown to mediate the degradation of DNA-PKcs (Parkinson et al., 1999), ND10 components (Everett et al., 1998a), centromeric proteins (Everett et al., 1999a; Lomonte and Morency, 2007; Lomonte et al., 2001), and the cellular deubiquitinating enzyme USP-7 (Boutell et al., 2005). As described in Chapter 2, RNF8 and RNF168 are restrictive to infection, and other studies have demonstrated that DNA-PKcs and PML body components are also restrictive (Everett et al., 2006; Lukashchuk and Everett, 2010; Parkinson et al., 1999). However, the effects of the individual proteins on HSV-1 infection are subtle. It is thus likely that ICP0 exerts its effects via a combinatorial strategy targeting many restrictive factors, some of which may be as yet unidentified.

ICP0 contains defined protein-interaction regions that have been described to bind some of its substrates. C-terminal regions of the protein are required for ICP0 to localize to PML bodies and bind USP7 (Everett et al., 1997; Maul and Everett, 1994), and as described in Chapter 3, a short linear phosphomotif at the N-terminus enables ICP0 to bind and degrade RNF8. It has thus become clear that ICP0 contains binding surfaces and motifs for its substrates, and we sought to use this property in order to identify novel cellular proteins and pathways intersecting with ICP0.

This Chapter describes a tandem-affinity purification and mass spectrometry approach to identify cellular proteins that can bind ICP0. We identify several pathways that appear to intersect with ICP0 and confirm these interactions. Most notably, ICP0 interacts with several DNA damage response proteins and appears to affect Nbs1 ubiquitylation. It also interacts with all three subunits of the CK2 kinase, RNA processing factors, and several chromatin-remodeling pathways. It remains to be determined whether any of the ICP0-interacting proteins are degradation targets of ICP0, and how they might contribute to or restrict HSV-1 infection.

Results

Identification of cellular proteins and pathways interacting with ICP0

To identify cellular proteins interacting with ICP0, we used a tandem-affinity purification method that uses streptavidin and calmodulin beads in succession, under naitve conditions, in order to purify protein complexes from cell lysates. We constructed a plasmid containing streptavidin-binding peptide (SBP) and calmodulin-binding peptide (CBP) fused to the N-terminus of ICP0 **(**TAP-ICP0, **Figure 4-1A)**. As controls we used a plasmid expressing TAP only (pNTAP) and a plasmid expressing TAP fused to an unrelated protein, the cellular cytidine deaminase APOBEC3A (TAP-A3A). To test the ability of TAP-ICP0 to bind known and novel substrates, we transfected TAP-ICP0, TAP, or TAP-A3A plasmid into 293T cells. 24 h post-transfection, lysates were prepared by 3X freeze-thaw between dry ice and cold water, and cleared lysates were incubated with Streptavidin beads to precipitate TAP-

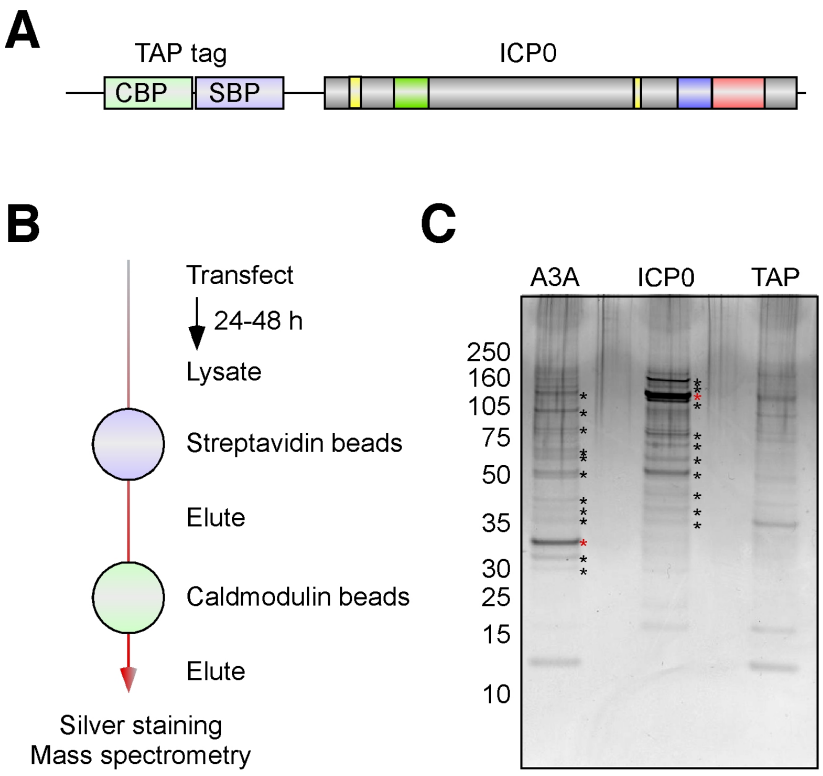

Figure 4-1. TAP-MS experimental approach. A. Streptavidin binding peptide (SBP) and Calmodulin binding peptide (CBP) sequences were cloned at the N-terminus of ICP0. **B.** TAP-ICP0, TAP-A3A, or pNTAP were transfected into 293T cells and harvested 24-48 h post-transfection. Lysates were prepared and purified over Streptavidin and Calmodulin beads using the InterPlay TAP purification kit (Stratagene). **C.** Purified proteins were analyzed by SDS-PAGE and silver staining. Bands unique to the TAP-ICP0 and TAP-A3A samples are marked with an asterisk. Red asterisk indicates TAP-ICP0 or TAP-A3A protein.

ICP0 via the SBP tag. Precipitated proteins were eluted, and the eluate was then incubated with Calmodulin beads, to bind TAP-ICP0 via the CBP region **(Figure 4-1B)**. This second round of purification ensured that proteins binding nonspecifically to Streptavidin were eliminated. Proteins bound to the Calmodulin beads were then eluted, and the eluates were analyzed by SDS-PAGE and silver staining. We observed that TAP-A3A and TAP-ICP0 precipitated distinct profiles of proteins, and that the TAP-only purification contained far fewer proteins **(Figure 4-1C)**.

We identified co-purifying proteins by mass spectrometry and eliminated those proteins that co-purified with both TAP-A3A and TAP-ICP0 as nonspecific interactors. Apart from ICP0, the protein in highest abundance in the TAP-ICP0 purifications was USP7, which is known to bind ICP0. We also observed p53 and DNA-PKcs to co-purify with ICP0, which is consistent with previous observations demonstrating that ICP0 can ubiquitylate and/or degrade these substrates. These observations indicated that the TAP-ICP0 purifications could contain other proteins that could be binding partners, ubiquitylation targets, and/or degradation targets of ICP0.

To gain a global picture of the complexes interacting with ICP0, we mapped the co-purifying proteins based on their known interactions to each other using the STRING database and algorithm (v 9.0, hstring-db.org). Proteins used in this analysis were restricted to those identified in at least three of six TAP-MS experiments. From this analysis we observed ICP0 to pull down proteins from the ribosomal subunits,

RNA processing and splicing factors, DDR proteins, chromatin remodeling proteins, and the CK2 kinase complex **(Figure 4-2)**.

To identify high-probability interaction candidates, we ranked proteins that appeared in at least four of six TAP-MS experiments by their abundance in the purifications. This can be reflected in the number of times the mass spectrometer observed spectra from a particular protein **(Table 4-1)**. Of approximately 300 proteins identified in these experiments **(Appendix Table 1)**, 35 appeared in at least four of six experiments. We identified these interacting proteins as the highest confidence candidates for further study. Among these were the DDR proteins Mre11 and Nbs1, and the HECT domain ubiquitin ligase EDD, which has been shown to interact with Chk2 and regulate checkpoint signaling (Henderson et al., 2006; Munoz et al., 2007). All three subunits of the CK2 kinase complex were also represented in this list, as well as two cancer-associated proteins, DICE1 (Deleted in cancer 1) and SART1 (squamous cell carcinoma antigen recognized by T-cells). We examined the relationship of these and other interacting proteins with ICP0 via co-purification and co-localization with ICP0, expression levels during HSV-1 infection, and ubiquitylation in the presence of ICP0 **(summarized in Table 4-2)**.

Analysis of high confidence and DDR candidates

To confirm ICP0 interaction with high confidence candidates, we transfected TAP-ICP0 or the TAP-only vector into 293T cells, tandem affinity purified protein complexes, and analyzed whether the candidate interactors were present in the

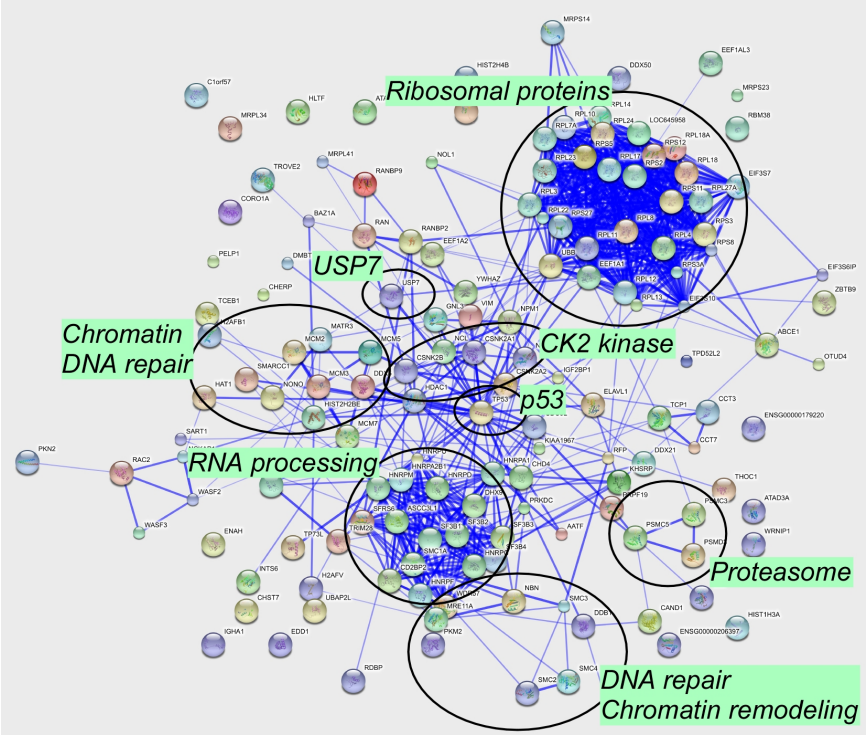

Figure 4-2. Overview of protein complexes co-purifying with TAP-ICP0. Proteins co-purifying with TAP-ICP0 at least 3 out of 6 times were mapped according to known previous associations using STRING v. 8.3. Notably, known ICP0 interacting proteins including USP-7 and p53 were identified in these studies.

Table 4-1. Highest confidence ICP0 interacting proteins.

PROTEIN NAME	RUN1	RUN2	RUN3	RUN4	RUN5	RUN6
USP7	>50	>50	>50	>50	>50	>50
U5 small nuclear ribonucleoprotein 200 kDa helicase	7	3	14	9	11	18
Probable RNA-dependent helicase p68 (DDX5)	3	3	5	6	5	13
PRP8 protein	3	3	3	8	7	11
Ubiquitin--protein ligase EDD (UBR5)	5	2	9	11	12	6
Similar to Double-strand break repair protein MRE11A	7	2	4	5	2	6
H2B	8	6	9	6	7	5
Casein kinase II beta subunit	4	2	5	3	2	3
DNA-dependent protein kinase catalytic subunit	7	3	6	5	35	30
ATP-dependent RNA helicase A (DEAH (Asp-Glu-Ala-His) box polypeptide 9)	5	5	6	3	6	10
NONO protein	4	3	6	3	6	5
NucleoliN		2	7	2	6	16
Transcription intermediary factor 1-beta	3	2	2		2	9
Nucleolar RNA helicase II (DDX21)	6	2	12	4		9
Splicing factor, proline-and glutamine-rich	3	3	3		4	6
Matrin 3		3	8	3	4	4
Histone H3	2	2	2		2	4
Splicing factor 3B Subunit 2	4	2	3	2		4
Nibrin	3	2		2	3	3
Casein kinase II, alpha' chain	3	2	3	4		2
H4 histone family, member M	4	6	8	7	8	
CSNK2A1 protein	10	5	12	6	3	
Nucleophosmin	2	2	3	6	2	
ATPase family, AAA domain containing 3A	2	2	3	5		
Pyruvate kinase M2			5	7	4	25
SART-1	8		2		5	5
DNA replication licensing factor MCM7	3			5	4	5
Heterogeneous nuclear ribonucleoprotein H1			4	5	3	5
40S ribosomal protein S2	6		5	6		5
DEAD/H (Asp-Glu-Ala-Asp/His) box polypeptide 3	2	2	5			5
Deleted in malignant brain tumors 1	4	2	3	6		
H2A histone family	5	4	4	3		
60S ribosomal protein L8	3	3	2	3		
Histone H2A.F/Z variant, isoform 1	5	4	5	2		
Candidate tumor suppressor protein DICE1	5	2	4	2		

Table Notes: Proteins identified in at least 4 out of 6 experiments are included in this table. Number of spectra identified for each protein is listed for each run.

purifications by SDS-PAGE and immunoblotting. We observed that Nbs1, USP7, SART1, DICE1, and the alpha subunit of the CK2 kinase complex (CK2α) co-purified with TAP-ICP0 but not the TAP only control **(Figure 4-3A)**. We also tested whether ATM and Rad50, which associate with Nbs1 and Mre11, co-purified with ICP0 and found that we could detect an interaction. We could detect a small amount of DNA-PKcs in the TAP-ICP0 purifications. In contrast, though Mre11 and EDD were among the top candidates from our TAP-MS analysis, we could not detect an interaction with these proteins by immunoblotting.

DDR interactions can be DNA dependent, and we have observed ICP0 to associate with chromatin fractions of cell lysates **(Appendix Figure A-4)**. To determine if the ICP0 interaction with the identified DDR proteins was DNA dependent, we repeated the pulldowns in the presence and absence of DNase and ethidium bromide (EtBr). For these experiments, we also constructed a TAP-mRFP plasmid to use as a negative control, as the TAP tag alone appeared to express poorly in cells. Cells were transfected with TAP-ICP0 or TAP-mRFP and harvested 24 h post-transfection. Lysates were prepared and treated with DNase (10 μg/ml) or EtBr (1 μg/ml) for 30 min prior to tandem affinity purification, and through the streptavidin binding phase of the purification. Purifying proteins were analyzed by SDS-PAGE and immunoblotting. We observed that both Rad50 and Nbs1 co-purified with TAP-ICP0 but not TAP-mRFP. Furthermore, they purified with TAP-ICP0 when lysates were treated with DNase and EtBr **(Figure 4-3B)**. These observations support our

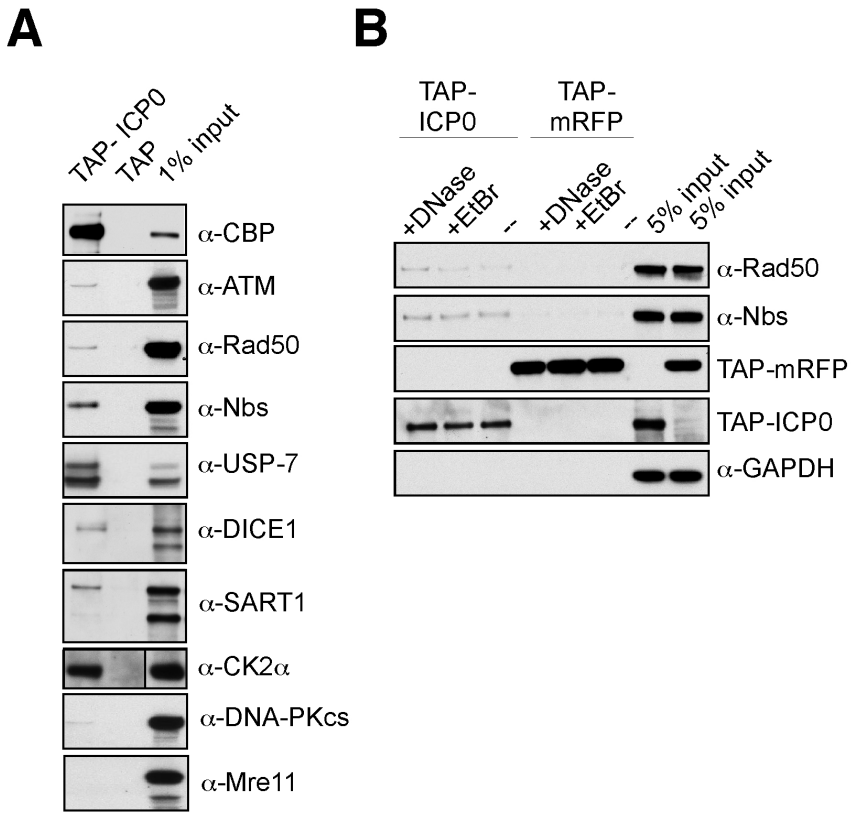

Figure 4-3. Validation of mass spectrometry results A. TAP-ICP0 or TAP only plasmid were transfected into 293T cells, harvested 24 h post-transfection, and tandem-affinity purified. Eluates were analyzed by SDS-PAGE and immunoblotting. USP-7 is used as a positive control. **B.** Interactions are not DNA dependent. TAP-ICP0 or TAP-mRFP plasmids were transfected into 293T cells and harvested 24 h post-transfection. Lysates were treated with DNase (50 μg/ml), EtBr (50 μg/ml), or untreated (--) before tandem affinity purification. TAP-mRFP and TAP-ICP0 were detected using α-CBP antibodies, which recognize the CBP portion of the TAP tag.

previous findings that Nbs1 and Rad50 associate with ICP0 and demonstrate that the association is DNA-independent.

To test whether ICP0 could affect the ubiquitylation status of Nbs1, we used His-ub pulldowns as described in Chapter 2. 293T cells were co-transfected with His-ub in the presence of ICP0 or ICP0 ΔRING and harvested 24 h post-transfection. To determine whether the ubiquitylation status changed after DNA damage, we also subjected cells to 10 Gy IR and harvested 1 h post-IR. His-ub conjugated proteins were purified under denaturing conditions using NiNTA beads and analyzed via SDS-PAGE and immunoblotting. As positive controls, we analyzed the ubiquitylation of p53 and ICP0, which are known to be ubiquitylated in cells, and USP7, which is a known degradation target of ICP0. We observed that p53 was ubiquitylated both in the presence and absence of ICP0, and there was a slight increase in p53 ubiquitylation in the presence of ICP0 **(Figure 4-4)**. We also observed significantly increased ubiquitylation of both Nbs1 and USP7 in the presence of ICP0, but not in the presence of the ΔRING mutant **(Figure 4-4)**. The ubiquitylation status of these proteins did not appear to change upon IR, though DDR-induced phosphorylation of Nbs1 was observed as reflected in a size shift in Nbs1 during SDS-PAGE. Combined, these observations indicate that Nbs1 is a potential ubiquitylation target of ICP0, although this will need to be directly tested via *in vitro* experiments. Similarly, the functional consequences of Nbs1 ubiquitylation in the presence of ICP0 need to be elucidated.

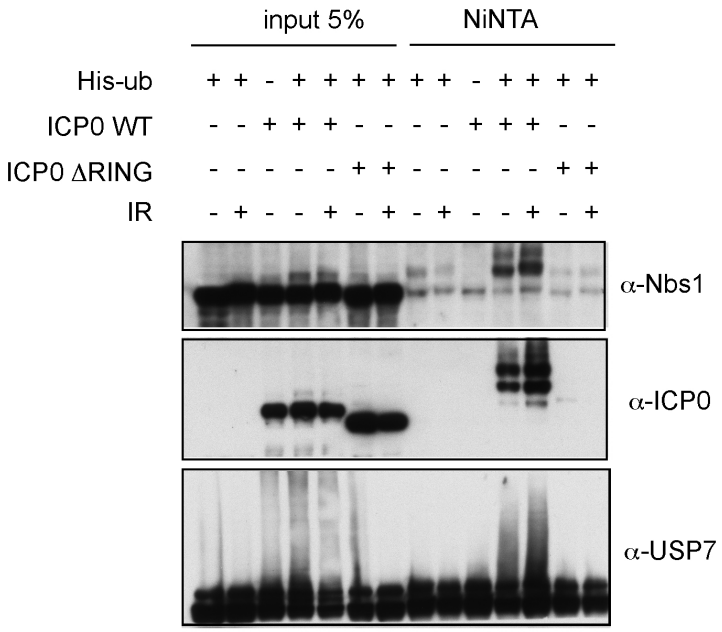

Figure 4-4. Nbs1 is ubiquitylated in the presence of ICP0. His-ub was co-transfected into 293T cells with ICP0 WT or ICP0 ΔRING, subject to 10 Gy IR 24 h post-transfection, and harvested 1 h post IR. His-ub conjugated proteins were purified under denaturing conditions using Ni-NTA beads and analyzed via SDS-PAGE and immunoblotting.

The CK2 kinase complex phosphorylates ICP0

All three subunits of the CK2 kinase complex co-purified in six of six TAP-MS experiments, and were among the highest abundance peptides. ICP0 interaction with the CK2α subunit was confirmed by immunoblotting **(see Figure 4-3A)**. We did not observe ICP0 to affect the ubiquitylation status or expression levels of CK2 **(summarized in Table 4-2)**. However, we noted that ICP0 contained several CK2 phosphorylation consensus sites, identified using the CK2 consensus sequences SXXD/E or TXXD/E. We therefore asked whether CK2 could phosphorylate ICP0. We expressed and purified a GST tagged N-terminal fragment of ICP0 containing the first 241 amino acids of ICP0 (GST-1-241), which contains several CK2 consensus sites. As a negative control, we purified a GST-tagged C-terminal fragment of ICP0 comprising the last 182 amino acids of ICP0 (GST-593-775), which did not contain any CK2 consensus sites. The purified proteins were subjected to *in vitro* phosphorylation with γ^{32}P-ATP in the presence or absence of CK2α/β holoenzyme, and the reaction products were analyzed by SDS-PAGE and visualized on a phosphorimager. We observed that GST-1-241 was phosphorylated by CK2 whereas the GST-593-775 fragment was not **(Figure 4-5)**. We could also detect several faint ^{32}P-labeled bands representing autophosphorylation of the CK2α/β subunits.

To more closely examine CK2-mediated phosphorylation of ICP0, the γ^{32}P -labeled GST-1-241 protein was extracted and purified from SDS-PAGE gels **(Figure 4-6A)**, and analyzed by phosphoamino acid analysis **(Figure 4-6B)** and phosphopeptide mapping **(Figure 4-6C)**. Phosphoamino acids were generated by

Table 4-2. Summary of the effects of ICP0 on candidate interactors

Protein	Co-purify	Co-localize	Ubiquitylated	Degraded
USP7	YES	N.D.	YES	YES
DNA-PKcs	YES (weak)	N.D.	N.D.	YES
CK2α/β	YES	N.D.	NO	NO
SART1	YES	NO	YES	NO
NONO	YES	NO	YES	NO
Mre11	NO	N.D.	N.D.	NO
EDD	NO	N.D.	NO	NO
Nbs1	YES	N.D.	YES	NO
Rad50	YES	N.D.	N.D.	NO
ATM	YES	N.D.	N.D.	NO
DICE1	YES	sometimes	YES	NO
ZNF198	N.D.	N.D.	NO	NO
SMARCA4	N.D.	NO	N.D.	NO
SMARCB1	N.D.	N.D.	N.D.	NO
SMARCC1	N.D.	N.D.	N.D.	NO
SMARCC2	N.D.	N.D.	N.D.	NO
CAF1-B	N.D.	N.D.	N.D.	NO

Table notes: N.D. = not determined or inconclusive. Co-purification was assessed via TAP or single-step streptavidin affinity purification. Ubiquitylation was assessed via His-ub assays. Endogenous protein levels were measured over an HSV-1 infection timecourse to determine degradation. Proteins listed in bold were present in TAP-MS experiments only after addition of proteasome inhibitors and were thus tested as potential ICP0 degradation targets.

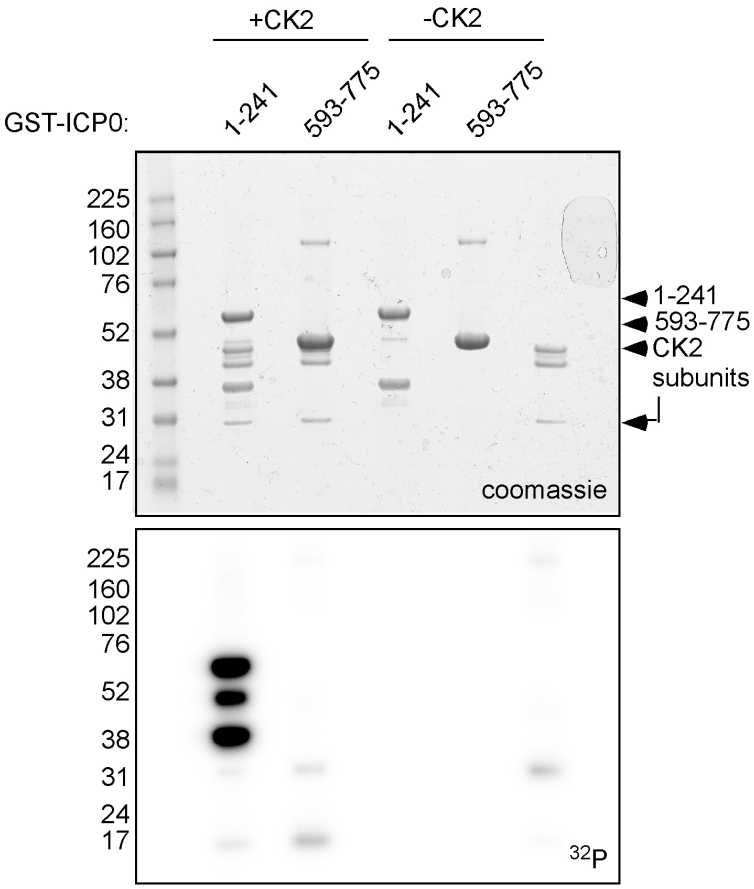

Figure 4-5. CK2 phosphorylates an N-terminal region of ICP0. GST-tagged ICP0 proteins containing amino acids 1-241 or 593-775 were purified from E. coli and phosphorylated in vitro using γ^{32}P ATP in the presence or absence of CK1. Reaction products were separated via SDS-PAGE. Total protein was visualized using coomassie staining, and ^{32}P-ATP incorporation was visualized on a phosphorimager.

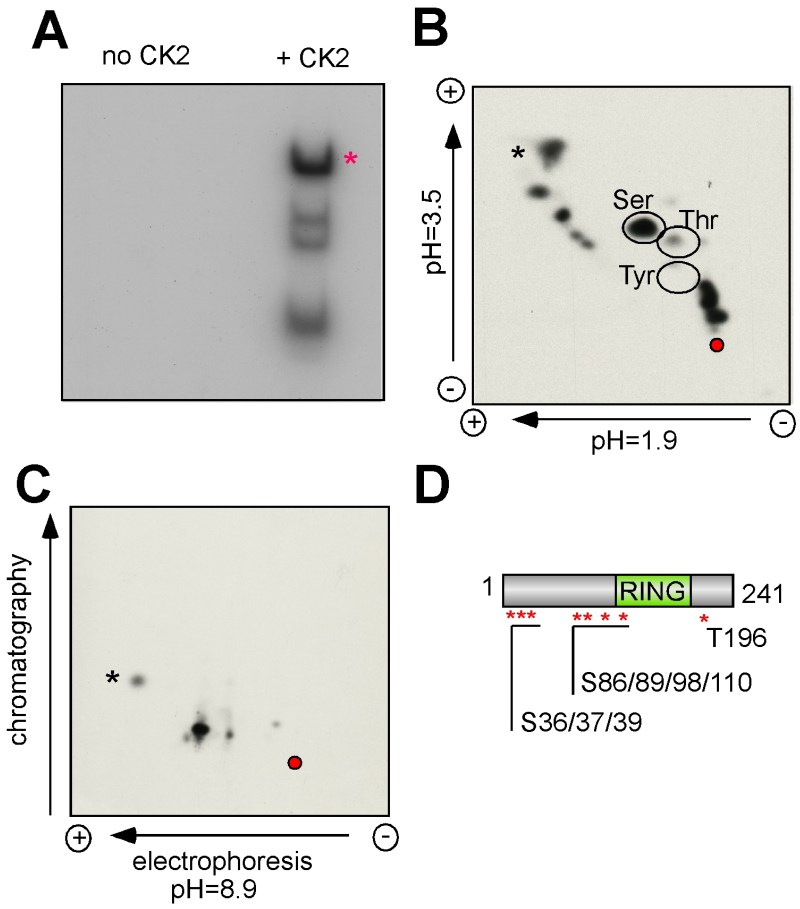

Figure 4-6. Identification of ICP0 residues phosphorylated by ICP0. A. Recombinant GST-ICP0 241 protein was phosphorylated *in vitro* by CK2 using γ^{32}P-ATP. Reaction products were analyzed by SDS-PAGE and ^{32}P signals were visualized using a phosphorimager. Phosphorylated products included the GST-241 protein, the alpha (α) and beta (β) subunits of CK2, and a cleavage product of GST-241. The full length protein (indicated with a red asterisk) was used for analysis. **B.** The phosphorylated GST-241 protein was extracted and hydrolyzed, and phosphorylated amino acids were identified by phosphoamino acid mapping (Thin layer chromatography using 2D electrophoresis). CK2 appeared to phosphorylate mainly Ser, with some Thr phosphorylation apparent. Red circle indicates origin; asterisk indicates free phosphate. **C.** Phosphorylated GST-241 protein was digested with trypsin, and 32P labeled tryptic peptides were analyzed by thin layer chromatography. Several phosphorylated peptides were apparent. **D.** Phosphorylated residues were identified by mass spectrometry analysis. The location of the RING domain of ICP0 is indicated in green.

hydrolysis in HCl and analyzed by 2D thin layer chromatography (TLC) using electrophoresis in the first and second dimensions. Labeled amino acids were visualized using autoradiography. We observed the majority of the ^{32}P-labeled residues to be Ser, with some phosphorylated Thr residues and no phosphorylated Tyr residues **(Figure 4-6B)**. For phosphopeptide mapping, the ^{32}P-labeled GST-241 protein was digested with trypsin, and the tryptic peptide products were analyzed using 2D TLC, with electrophoresis in the first dimension and chromatography in the second dimension. We observed several ^{32}P-labeled tryptic peptides **(Figure 4-6C)**, indicating that ICP0 can phosphorylate several residues on GST-1-241.

To identify the phosphorylated residues, GST-1-241 protein was phosphorylated *in vitro* with CK2 using cold ATP, purified using Glutathione resin, and digested with the proteinase Glu-C. Phosphorylated residues from the resulting peptides were identified by mass spectrometry. We observed ICP0 to be phosphorylated at S36/37/39, S86/89/98/110, and T196 **(Figure 4-6D)**. Combined, these observations indicate that the CK2-ICP0 interaction may serve to facilitate phosphorylation of ICP0 on CK2 consensus sites and contribute to ICP0 function.

SART1 associates with and is ubiquitylated in the presence of ICP0

SART1 is a component of the spliceosome (Makarova et al., 2001), and in squamous cell carcinomas, antigenic peptides from SART1 are recognized by cytotoxic (CD8+) T-lymphocytes (Shichijo et al., 1998). SART1 co-purified with TAP-ICP0 in four of six TAP-MS experiments and association of endogenous SART1

was confirmed by immunoblotting **(see Figure 4-3A)**. We constructed a Flag-SART1 expression construct to analyze the SART1-ICP0 relationship. The Flag-SART1 expression plasmid was co-transfected with TAP-mRFP or TAP-ICP0 into 293T cells, harvested 24 h post transfection, and TAP-ICP0 was purified using streptavidin beads. We observed that Flag-SART1 co-purified with TAP-ICP0 but not TAP-mRFP **(Figure 4-7A)**, confirming the results with endogenous SART1 protein as described above. We next analyzed the ubiquitylation status of Flag-SART1 using His-ub pulldowns. 293T cells were co-transfected with His-ub and Flag-SART1 in the presence or absence of ICP0. We observed that SART1 was ubiquitylated both in the presence and absence of ICP0, but that ubiquitylated levels increased in the presence of ICP0 **(Figure 4-7B)**, providing evidence that ICP0 can promote the ubiquitylation of SART1 in cells. We next analyzed whether SART1 co-localized with ICP0. Flag-SART1 and eGFP-ICP0 were co-transfected into HeLa cells and processed for immunofluorescence 24 h post infection. Flag-SART1 was diffusely nuclear in the absence of eGFP-ICP0, and did not re-localize to ICP0 foci upon eGFP-ICP0 expression **(Figure 4-7C)**.

Analysis of SART1 expression during HSV-1 infection revealed that endogenous SART1 proteins levels remained constant, indicating that SART1 is not a degradation target of ICP0 **(see Table 4-2)**. Combined, these observations suggest that SART1 may play a role during HSV-1 infection via its recruitment to HSV-1 replication centers, and that it may be subject to non-degradative ubiquitylation by ICP0 during HSV-1 infection to alter its function.

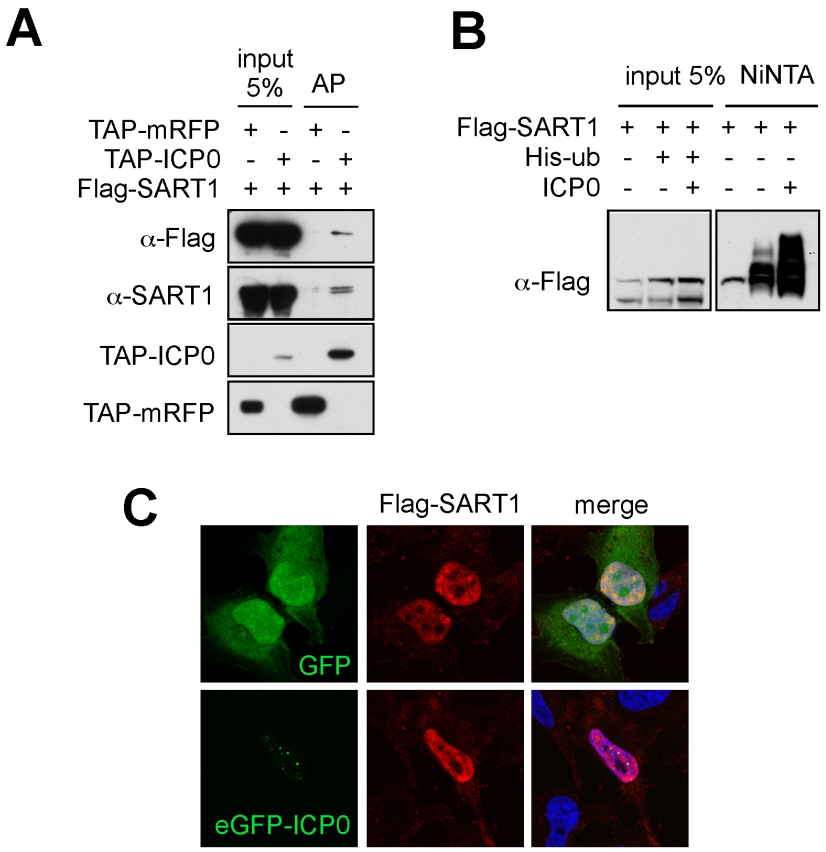

Figure 4-7. Analysis of SART1 association with ICP0. A. Flag-SART1 co-purifies with TAP-ICP0. Flag-SART1 was co-transfected with TAP-ICP0 or TAP-mRFP into 293T cells, harvested 24 h post-transfection, and tandem affinity purified. **B.** Flag-SART1 is ubiquitylated in the presence of ICP0. Flag-SART1 was co-transfected with His-ub in the presence and absence of ICP0, harvested 24 h post-transfection, and His-ub conjugated proteins were purified over NiNTA beads. **C.** Flag-SART1 does not localize to ICP0 foci or IRIF, but does localize to HSV-1 replication centers. Flag-SART1 was co-transfected transfected into HeLa cells with GFP or eGFP-ICP0 and analyzed for localization via immunofluorescence.

DICE1 associates with and is ubiquitylated in the presence of ICP0

DICE1 is frequently deleted or downregulated in prostate and other cancers (Li et al., 2003; Ropke et al., 2005). Functionally, it is a DEAD box RNA helicase that is a member of the Integrator complex, which associates with the C terminal domain of RNA polymerase II and promotes splicing of small nuclear RNAs (Baillat et al., 2005). DICE1 appeared in three of six TAP-MS experiments and ICP0 association with endogenous DICE1 was confirmed via immunoblotting **(see Figure 4-3A)**. We constructed a DICE1-HA expression construct to further analyze the DICE1-ICP0 relationship. The DICE1-HA expression plasmid that was co-transfected with TAP-mRFP or TAP-ICP0 into 293T cells, harvested 24 h post transfection, and TAP-ICP0 was affinity purified using streptavidin beads. We observed that DICE1-HA co-purified with TAP-ICP0 but not TAP-mRFP **(Figure 4-8A)**, supporting the observations with endogenous protein as described above. We next analyzed the ubiquitylation status of DICE1 using His-ub pulldowns. 293T cells were co-transfected with His-ub and DICE1-HA in the presence or absence of ICP0. As an additional negative control, we also examined DICE1-HA ubiquitylation in the presence of the ICP0 ΔRING mutant. We observed ubiquitylation of DICE1-HA in the presence of ICP0, but not in the presence of the ΔRING mutant or in the absence of ICP0 **(Figure 4-8B)**, providing evidence that ICP0 can promote the ubiquitylation of DICE1 in cells. We next analyzed whether DICE1 co-localized with ICP0. DICE1-HA and eGFP-ICP0 were co- transfected into HeLa cells and processed for immunofluorescence 24 h post-infection. DICE1-HA was diffusely nuclear when co-

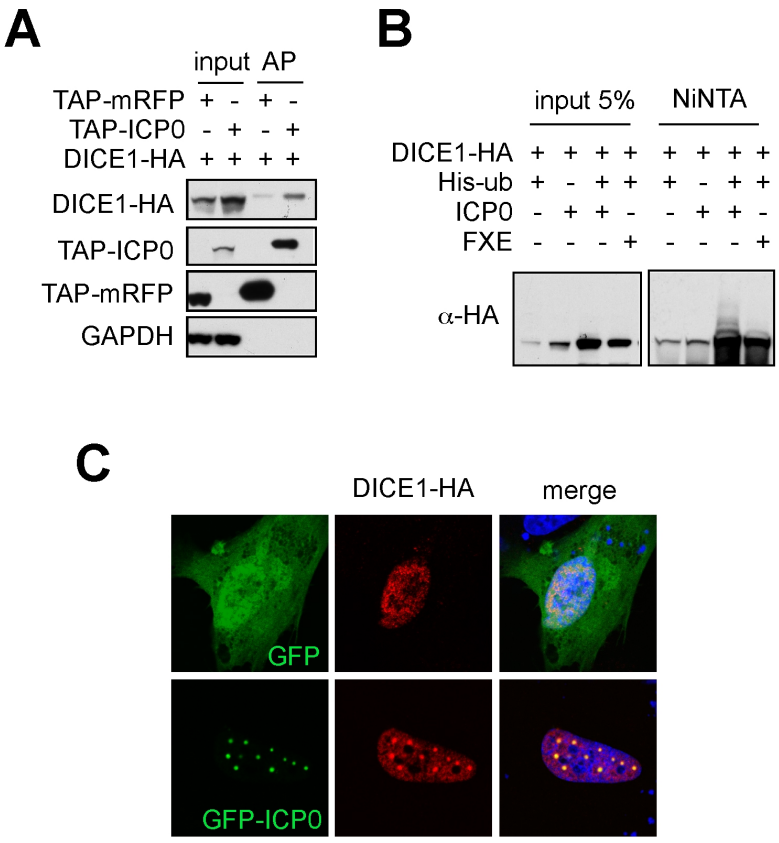

Figure 4-8. Analysis of DICE1 association with ICP0. A. DICE1-HA was co-transfected with TAP-ICP0 or TAP-mRFP into 293T cells and harvested 24 h post-transfection. Lysates were purified using streptavidin beads and analyzed via SDS-PAGE and immunoblotting. **B.** DICE1 ubiquitylation is increased in the presence of ICP0. DICE1-HA was co-transfected with His-ub in the presence or absence of ICP0 and cells were harvested 24 h post-transfection. His-ub conjugated proteins were purified using NiNTA beads and analyzed by SDS-PAGE and immunoblotting. **C.** DICE1-HA can co-localize with ICP0. DICE1-HA was co-transfected with GFP or eGFP-ICP0 into HeLa cells and protein localization was analyzed by immunofluorescence.

transfected with GFP, but upon expression of eGFP-ICP0 we observed DICE1-HA to localize to eGFP-ICP0 foci. However, this was only observed in a subset of cells (approximately 10%) **(Figure 4-8C)**. During a timecourse of HSV-1 infection, DICE1 levels remained constant, indicating that it is not degradation target of ICP0 **(summarized in Table 4-2)**. Combined, these results indicate that DICE1 may interact with ICP0 and that this may affect its ubiquitylation status, but the effects of ICP0 on DICE1 function are more likely occurring through non-degradative ubiquitylation.

Analysis of potential ICP0 degradation targets

As described above, none of the high confidence ICP0-interaction proteins represents ICP0 degradation targets, but it was very likely that true degradation targets were degraded during the course of the TAP-MS experiments. To specifically identify those proteins that could be ICP0 degradation targets, the TAP-MS experiments were repeated in the presence of proteasome inhibitors. Silver stain analysis of purifications in the presence or absence of proteasome inhibitors revealed that more proteins co-purified with TAP-ICP0 in the presence of proteasome inhibitors **(Figure 4-9A)**. In addition, the protein levels appeared to be increased in these purifications. Importantly, in TAP-mRFP purifications we did not observe a significant difference in protein purifications in the presence or absence of proteasome inhibitors. Combined, these observations provided evidence that analysis of TAP-ICP0 interacting proteins in the presence of proteasome inhibitors could potentially identify ICP0 degradation

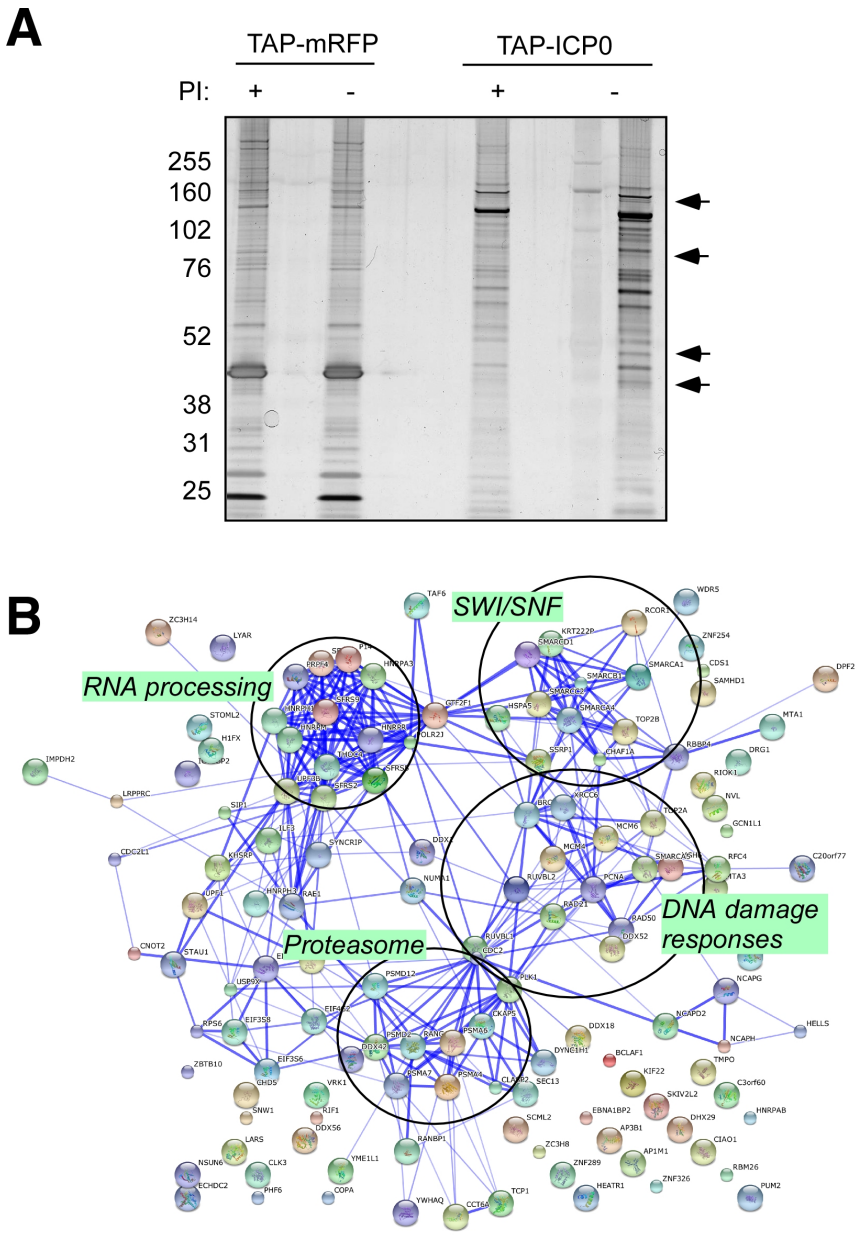

Figure 4-9. Identification of potential ICP0 degradation targets. A. 293T cells were transfected with TAP-mRFP or TAP-ICP0. Where indicated proteasome inhibitors (PI) were added 6 h post transfection and cells were harvested 16 h post transfection. Proteins were tandem affinity purified and analyzed by SDS-PAGE and silver staining. Arrows indicate bands appearing in TAP-ICP0 purification only in the presence of proteasome inhibitors. **B.** Mass spectrometry identification of proteins co-purifying with ICP0 in the presence of proteasome inhibitors. The four major groups of proteins represented were proteasome subunits, RNA splicing and processing factors, SWI/SNF chromatin remodeling proteins, and DNA damage response and repair factors.

targets. Mass spectrometry identification of proteins co-purifying in the presence of proteasome inhibitors revealed the presence several protein complexes **(Figure 4-9B)**.

The most distinct group of proteins represented in the proteasome-inhibitor tandem affinity purifications comprised members of the SWI/SNF chromatin remodeling complex **(Figure 4-10A)**, which regulates differentiation and proliferation (reviewed in (Roberts and Orkin, 2004)). These included SMARCD1 (BAF60), SMARCB1 (BAF47), SMARCC2 (BAF170), SMARCA4 (BRG1), SMARCE1 (BAF57) and SMARCA1 **(Figure 4-10B)**. We also noted that a zinc finger protein called ZNF198, and A and C subunits of the chromatin assembly factor (CAF-1) complex, interacted in a proteasome-dependent manner. Because they appeared to interact with ICP0 only in the presence of proteasome inhibitors, we hypothesized that they could represent ICP0 degradation targets. To test this, we analyzed protein levels during a timecourse of HSV-1 infection. HeLa cells were infected with HSV-1 or HSV-1 ΔICP0, harvested between 0.5 and 8 hpi, and protein levels analyzed by SDS-PAGE and immunoblotting. We detected lower levels of DNA-PKcs and RNF8 during the course of WT HSV-1 infection in a proteasome- and ICP0- dependent manner. In contrast, protein levels of the SWI/SNF complex members, ZNF198, and CAF1-A remained constant during infection **(Figure 4-11A)**. Combined, these observations lead us to conclude that these proteins do not represent degradation targets of ICP0. While we tested several SWI/SNF complex members in the above experiment, we did not have antibodies available to test whether SMARCA1 and

A

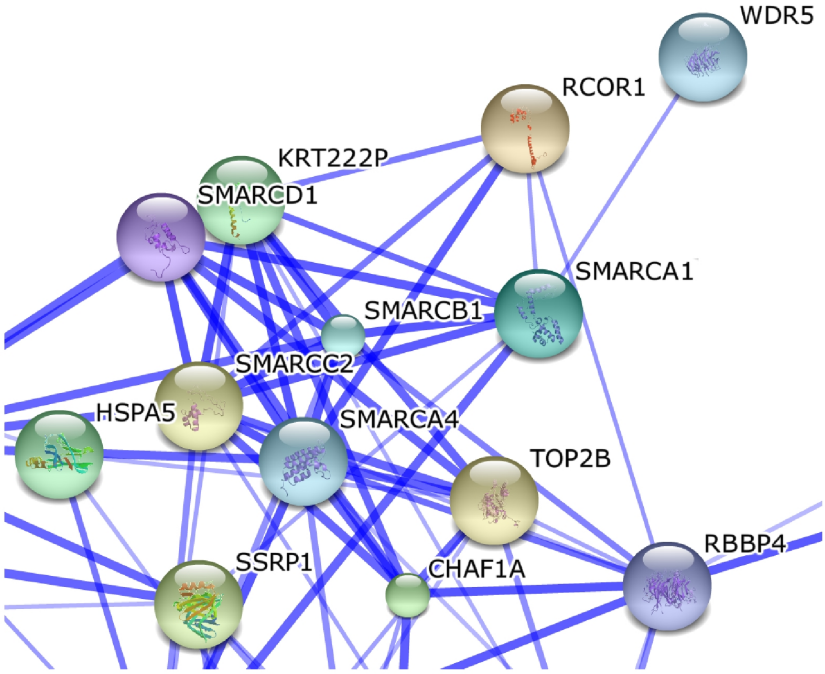

B

Protein	#spectra	Description
SMARCD1	4	SWI/SNF (BAF 60)
SMARCB1	2	SWI/SNF (BAF 57)
SMARCC2	6	SWI/SNF (BAF 170)t
SMARCA4	6	SWI/SNF (BRG-1)
SMARCA1	2	SWI/SNF
RCOR1	3	Co-REST (HDAC)
SSRP1	2	nucleosome reorganization
RBBP4	2	CAF1 subunit C
CHAF1A	2	CAF1 subunit A
TOP2B	8	topoisomerase II, beta isozyme
KRT222P	2	BAF 57kDa subunit
WDR5	2	WD repeats/transcriptional regulation

Figure 4-10. Members of the SWI/SNF chromatin remodeling complex associate with ICP0 in the presence of proteasome inhibitors. **A.** STRING map highlighting the SWI/SNF region of proteins co-purifying with ICP0 in the presence of proteasome inhibitors. **B.** Number of spectra observed for each protein in the SWI/SNF node of the STRING map, with protein description and function.

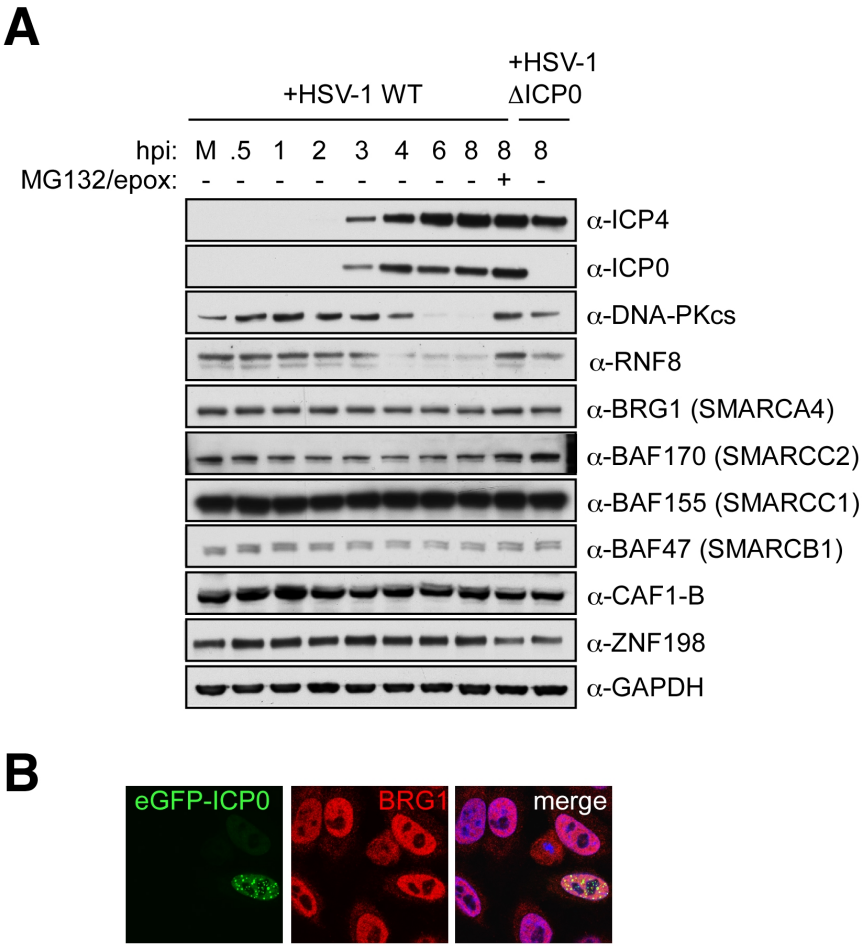

Figure 4-11. Analysis of proteins that interact with ICP0 in a proteasome-dependent manner. A. HeLa cells were infected with WT HSV-1 (strain 17 *syn+)* or DICP0 and harvested at the indiated timepoints. Where indicated, proteasome inhibitors (MG132, 10 μM; epoxomycin, 1 μM) were added 2 h post-infection. Protein levels were analyzed by SDS-PAGE and immunoblotting. **B.** HeLa cells were transfected with eGFP-ICP0, fixed 24 h post-transfection, and BRG1 (SMARCA4) levels and localization were analyzed by immunostaining.

SMARCD1 were affected, and it is possible that degradation of one complex member could affect the integrity of the entire complex.

We next analyzed whether SMARCA4, also known as BRG1 and the ATPase of the SWI/SNF complex, was recruited to ICP0 foci. eGFP-ICP0 was transfected into cells and protein localization was assessed by immunofluorescence. We observed that SMARCA4 was diffusely nuclear both in the presence and absence of eGFP-ICP0 **(Figure 4-11B),** indicating that SMARCA4 does not co-localize with ICP0. As the SWI/SNF complex core subunits associate in cells it is likely that the other complex members do not localize to ICP0 foci, but further study will be needed to determine whether this is the case.

Discussion

The preliminary data presented above demonstrate that it may be possible to identify novel ubiquitylation and degradation targets of ICP0 by defining the cellular proteins that associate with ICP0. Among the interacting proteins, the DDR protein Nbs1 reproducibly associates with ICP0 and is ubiquitylated in the presence of ICP0, both in the presence and absence of DNA damage. As Nbs1 levels remain constant during HSV-1 infection (Lilley et al., 2005), this ubiquitylation is likely non-degradative and may serve to alter Nbs1 function. Interestingly, Nbs1 was also identified as an interacting protein with the pT67 peptide of ICP0 in Chapter 3, providing supporting evidence that these two proteins interact and suggesting that this may occur through the FHA domain of Nbs1. A mutant analysis of the functional

domains of Nbs1, which contains defined BRCT, FHA and ATM binding domains, will help determine the mechanism by which Nbs1 and ICP0 associate.

The CK2 kinase complex reliably associates with ICP0 in TAP-ICP0 pulldowns **(Figure 4-2 and Table 4-1)**. Consistent with these observations, many CK2 phosphorylation consensus sites have been identified on ICP0, and CK2 can phosphorylate several N-terminal Ser and Thr residues *in vitro*. We did not observe the alpha subunit of the CK2 complex to be ubiquitylated or degraded in the presence of ICP0, and we thus hypothesize that the interaction between ICP0 and CK2 serves to facilitate CK2-mediated phosphorylation of ICP0. An additional possibility is that the interaction with CK2 facilitates recruitment of CK2 to PML bodies. This has been demonstrated in the case of the EBNA1 protein of EBV. EBNA1 has been shown to bind the CK2 complex via the CK2β subunit and recruit the complex to PML bodies, where it then promotes CK2-mediated PML phosphorylation and subsequent PML degradation (Sivachandran et al., 2010). This may represent another example of viral hijacking, as CK2-mediated phosphorylation of PML promotes PML degradation outside the context of infection (Scaglioni et al., 2006; Scaglioni et al., 2008). EBNA1 shares many characteristics of ICP0, including localization to ND10 and association with USP7. Like ICP0, the EBNA1 interaction with CK2 was identified via biochemical association studies. It is thus possible that ICP0 interacts with CK2 to promote PML degradation as well, and future studies will be needed to address whether this is the case.

SART1 and DICE1 appear to be affected by ICP0 in a similar manner as Nbs1, as they associate with and are ubiquitylated in the presence of ICP0, but are not degradation targets **(summarized in Table 4-2)**. ICP0 may modify these proteins in order to promote HSV-1 infection, and it may therefore be worth assessing the effects of these proteins on transcription, replication, or progeny production of WT and ΔICP0 viruses. DICE1 has also been identified as an ICP0 interacting protein via yeast-two-hybrid analysis (R. Everett, personal communication), supporting the findings presented here and providing evidence that the association is direct. Interestingly, SART1 is known to be SUMOylated (Schimmel et al., 2010; Vertegaal et al., 2006), and recent evidence demonstrates that ICP0 contains several SUMO-interacting motif-like sequences (SLSs) that can bind SUMO (C. Boutell, personal communication). It is possible that ICP0 could bind SART1 via a SUMO-SLS interaction.

We were unable to analyze cellular protein association with a TAP-ICP0 ΔRING protein, to prevent degradation of potential ICP0 targets, because this protein appeared to be insoluble under the lysis conditions we used. Subsequent biochemical fractionation studies indicated that the ΔRING protein was highly associated with the chromatin insoluble fractions **(Appendix Figure A-4)**, and FRAP analysis demonstrated that the ΔRING protein was largely immobile **(Appendix Figure A-5)**. We therefore used proteasome inhibitors to attempt to identify potential ICP0 degradation targets. A better approach for future experiments may be to use other mutants of ICP0 that are more soluble than the ΔRING mutant, but which are similarly

unable to degrade target substrates. These could include E2 binding mutants, or C-and N- terminal fragments of ICP0 that appear to mediate substrate binding and targeting. An ICP0 mutant containing catalytically inactivating point mutations within the RING domain (C116G/C156A) is more soluble than the ΔRING mutant, and may also be useful in TAP-MS experiments in the future. While we have not yet identified any ICP0-associated proteins that are degraded during HSV-1 infection, other candidates remain untested. It is also possible that ICP0 expression may change the localization or chromatin association of the SWI/SNF factors, and experiments addressing these possibilities may help us gain a greater understanding of how ICP0 may be affecting these chromatin remodeling pathways.

Materials and Methods

Cell lines and viruses

Cell lines and viruses are described in Chapter 2. HSV-1 timecourses to analyze protein degradation were also carried out as described in Chapter 2.

Plasmids and transfections

The eGFP-ICP0, ICP0, and TAP-ICP0 plasmids, and all mutants thereof, are described in Chapters 2 and 3. DICE1 cDNA was amplified from HeLa cDNA using primers CTCGAGATGCCCATCTTACTGTTCCTG (F) and CTCGAGTTAGTAATCTGGAACATCGTA (R) containing *XhoI* restriction sites, digested, and inserted into pcDNA3.1(+). Flag-SART1 was generated by Gateway

cloning of SART1 from a Gateway vector into a Flag destination vector (A gift from C. O'Shea). Transfections were performed as described in Chapter 2.

Antibodies

Antibodies to ICP0 and RNF8 are described in Chapter 2. SMARCA4 (BRG-1), SMARCC2 (BAF170), and SMARCC1 (BAF155) antibodies were from Santa Cruz. SMARCB1 (BAF47) was from BD Biosciences. DICE1, SART1, and CK2 antibodies were from Abcam. USP7 was from Bethyl.

NiNTA purifications

NiNTA purifications were performed and analyzed as described in Chapter 2.

Immunofluorescence and Immunoblotting

All immunofluorescence and immunoblotting were performed as described in Chapters 2 and 3.

Tandem Affinity Purification

For tandem affinity purification of ICP0, TAP-ICP0 was transfected into 293T cells and cells were harvested 24 h post transfection. Where indicated, proteasome inhibitors (10 μM MG132 and 1 μM epoxomycin) were added 6 h post transfection and cells were harvested 12 h after addition of proteasome inhibitors. Cells were lysed and purified using the InterPlay TAP purification kit (Stratagene) according to the

manufacturer's protocol. Purification products were analyzed by SDS-PAGE and silver staining (Silver Quest, Invitrogen) or by immunoblotting as indicated. Single-step streptavidin affinity purifications were performed as described in Chapter 3.

Phosphopeptide mapping

Phosphopeptide mapping and phosphoamino acid analysis were performed as described (Meisenhelder et al., 2001; van der Geer and Hunter, 1994). CK2 phosphorylation reactions were separated by SDS-PAGE, and ^{32}P labeled GST-241 protein was excised from the dried SDS-PAGE gel and hydrated in 50 mM ammonium bicarbonate buffer (pH=7.5). Protein was extracted by adding 500 μl 50 mM ammonium bicarbonate buffer, 10 μl β-mercaptoethanol, and 10 ml 20% SDS, boiled for 2 min, and incubated on a rocker overnight. Protein from eluates were precipitated in TCA and the protein pellet was washed in 96% EtOH. To oxidize the ^{32}P labeled protein, the protein pellet was resuspended in 50 μl chilled performic acid and incubated for 1 h on ice. The protein was then diluted in 400 μl ddH_2O and freeze dried on ice, and evaporated in a SpeedVac. For trypsin digestion, the protein pellet was resuspended in 50 μl 50 mM ammonium bicarbonate (pH=8.0). 10 μg trypsin was added, and the digest was incubated overnight at 37^{o}C, with addition of 10 μg additional trypsin at 4 h. The digest was diluted in ddH_2O and evaporated in a SpeedVac, and repeated four times. The tryptic peptides were resuspended in electrophoresis buffer pH=1.9 (50 ml formic acid (88% w/v), 156 ml glacial acetic acid, 1794 ml ddH_2O), and spotted onto thin-layer chromatography plates. Peptides

were separated by electrophoresis in the first dimension (pH=1.9), air dried, and then separated by chromatography in phospho-chromatography buffer (150 glacial acetic acid, 500 ml pyridine, 600 ml ddH_2O, 750 ml *n*-butanol) in the second dimension. ^{32}P-labeled tryptic peptides were visualized by autoradiography.

For phosphoamino acid analysis, lyophilized ^{32}P protein was hydrolyzed using HCl and incubated for 1 h at 110^{o}C. The protein was lyophilized using a SpeedVac, resuspended in electrophoresis buffer and analyzed by TLC using electrophoresis in the first dimension (pH=1.9) and second dimension (pH=3.5, 10ml pyridine, 100ml acetic acid, 10 ml 100 mM EDTA, 1880 ml ddH_2O).

Mass spectrometry analysis

TAP-ICP0 purifications were precipitated in TCA, digested with trypsin, and tryptic peptides were identified by mass spectrometry as described in Chapter 3. For identification of phosphorylated residues from in vitro phosphorylation reactions, GST-ICP0-241 was purified from *in vitro* reactions using glutathione beads, eluted, and precipitated in TCA. Samples were first denatured in 8M urea and then reduced and alkylated with 10 mM Tris(2-carboxyethyl)phosphine hydrochloride (Roche) and 55 mM iodoacetamide (Sigma-Aldrich) respectively. Samples were then digested over-night with trypsin (Promega) or endoproteinase Glu-C (Roche Applied Science) according to the manufacturer's specifications.

The protein digests were pressure-loaded onto a 250 micron i.d. fused silica capillary (Polymicro Technologies) column with a Kasil frit packed with 3 cm of 5 micron Partisphere strong cation exchange (SCX) resin (Whatman) and 3 cm of 5 micron C18 resin (Phenomenex). After desalting, this bi-phasic column was connected to a 100 micron i.d. fused silica capillary (Polymicro Technologies) analytical column with a 5 micron pulled-tip, packed with 10 cm of 5 micron C18 resin (Phenomenex). The MudPIT column was placed inline with an 1100 quaternary HPLC pump (Agilent) and the eluted peptides were electrosprayed directly into an LTQ mass spectrometer (Thermo Scientific). The buffer solutions used were 5% acetonitrile/0.1% formic acid (buffer A), 80% acetonitrile/0.1% formic acid (buffer B) and 500 mM ammonium acetate/5% acetonitrile/0.1% formic acid (buffer C). MudPIT of up to six steps was run with salt pulses of 0%, 20%, 40%, 70% and 100% buffer C and 90% buffer C/10% buffer B. A cycle consisted of one full scan mass spectrum (300-2000 m/z) followed by eight data-dependent collision induced dissociation (CID) MS/MS spectra with neutral loss triggered MS3. Application of mass spectrometer scan functions and HPLC solvent gradients were controlled by the Xcalibur data system (Thermo Scientific). MS/MS and MS3 spectra were extracted using RawXtract (version 1.9.9) (McDonald et al., 2004). For the ICP0 pulldown experiments, MS/MS spectra were searched with the Sequest algorithm (Eng et al., 1994) against a human International Protein Index (IPI) database supplemented with the human herpesvirus ICP0 protein (P08393) concatenated to a decoy database in which the sequence for each entry in the original database was reversed (Peng et al., 2003). The MS/MS Sequest search was

performed using no enzyme specificity and a static modification of cysteine due to carboxyamidomethylation. Sequest search results were assembled and filtered using the DTASelect (version 2.0) algorithm (Tabb et al., 2002), requiring peptides to be at least half tryptic and a minimum of two peptides per protein identification. The protein identification false positive rate was below four percent for each sample. For the *in vitro* phosphorylation experiments, MS/MS and MS3 spectra were searched with the Sequest algorithm (Eng et al., 1994) against protein sequences from Escherichia coli, Sacchromyces Genome Database (SGD), GST-ICP0 and human casein kinase subunits concatenated to a decoy database in which the sequence for each entry in the original database was reversed (Peng et al., 2003). The MS/MS Sequest search was performed using full enzyme specificity and a static modification of cysteine due to carboxyamidomethylation. A differential modification search of serine and threonine due to phosphorylation was performed with a maximum of three modifications and up to two missed cleavages per peptide. The MS3 Sequest search was performed using no enzyme specificity and a static modification of cysteine due to carboxyamidomethylation. A differential modification search of serine and threonine due to phosphorylation (-18) was performed with a maximum of two modifications per peptide. Sequest search results were assembled and filtered using the DTASelect (version 2.0) algorithm (Tabb et al., 2002), requiring a minimum of two peptides per protein identification. The protein identification false positive rate was below two percent for each sample. Phosphopeptide validation was performed

using DeBunker (Lu et al., 2007). Phosphorylation site localization was evaluated with AScore (Beausoleil et al., 2006).

Acknowledgements

I am very grateful to Aaron Aslanian, who analyzed TAP-ICP0 pulldowns and *in vitro* CK2 phosphorylation reactions by mass spectrometry, and provided useful advice for protein purifications. We also thank Jill Meisenhelder for help analyzing CK2-mediated phosphorylation of ICP0 using phosphopeptide mapping and phosphoamino acid analysis. We thank K. Jones for providing antibodies to the SWI/SNF complex members.

Chapter 5. Discussion

Summary

The findings presented in this Dissertation define the cellular DNA damage response as an intrinsic antiviral defense that recognizes incoming HSV-1 genomes and restricts their transcriptional competence, resulting in impaired progeny production. This cellular defense is counteracted by the viral E3 ligase ICP0, which targets the cellular E3 ligases RNF8 and RNF168 for degradation. This targeting leads to loss of ubiquitylated H2A and H2AX, disruption of the DDR, and relief of transcriptional repression on the viral genome. These findings highlight the use of ubiquitylation as both a cellular defense and viral counterattack during HSV-1 infection **(Figure 5-1)**. In uncovering the binding interface between ICP0 and RNF8, we identify a novel phosphosite on ICP0, pT67, present within a short linear motif that mimics cellular phosphosites. ICP0 uses this phosphosite mimicry to bind the RNF8 FHA domain and target RNF8 for degradation. We further identify CK1 as the kinase catalyzing phosphorylation to target RNF8. Using mass spectrometry-based approaches, we have identified other cellular proteins that can be targeted by ICP0, via interaction with the mimicking ICP0 phosphosite at T67 or via interaction with the entire ICP0 protein. These findings have implications for our general understanding of the distinct phases of the HSV-1 life cycle and the associated epigenetic marks contributing to establishment of the respective transcriptional states. Furthermore, they describe what may be a prototype mechanism by which viruses intersect with cellular pathways, through mimicking of cellular FHA consensus phosphosites

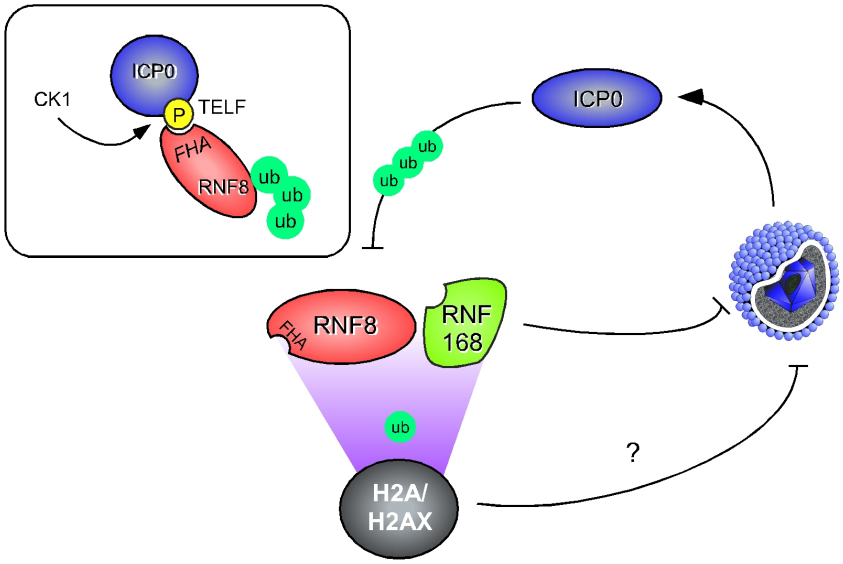

Figure 5-1. Ubiquitylation as cellular defense and viral counterattack. Work in this Dissertation has demonstrated that the cellular E3 ubiquitin ligases, RNF8 and RNF168, which function in the DDR, are restrictive to HSV-1 infection. In turn, HSV-1 encodes its own E3 ligase, ICP0, which targets RNF8 and RNF168 for degradation. In the case of RNF8, we have demonstrated that a phosphorylation-dependent targeting mechanism results in its ICP0-mediated ubiquitylation and degradation. We have also shown that ICP0 expression results in loss of ubH2A and ubH2AX, and given the defined roles of RNF8 and RNF168 as ubiquitin ligases for H2A and H2AX, it is possible that repression occurs through deposition of ubH2A on the viral genome. This hypothesis is supported by demonstrations that DDR proteins are recruited to sites associated with incoming viral genomes and that IE gene transcription is impaired during ΔICP0 infection in the presence of RNF8 and RNF168.

and targeting FHA domain proteins. Finally, they provide a basis to begin to understand fundamental cellular questions including how the DDR is regulated, and how endogenous levels of E3 ligases may be regulated.

The DDR in HSV-1 infection: two layers

Cellular proteins functioning as intrinsic antiviral defenses are constitutively expressed, can redirect their functions to restrict viral infection, and are often countered by viral regulatory proteins. As described in this Dissertation, the cellular E3 ligases RNF8 and RNF168, which function in the DDR, fulfill these three requirements as they are constitutively expressed, are repressive to HSV-1 infection, and are degraded by the HSV-1 encoded E3 ligase ICP0. These findings are especially surprising given previous demonstrations that the ATM-spearheaded branch of the DDR can be beneficial to viral infection. In contrast to RNF8 and RNF168, HSV-1 infection is impaired in the absence of ATM and Mre11 (Lilley et al., 2005), which function upstream of RNF8 and RNF168 in the DDR. It thus appears that, in contrast to an absolute activation or inactivation of the pathway, HSV-1 has evolved a mechanism to activate upstream DDR events while disabling downstream events. This dissection of the pathway, which occurs at the interface of phosphorylation-dependent and ubiquitin-dependent events, highlights the complex relationship between HSV-1 and the DDR.

What are the detrimental functions of the downstream DDR events? RNF8 and RNF168 are clearly restrictive to progeny production, and the data presented in

this Dissertation suggest that impaired immediate-early transcription events are at least partially responsible for this defect. As RNF8 and RNF168 are ubiquitin ligases for H2A and H2AX, it is tempting to speculate that RNF8- and RNF168-mediated deposition of ubH2A on the viral genome constitutes a cellular mechanism to attempt to repress the viral genome. This is particularly intriguing in light of the recent demonstration that ubH2A generated on the chromatin surrounding a DSB contributes to transcriptional silencing at the site of the break (Shanbhag et al., 2010). This silencing is regulated by RNF8, RNF168, ubH2A, and ATM. Importantly, the DDR-dependent effects on transcription at the site of a DSB occur *in cis*, not *in trans*. These observations support a model whereby DDR events directly target the incoming viral genomes to restrict transcription. It will therefore be interesting to determine whether DDR proteins can be detected on HSV-1 genomes through ChIP analysis, and especially whether the associated proteins change in the presence or absence of ICP0 and at distinct stages of the viral life cycle.

A novel epigenetic mark on viral genomes?

As described in detail in Chapter 1, the chromatin state of the HSV-1 genome is markedly distinct between the lytic and latent phases of the viral lifecycle, as demonstrated by changes in the overall nucleosome occupancy and specific epigenetic landscapes associated with lytic and latent promoters. Two viral components that affect the chromatin state appear to be the LATs and ICP0, although it is unclear how they manipulate the deposition of specific epigenetic marks during different phases of

the viral life cycle. It is likely that they somehow intersect with cellular chromatin modifying pathways, but to date such interactions have not been described. In Chapter 2, we demonstrate that ICP0 degrades cellular E3 ligases that ubiquitylate H2A, resulting in loss of ubH2A and ubH2AX levels in the cell. These observations provide a potential mechanism by which ICP0 could affect the chromatin state of the viral genome, as well as identify a potentially novel epigenetic mark, ubH2A, present on the viral genome after entry into the cell. These findings also shed light on a unique feature of ICP0, which is its ability to transactivate promoters in a sequence-independent manner, and without binding DNA.

Though it has often been described as a transcriptional transactivator, it is possible that by preventing the accumulation of ubH2A on viral promoters, ICP0 is actually functioning as a transcriptional de-repressor. Supporting this hypothesis, preliminary experiments on our lab have determined that ICP0 can overcome the RNF8-, RNF168-, and ubH2A- dependent transcriptional silencing at a DSB (C. Lilley, unpublished observations), and that this is dependent on the RING domain of ICP0. Interestingly, it has been previously demonstrated that silencing at a DSB is only partially dependent on RNF8 and RNF168, indicating that other cellular factors contribute as well. ICP0 appears to completely overcome transcriptional silencing at a DSB, suggesting that it may also target the other contributing cellular proteins. Thus, identifying other substrates of ICP0 may shed light on the full mechanism governing transcriptional silencing at a DSB, and it is likely that these same pathways may function to repress transcription from the HSV-1 genome. The contribution of other

cellular proteins also highlights the need to identify novel cellular substrates of ICP0, and it is possible that further examination of the ICP0 interacting proteins described in Chapters 3 and 4 may yield new players in the DNA damage response, chromatin remodeling, or transcriptional silencing relevant to the DDR and intrinsic antiviral defense during HSV-1 infection.

Hijacking cellular mechanisms of substrate targeting

In Chapter 3, we demonstrate that ICP0 contains a phosphosite that is used to bind the RNF8 FHA domain. These observations are particularly intriguing given that RNF8 localizes to its own substrates by virtue of its FHA domain, which binds phosphosites on Mdc1 anchored at the sites of DNA damage. In the presence of ICP0, the very mechanism used by RNF8 is hijacked and redirected, to then target RNF8 itself for degradation. As described in more detail in Chapter 3, the variations in the amino acid sequences within the phosphosite lead to distinct phosphorylation mechanisms, and may enable ICP0 to target structurally distinct FHA domains.

In the case of FOXK2, its FHA-dependent interaction with phosphorylated residues on viral regulatory proteins including Ad5 E1A and HPV E6 indicate that the same mechanism is likely used for association with ICP0. As FOXK2 does not appear to be targeted for degradation (unpublished observations), it is possible that modification by ICP0 affects FOXK2 function. In Chapter 4, we demonstrate that Nbs1 can co-purify with full-length ICP0 protein and the pT67 peptide, and that it is ubiquitylated in the presence of ICP0. It will be interesting to determine whether

interaction occurs through the FHA domain as well as identify the consequences of ICP0 interaction and the effects of Nbs1 ubiquitylation.

ICP0 is a heavily phosphorylated protein (Davido et al., 2005), and it is possible that one function of these phosphosites could be to bind other substrates of ICP0. It is as yet unclear whether phosphorylation of these sites is regulated or constitutive, although phosphorylation of T67 by CK1 as described in Chapter 3 would likely be constitutive. It will be necessary to more closely examine the observed ICP0 phosphosites, particularly with respect to kinases catalyzing these phosphorylations and potential protein-interacting motifs that may be generated. Many of the described sites are Ser residues, highlighting the possibility that ICP0 does not only target FHA domain proteins, but may be able to hijack other phospho-binding modules. Future studies can elucidate whether other phospho-dependent interactions are responsible for substrate targeting, in the case of ICP0 as well as other viral ubiquitin ligases.

ICP0 likely also hijacks other cellular mechanisms of substrate targeting, including the recently described SUMO-based mechanisms (Prudden et al., 2007; Sun et al., 2007), referred to briefly in Chapters 3 and 4. SUMO-targeted ubiquitin ligases (STUbLs) contain SUMO-interacting motifs (SIMs) that bind SUMO-modified proteins to target them for ubiquitylation. ICP0 has several SIM-like sequences (SLSs) that can interact with SUMO, and it appears this mechanism is used to target SUMOylated forms of PML for degradation (C. Boutell, personal communication). It will be interesting to determine whether other cellular proteins can be targeted through

this mechanism, how they affect HSV-1 infection, and what roles they play in cellular pathways.

Summary

Viruses have evolved a complex relationship with the cellular DNA damage response, and our work here demonstrates how the cellular DDR signaling events can recognize and manipulate the transcriptional competence of incoming viral genomes. It is likely that further study of ICP0, including the identification of new substrates, will shed light on how the DDR is regulated and lead to greater understanding of epigenetic and transcriptional control of HSV-1 genomes and at DSBs. Finally, they have important implications for the molecular basis of transition between latent and lytic infection, highlighting how the cell attempts to modulate the viral genome and how the virus counters these attempts.

Appendix

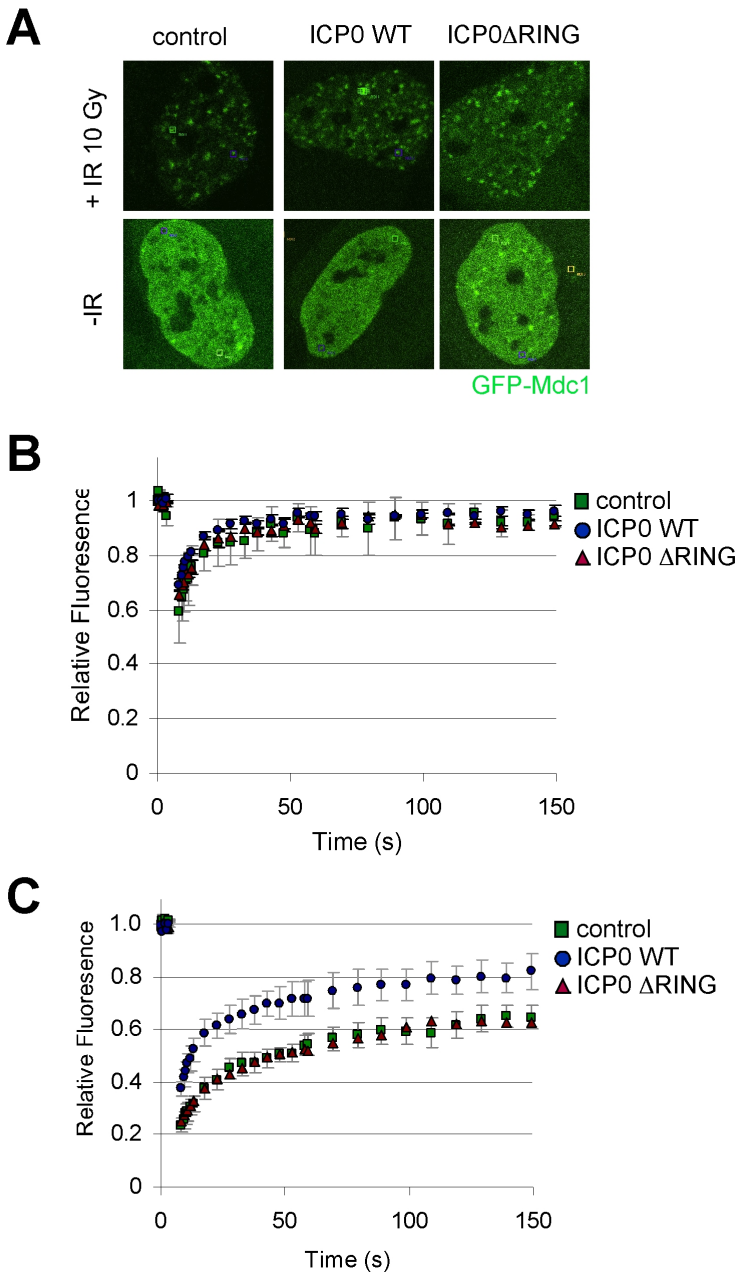

Figure A-1. Mdc1 residence time at IRIF is decreased in the presence of ICP0. A. U2OS cells stably expressing GFP-Mdc1 were transfected with WT or ΔRING ICP0, irradiated 24 h post transfection, and localization analyzed using live cell fluorescence microscopy. GFP-Mdc1 fluorescence recovery after photobleaching was asssessed before **(B)** or after **(C)** IR. Values are represented as the fraction of fluorescence intensity at each timepoint compared to the pre-bleach intensity, normalized for photobleaching during image acquisition and subtracted for background fluorescence. Error is the SEM of three independent experiments, examining 10 ROIs in each experiment.

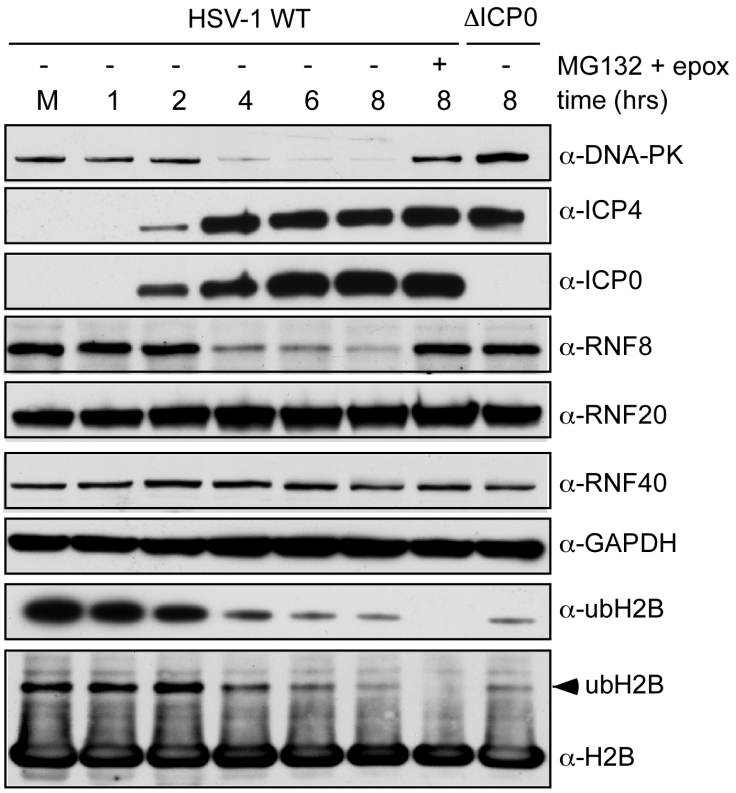

Figure A-2. Ubiquitylated H2B is decreased during HSV-1 infection in an ICP0-independent manner. HSV-1 WT or ΔICP0 viruses were used to infect HeLa cells at MOI=3 and harvested at the indicated timepoints. Protein levels were analyzed by SDS-PAGE and immunoblotting. Where indicated, proteasome inhibitors (MG132, 10 μM and epoxomycin, 1 μM) were added 2 h post-infection. The loss of ubH2B in the presence of proteasome inhibitors likely reflects the sequestration of poly-ubiquitin chains in the cytoplasm, depleting the nuclear supply.

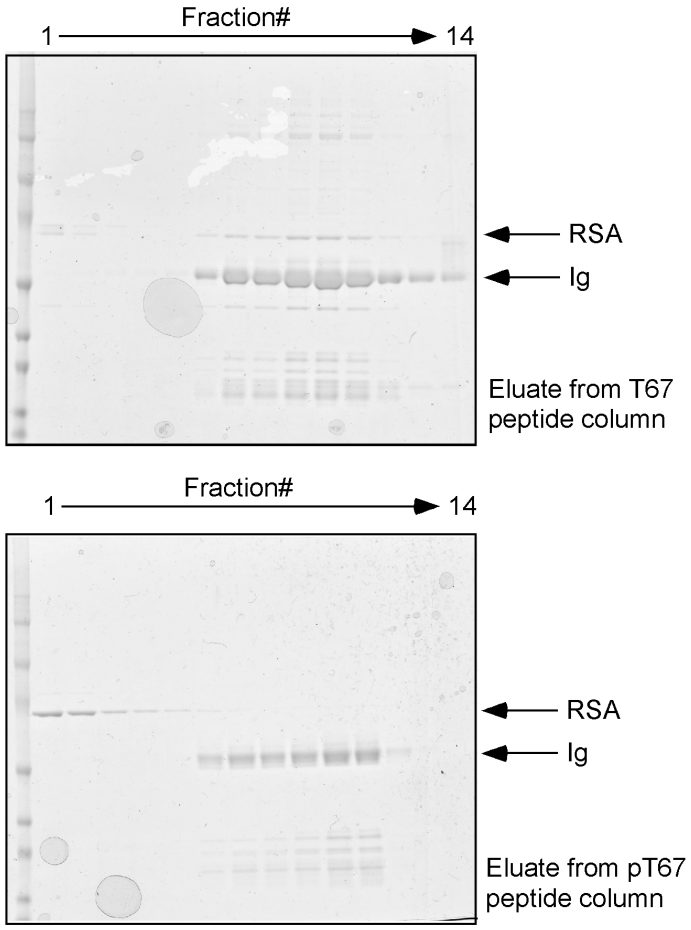

Figure A-3. Purification of α-pT67 antibodies. Rabbit sera were purified over an unphosphorylated T67 column to remove antibodies binding the ICP0 T67 in a non-phosphorylation dependent manner, and the flowthrough was then purified over a phosphorylated T67 column. Eluates were collected in 0.5 ml fractions. Eluates from the unphosphorylated column (upper panel) contained antibodies capable of recognizing both phosphorylated and unphosphorylated T67 peptide and the eluate from the phosphorylated column (lower panel) was specific for phosphorylated ICP0 T67 protein, as described in Chapter 3. RSA= rabbit serumn albumin; Ig= immunoglobulin proteins.

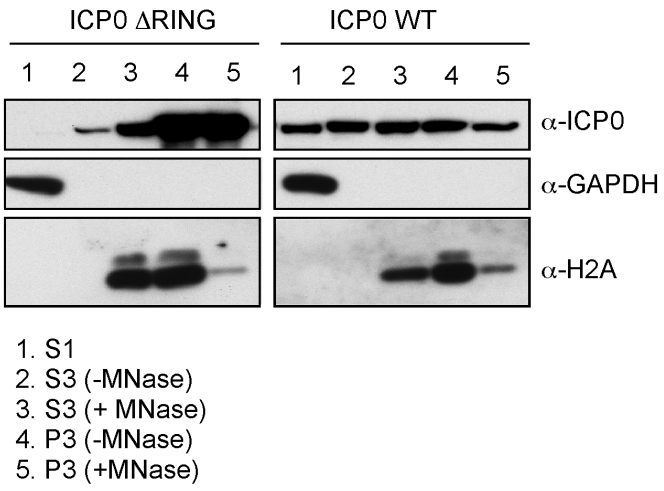

Figure A-4. ICP0 associates with the chromatin fraction of cell lysates. HeLa cells were transfected with ICP0 WT or ICP0 ΔRING and fractionated to yield cytoplasmic soluble proteins (S1), nuclear soluble proteins (S3), and insoluble proteins (P3). To release chromatin-associated proteins into the soluble fraction, the insoluble material was subjected to microccocal nuclease (MNase) digestion and the MNase treated S3 and P3 fractions were analyzed (S3+MNase, P3+MNase). GAPDH was used as a control for cytoplasmic soluble proteins, and H2A was used to analyze the nuclear fraction. After MNase treatment, H2A re-localizes from the insoluble fraction (lane 4) to the soluble fraction (lane 3; also compare to decrease in lane 5 and increase from lane 2). WT ICP0 appears in all fractions, and the ΔRING mutant appears to localize more predominantly to the chromatin fraction.

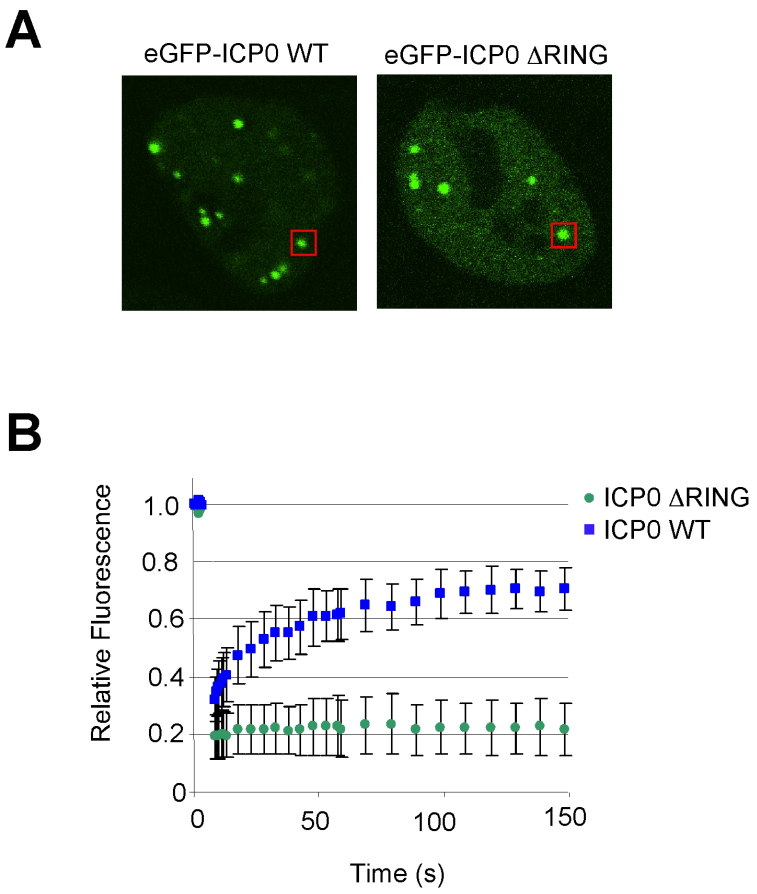

Figure A-5. The ΔRING mutant of ICP0 localizes to PML bodies, but is largely immobile at these sites. **A.** HeLa cells were transfected with eGFP-ICP0 or eGFP-ICP0 ΔRING and localization was analyzed by live-cell fluorescence microscopy. Red boxes indicate sample regions used for FRAP analysis. **B.** FRAP analysis of eGFP-ICP0 WT and ΔRING proteins. eGFP-ICP0 localized to foci as in (A) were photobleached and recovery of GFP signal was assessed at 5- and 10-second intervals post-bleach for 140 sec. Values shown are the adjusted integrated fluorescence intensity of the pre-bleach intensity, normalized for photobleaching during image acquisition and subtracted for background fluorescence. Error bars are standard error of 10 foci analyzed for WT and ΔRING mutants.

References

Baillat, D., Hakimi, M.A., Naar, A.M., Shilatifard, A., Cooch, N., and Shiekhattar, R. (2005). Integrator, a multiprotein mediator of small nuclear RNA processing, associates with the C-terminal repeat of RNA polymerase II. Cell *123*, 265-276.

Bakkenist, C.J., and Kastan, M.B. (2003). DNA damage activates ATM through intermolecular autophosphorylation and dimer dissociation. Nature *421*, 499-506.

Beausoleil, S.A., Villen, J., Gerber, S.A., Rush, J., Gygi, S.P. (2006) A probability-based approach for high-throughput protein phosphorylation analysis and site localization. Nature Biotechnology *24,* 1285-1292.

Bekker-Jensen, S., Lukas, C., Kitagawa, R., Melander, F., Kastan, M.B., Bartek, J., and Lukas, J. (2006). Spatial organization of the mammalian genome surveillance machinery in response to DNA strand breaks. J Cell Biol *173*, 195-206.

Bekker-Jensen, S., Lukas, C., Melander, F., Bartek, J., and Lukas, J. (2005). Dynamic assembly and sustained retention of 53BP1 at the sites of DNA damage are controlled by Mdc1/NFBD1. J Cell Biol *170*, 201-211.

Bekker-Jensen, S., Rendtlew Danielsen, J., Fugger, K., Gromova, I., Nerstedt, A., Lukas, C., Bartek, J., Lukas, J., and Mailand, N. (2010). HERC2 coordinates ubiquitin-dependent assembly of DNA repair factors on damaged chromosomes. Nat Cell Biol *12*, 80-86; sup pp 81-12.

Berkovich, E., Monnat, R.J., Jr., and Kastan, M.B. (2007). Roles of ATM and NBS1 in chromatin structure modulation and DNA double-strand break repair. Nat Cell Biol *9*, 683-690.

Bieniasz, P.D. (2004). Intrinsic immunity: a front-line defense against viral attack. Nat Immunol *5*, 1109-1115.

Bohgaki, T., Bohgaki, M., Cardoso, R., Panier, S., Zeegers, D., Li, L., Stewart, G.S., Sanchez, O., Hande, M.P., Durocher, D*., et al.* (2011). Genomic Instability, Defective Spermatogenesis, Immunodeficiency, and Cancer in a Mouse Model of the RIDDLE Syndrome. PLoS Genet *7*, e1001381.

Botuyan, M.V., Lee, J., Ward, I.M., Kim, J.E., Thompson, J.R., Chen, J., and Mer, G. (2006). Structural basis for the methylation state-specific recognition of histone H4-K20 by 53BP1 and Crb2 in DNA repair. Cell *127*, 1361-1373.

Boutell, C., Canning, M., Orr, A., and Everett, R.D. (2005). Reciprocal activities between herpes simplex virus type 1 regulatory protein ICP0, a ubiquitin E3 ligase, and ubiquitin-specific protease USP7. J Virol *79*, 12342-12354.

Boutell, C., and Everett, R.D. (2003). The herpes simplex virus type 1 (HSV-1) regulatory protein ICP0 interacts with and Ubiquitylates p53. J Biol Chem *278*, 36596-36602.

Boutell, C., and Everett, R.D. (2004). Herpes simplex virus type 1 infection induces the stabilization of p53 in a USP7- and ATM-independent manner. J Virol *78*, 8068-8077.

Boutell, C., Sadis, S., and Everett, R.D. (2002). Herpes simplex virus type 1 immediate-early protein ICP0 and is isolated RING finger domain act as ubiquitin E3 ligases in vitro. J Virol *76*, 841-850.

Brzovic, P.S., Rajagopal, P., Hoyt, D.W., King, M.C., and Klevit, R.E. (2001). Structure of a BRCA1-BARD1 heterodimeric RING-RING complex. Nat Struct Biol *8*, 833-837.

Buchwald, G., van der Stoop, P., Weichenrieder, O., Perrakis, A., van Lohuizen, M., and Sixma, T.K. (2006). Structure and E3-ligase activity of the Ring-Ring complex of polycomb proteins Bmi1 and Ring1b. EMBO J *25*, 2465-2474.

Burma, S., Chen, B.P., Murphy, M., Kurimasa, A., and Chen, D.J. (2001). ATM phosphorylates histone H2AX in response to DNA double-strand breaks. J Biol Chem *276*, 42462-42467.

Cai, W., Astor, T.L., Liptak, L.M., Cho, C., Coen, D.M., and Schaffer, P.A. (1993). The herpes simplex virus type 1 regulatory protein ICP0 enhances virus replication during acute infection and reactivation from latency. J Virol *67*, 7501-7512.

Cai, W., and Schaffer, P.A. (1992). Herpes simplex virus type 1 ICP0 regulates expression of immediate-early, early, and late genes in productively infected cells. J Virol *66*, 2904-2915.

Cai, W.Z., and Schaffer, P.A. (1989). Herpes simplex virus type 1 ICP0 plays a critical role in the de novo synthesis of infectious virus following transfection of viral DNA. J Virol *63*, 4579-4589.

Cardozo, T., and Pagano, M. (2004). The SCF ubiquitin ligase: insights into a molecular machine. Nat Rev Mol Cell Biol *5*, 739-751.

Carson, C.T., Orazio, N.I., Lee, D.V., Suh, J., Bekker-Jensen, S., Araujo, F.D., Lakdawala, S.S., Lilley, C.E., Bartek, J., Lukas, J.*, et al.* (2009). Mislocalization of the

MRN complex prevents ATR signaling during adenovirus infection. EMBO J *28*, 652-662.

Carson, C.T., Schwartz, R.A., Stracker, T.H., Lilley, C.E., Lee, D.V., and Weitzman, M.D. (2003). The Mre11 complex is required for ATM activation and the G2/M checkpoint. EMBO J *22*, 6610-6620.

Celeste, A., Petersen, S., Romanienko, P.J., Fernandez-Capetillo, O., Chen, H.T., Sedelnikova, O.A., Reina-San-Martin, B., Coppola, V., Meffre, E., Difilippantonio, M.J.*, et al.* (2002). Genomic instability in mice lacking histone H2AX. Science *296*, 922-927.

Chagraoui, J., Hebert, J., Girard, S., and Sauvageau, G. (2011). An anticlastogenic function for the Polycomb Group gene Bmi1. Proc Natl Acad Sci U S A *108*, 5284-5289.

Chapman, J.R., and Jackson, S.P. (2008). Phospho-dependent interactions between NBS1 and MDC1 mediate chromatin retention of the MRN complex at sites of DNA damage. EMBO Rep *9*, 795-801.

Chaudhuri, J., and Alt, F.W. (2004). Class-switch recombination: interplay of transcription, DNA deamination and DNA repair. Nat Rev Immunol *4*, 541-552.

Chun, H.H., and Gatti, R.A. (2004). Ataxia-telangiectasia, an evolving phenotype. DNA Repair (Amst) *3*, 1187-1196.

Ciechanover, A., and Schwartz, A.L. (2004). The ubiquitin system: pathogenesis of human diseases and drug targeting. Biochim Biophys Acta *1695*, 3-17.

Cimprich, K.A., and Cortez, D. (2008). ATR: an essential regulator of genome integrity. Nat Rev Mol Cell Biol *9*, 616-627.

Clements, G.B., and Stow, N.D. (1989). A herpes simplex virus type 1 mutant containing a deletion within immediate early gene 1 is latency-competent in mice. J Gen Virol *70 (Pt 9)*, 2501-2506.

Cliffe, A.R., Garber, D.A., and Knipe, D.M. (2009). Transcription of the herpes simplex virus latency-associated transcript promotes the formation of facultative heterochromatin on lytic promoters. J Virol *83*, 8182-8190.

Cliffe, A.R., and Knipe, D.M. (2008). Herpes simplex virus ICP0 promotes both histone removal and acetylation on viral DNA during lytic infection. J Virol *82*, 12030-12038.

Corey, L. (2007). Herpes simplex virus type 2 and HIV-1: the dialogue between the 2 organisms continues. J Infect Dis *195*, 1242-1244.

Corey, L., and Wald, A. (2009). Maternal and neonatal herpes simplex virus infections. N Engl J Med *361*, 1376-1385.

Davey, N.E., Trave, G., and Gibson, T.J. (2011). How viruses hijack cell regulation. Trends Biochem Sci *36*, 159-169.

Davido, D.J., von Zagorski, W.F., Lane, W.S., and Schaffer, P.A. (2005). Phosphorylation site mutations affect herpes simplex virus type 1 ICP0 function. J Virol *79*, 1232-1243.

Delius, H., and Clements, J.B. (1976). A partial denaturation map of herpes simplex virus type 1 DNA: evidence for inversions of the unique DNA regions. J Gen Virol *33*, 125-133.

Dennett, C., Cleator, G.M., and Klapper, P.E. (1997). HSV-1 and HSV-2 in herpes simplex encephalitis: a study of sixty-four cases in the United Kingdom. J Med Virol *53*, 1-3.

Deshmane, S.L., and Fraser, N.W. (1989). During latency, herpes simplex virus type 1 DNA is associated with nucleosomes in a chromatin structure. J Virol *63*, 943-947.

Devgan, S.S., Sanal, O., Doil, C., Nakamura, K., Nahas, S.A., Pettijohn, K., Bartek, J., Lukas, C., Lukas, J., and Gatti, R.A. (2011). Homozygous deficiency of ubiquitin-ligase ring-finger protein RNF168 mimics the radiosensitivity syndrome of ataxia-telangiectasia. Cell Death Differ.

Doil, C., Mailand, N., Bekker-Jensen, S., Menard, P., Larsen, D.H., Pepperkok, R., Ellenberg, J., Panier, S., Durocher, D., Bartek, J.*, et al.* (2009). RNF168 binds and amplifies ubiquitin conjugates on damaged chromosomes to allow accumulation of repair proteins. Cell *136*, 435-446.

Durocher, D., Henckel, J., Fersht, A.R., and Jackson, S.P. (1999). The FHA domain is a modular phosphopeptide recognition motif. Mol Cell *4*, 387-394.

Durocher, D., and Jackson, S.P. (2002). The FHA domain. FEBS Lett *513*, 58-66.

Durocher, D., Taylor, I.A., Sarbassova, D., Haire, L.F., Westcott, S.L., Jackson, S.P., Smerdon, S.J., and Yaffe, M.B. (2000). The molecular basis of FHA domain:phosphopeptide binding specificity and implications for phospho-dependent signaling mechanisms. Mol Cell *6*, 1169-1182.

Elion, G.B. (1983). The biochemistry and mechanism of action of acyclovir. J Antimicrob Chemother *12 Suppl B*, 9-17.

Eng, J.K., McCormack, A.L., and Yates, J.R., 3rd (1994). An Approach to Correlate Tandem Mass Spectral Data of Peptides with Amino Acid Sequences in a Protein Database. Journal of the American Society of Mass Spectrometry *5*, 976-989.

Everett, R.D. (1987). A detailed mutational analysis of Vmw110, a trans-acting transcriptional activator encoded by herpes simplex virus type 1. EMBO J *6*, 2069-2076.

Everett, R.D. (2000a). ICP0 induces the accumulation of colocalizing conjugated ubiquitin. J Virol *74*, 9994-10005.

Everett, R.D. (2000b). ICP0, a regulator of herpes simplex virus during lytic and latent infection. Bioessays *22*, 761-770.

Everett, R.D., Cross, A., and Orr, A. (1993). A truncated form of herpes simplex virus type 1 immediate-early protein Vmw110 is expressed in a cell type dependent manner. Virology *197*, 751-756.

Everett, R.D., Earnshaw, W.C., Findlay, J., and Lomonte, P. (1999a). Specific destruction of kinetochore protein CENP-C and disruption of cell division by herpes simplex virus immediate-early protein Vmw110. EMBO J *18*, 1526-1538.

Everett, R.D., Freemont, P., Saitoh, H., Dasso, M., Orr, A., Kathoria, M., and Parkinson, J. (1998a). The disruption of ND10 during herpes simplex virus infection correlates with the Vmw110- and proteasome-dependent loss of several PML isoforms. J Virol *72*, 6581-6591.

Everett, R.D., and Maul, G.G. (1994). HSV-1 IE protein Vmw110 causes redistribution of PML. EMBO J *13*, 5062-5069.

Everett, R.D., Meredith, M., and Orr, A. (1999b). The ability of herpes simplex virus type 1 immediate-early protein Vmw110 to bind to a ubiquitin-specific protease contributes to its roles in the activation of gene expression and stimulation of virus replication. J Virol *73*, 417-426.

Everett, R.D., Meredith, M., Orr, A., Cross, A., Kathoria, M., and Parkinson, J. (1997). A novel ubiquitin-specific protease is dynamically associated with the PML nuclear domain and binds to a herpesvirus regulatory protein. EMBO J *16*, 566-577.

Everett, R.D., and Murray, J. (2005). ND10 components relocate to sites associated with herpes simplex virus type 1 nucleoprotein complexes during virus infection. J Virol *79*, 5078-5089.

Everett, R.D., Orr, A., and Elliott, M. (1991). High level expression and purification of herpes simplex virus type 1 immediate early polypeptide Vmw110. Nucleic Acids Res *19*, 6155-6161.

Everett, R.D., Orr, A., and Preston, C.M. (1998b). A viral activator of gene expression functions via the ubiquitin-proteasome pathway. EMBO J *17*, 7161-7169.

Everett, R.D., Parada, C., Gripon, P., Sirma, H., and Orr, A. (2008). Replication of ICP0-null mutant herpes simplex virus type 1 is restricted by both PML and Sp100. J Virol *82*, 2661-2672.

Everett, R.D., Rechter, S., Papior, P., Tavalai, N., Stamminger, T., and Orr, A. (2006). PML contributes to a cellular mechanism of repression of herpes simplex virus type 1 infection that is inactivated by ICP0. J Virol *80*, 7995-8005.

Everett, R.D., Sourvinos, G., Leiper, C., Clements, J.B., and Orr, A. (2004). Formation of nuclear foci of the herpes simplex virus type 1 regulatory protein ICP4 at early times of infection: localization, dynamics, recruitment of ICP27, and evidence for the de novo induction of ND10-like complexes. J Virol *78*, 1903-1917.

Falck, J., Coates, J., and Jackson, S.P. (2005). Conserved modes of recruitment of ATM, ATR and DNA-PKcs to sites of DNA damage. Nature *434*, 605-611.

Ferenczy, M.W., and DeLuca, N.A. (2009). Epigenetic modulation of gene expression from quiescent herpes simplex virus genomes. J Virol *83*, 8514-8524.

Ferenczy, M.W., and DeLuca, N.A. (2011). Reversal of heterochromatic silencing of quiescent herpes simplex virus type 1 by ICP0. J Virol *85*, 3424-3435.

Flotow, H., Graves, P.R., Wang, A.Q., Fiol, C.J., Roeske, R.W., and Roach, P.J. (1990). Phosphate groups as substrate determinants for casein kinase I action. J Biol Chem *265*, 14264-14269.

Flotow, H., and Roach, P.J. (1991). Role of acidic residues as substrate determinants for casein kinase I. J Biol Chem *266*, 3724-3727.

Friedmann, A., Shlomai, J., and Becker, Y. (1977). Electron microscopy of herpes simplex virus DNA molecules isolated from infected cells by centrifugation in CsCl density gradients. J Gen Virol *34*, 507-522.

Garber, D.A., Beverley, S.M., and Coen, D.M. (1993). Demonstration of circularization of herpes simplex virus DNA following infection using pulsed field gel electrophoresis. Virology *197*, 459-462.

Ginjala, V., Nacerddine, K., Kulkarni, A., Oza, J., Hill, S.J., Yao, M., Citterio, E., van Lohuizen, M., and Ganesan, S. (2011). BMI1 Is Recruited to DNA Breaks and Contributes to DNA Damage-Induced H2A Ubiquitylation and Repair. Mol Cell Biol *31*, 1972-1982.

Grawunder, U., Zimmer, D., and Leiber, M.R. (1998). DNA ligase IV binds to XRCC4 via a motif located between rather than within its BRCT domains. Curr Biol *8*, 873-876.

Greil, W., Igo-Kemenes, T., and Zachau, H.G. (1976). Nuclease digestion in between and within nucleosomes. Nucleic Acids Res *3*, 2633-2644.

Gripon, P., Rumin, S., Urban, S., Le Seyec, J., Glaise, D., Cannie, I., Guyomard, C., Lucas, J., Trepo, C., and Guguen-Guillouzo, C. (2002). Infection of a human hepatoma cell line by hepatitis B virus. Proc Natl Acad Sci U S A *99*, 15655-15660.

Harris, R.A., Everett, R.D., Zhu, X.X., Silverstein, S., and Preston, C.M. (1989). Herpes simplex virus type 1 immediate-early protein Vmw110 reactivates latent herpes simplex virus type 2 in an in vitro latency system. J Virol *63*, 3513-3515.

Hayward, G.S., Jacob, R.J., Wadsworth, S.C., and Roizman, B. (1975). Anatomy of herpes simplex virus DNA: evidence for four populations of molecules that differ in the relative orientations of their long and short components. Proc Natl Acad Sci U S A *72*, 4243-4247.

Henderson, M.J., Munoz, M.A., Saunders, D.N., Clancy, J.L., Russell, A.J., Williams, B., Pappin, D., Khanna, K.K., Jackson, S.P., Sutherland, R.L.*, et al.* (2006). EDD mediates DNA damage-induced activation of CHK2. J Biol Chem *281*, 39990-40000.

Herrera, F.J., and Triezenberg, S.J. (2004). VP16-dependent association of chromatin-modifying coactivators and underrepresentation of histones at immediate-early gene promoters during herpes simplex virus infection. J Virol *78*, 9689-9696.

Hill, A., Jugovic, P., York, I., Russ, G., Bennink, J., Yewdell, J., Ploegh, H., and Johnson, D. (1995). Herpes simplex virus turns off the TAP to evade host immunity. Nature *375*, 411-415.

Hobbs, W.E., Brough, D.E., Kovesdi, I., and DeLuca, N.A. (2001). Efficient activation of viral genomes by levels of herpes simplex virus ICP0 insufficient to affect cellular gene expression or cell survival. J Virol *75*, 3391-3403.

Hofmann, K., and Bucher, P. (1995). The FHA domain: a putative nuclear signalling domain found in protein kinases and transcription factors. Trends Biochem Sci *20*, 347-349.

Honess, R.W., and Roizman, B. (1974). Regulation of herpesvirus macromolecular synthesis. I. Cascade regulation of the synthesis of three groups of viral proteins. J Virol *14*, 8-19.

Huen, M.S., Grant, R., Manke, I., Minn, K., Yu, X., Yaffe, M.B., and Chen, J. (2007). RNF8 transduces the DNA-damage signal via histone ubiquitylation and checkpoint protein assembly. Cell *131*, 901-914.

Hunter, T. (2007). The age of crosstalk: phosphorylation, ubiquitylation, and beyond. Mol Cell *28*, 730-738.

Ismail, I.H., Andrin, C., McDonald, D., and Hendzel, M.J. (2010). BMI1-mediated histone ubiquitylation promotes DNA double-strand break repair. J Cell Biol *191*, 45-60.

Jackson, S.A., and DeLuca, N.A. (2003). Relationship of herpes simplex virus genome configuration to productive and persistent infections. Proc Natl Acad Sci U S A *100*, 7871-7876.

Jackson, S.P., and Bartek, J. (2009). The DNA-damage response in human biology and disease. Nature *461*, 1071-1078.

Jacob, R.J., Morse, L.S., and Roizman, B. (1979). Anatomy of herpes simplex virus DNA. XII. Accumulation of head-to-tail concatemers in nuclei of infected cells and their role in the generation of the four isomeric arrangements of viral DNA. J Virol *29*, 448-457.

Johnson, D.C., and Baines, J.D. (2011). Herpesviruses remodel host membranes for virus egress. Nat Rev Microbiol *9*, 382-394.

Kent, J.R., Zeng, P.Y., Atanasiu, D., Gardner, J., Fraser, N.W., and Berger, S.L. (2004). During lytic infection herpes simplex virus type 1 is associated with histones bearing modifications that correlate with active transcription. J Virol *78*, 10178-10186.

Kim, S.T., Lim, D.S., Canman, C.E., and Kastan, M.B. (1999). Substrate specificities and identification of putative substrates of ATM kinase family members. J Biol Chem *274*, 37538-37543.

Koch, C.A., Agyei, R., Galicia, S., Metalnikov, P., O'Donnell, P., Starostine, A., Weinfeld, M., and Durocher, D. (2004). Xrcc4 physically links DNA end processing by polynucleotide kinase to DNA ligation by DNA ligase IV. EMBO J *23*, 3874-3885.

Kolas, N.K., Chapman, J.R., Nakada, S., Ylanko, J., Chahwan, R., Sweeney, F.D., Panier, S., Mendez, M., Wildenhain, J., Thomson, T.M.*, et al.* (2007). Orchestration of the DNA-damage response by the RNF8 ubiquitin ligase. Science *318*, 1637-1640.

Komorek, J., Kuppuswamy, M., Subramanian, T., Vijayalingam, S., Lomonosova, E., Zhao, L.J., Mymryk, J.S., Schmitt, K., and Chinnadurai, G. (2010). Adenovirus type 5 E1A and E6 proteins of low-risk cutaneous beta-human papillomaviruses suppress cell

transformation through interaction with FOXK1/K2 transcription factors. J Virol *84*, 2719-2731.

Kozlov, S.V., Graham, M.E., Jakob, B., Tobias, F., Kijas, A.W., Tanuji, M., Chen, P., Robinson, P.J., Taucher-Scholz, G., Suzuki, K.*, et al.* (2011). Autophosphorylation and ATM activation: additional sites add to the complexity. J Biol Chem *286*, 9107-9119.

Kozlov, S.V., Graham, M.E., Peng, C., Chen, P., Robinson, P.J., and Lavin, M.F. (2006). Involvement of novel autophosphorylation sites in ATM activation. EMBO J *25*, 3504-3514.

Kubat, N.J., Tran, R.K., McAnany, P., and Bloom, D.C. (2004). Specific histone tail modification and not DNA methylation is a determinant of herpes simplex virus type 1 latent gene expression. J Virol *78*, 1139-1149.

Kwiatkowski, D.L., Thompson, H.W., and Bloom, D.C. (2009). The polycomb group protein Bmi1 binds to the herpes simplex virus 1 latent genome and maintains repressive histone marks during latency. J Virol *83*, 8173-8181.

Lacasse, J.J., and Schang, L.M. (2010). During lytic infections, herpes simplex virus type 1 DNA is in complexes with the properties of unstable nucleosomes. J Virol *84*, 1920-1933.

Lees-Miller, S.P., Long, M.C., Kilvert, M.A., Lam, V., Rice, S.A., and Spencer, C.A. (1996). Attenuation of DNA-dependent protein kinase activity and its catalytic subunit by the herpes simplex virus type 1 transactivator ICP0. J Virol *70*, 7471-7477.

Leib, D.A., Coen, D.M., Bogard, C.L., Hicks, K.A., Yager, D.R., Knipe, D.M., Tyler, K.L., and Schaffer, P.A. (1989). Immediate-early regulatory gene mutants define different stages in the establishment and reactivation of herpes simplex virus latency. J Virol *63*, 759-768.

Li, L., Halaby, M.J., Hakem, A., Cardoso, R., El Ghamrasni, S., Harding, S., Chan, N., Bristow, R., Sanchez, O., Durocher, D.*, et al.* (2010). Rnf8 deficiency impairs class switch recombination, spermatogenesis, and genomic integrity and predisposes for cancer. J Exp Med *207*, 983-997.

Li, W.J., Hu, N., Su, H., Wang, C., Goldstein, A.M., Wang, Y., Emmert-Buck, M.R., Roth, M.J., Guo, W.J., and Taylor, P.R. (2003). Allelic loss on chromosome 13q14 and mutation in deleted in cancer 1 gene in esophageal squamous cell carcinoma. Oncogene *22*, 314-318.

Liang, Y., Vogel, J.L., Narayanan, A., Peng, H., and Kristie, T.M. (2009). Inhibition of the histone demethylase LSD1 blocks alpha-herpesvirus lytic replication and reactivation from latency. Nat Med *15*, 1312-1317.

Liashkovich, I., Hafezi, W., Kuhn, J.M., Oberleithner, H., and Shahin, V. (2011). Nuclear delivery mechanism of herpes simplex virus type 1 genome. J Mol Recognit *24*, 414-421.

Lilley, C.E., Carson, C.T., Muotri, A.R., Gage, F.H., and Weitzman, M.D. (2005). DNA repair proteins affect the lifecycle of herpes simplex virus 1. Proc Natl Acad Sci U S A *102*, 5844-5849.

Lilley, C.E., Schwartz, R.A., and Weitzman, M.D. (2007). Using or abusing: viruses and the cellular DNA damage response. Trends Microbiol *15*, 119-126.

Lloyd, J., Chapman, J.R., Clapperton, J.A., Haire, L.F., Hartsuiker, E., Li, J., Carr, A.M., Jackson, S.P., and Smerdon, S.J. (2009). A supramodular FHA/BRCT-repeat architecture mediates Nbs1 adaptor function in response to DNA damage. Cell *139*, 100-111.

Lomonte, P., and Morency, E. (2007). Centromeric protein CENP-B proteasomal degradation induced by the viral protein ICP0. FEBS Lett *581*, 658-662.

Lomonte, P., Sullivan, K.F., and Everett, R.D. (2001). Degradation of nucleosome-associated centromeric histone H3-like protein CENP-A induced by herpes simplex virus type 1 protein ICP0. J Biol Chem *276*, 5829-5835.

Lou, Z., Minter-Dykhouse, K., Wu, X., and Chen, J. (2003). MDC1 is coupled to activated CHK2 in mammalian DNA damage response pathways. Nature *421*, 957-961.

Lu, B., Ruse, C., Xu, T., Park, S.K., Yates J 3rd. (2007) Automatic validation of phosphopeptide identifications from tandem mass spectra. Anal Chem *79*, 1301-10.

Lukashchuk, V., and Everett, R.D. (2010). Regulation of ICP0-null mutant herpes simplex virus type 1 infection by ND10 components ATRX and hDaxx. J Virol *84*, 4026-4040.

Mailand, N., Bekker-Jensen, S., Faustrup, H., Melander, F., Bartek, J., Lukas, C., and Lukas, J. (2007). RNF8 ubiquitylates histones at DNA double-strand breaks and promotes assembly of repair proteins. Cell *131*, 887-900.

Makarova, O.V., Makarov, E.M., and Luhrmann, R. (2001). The 65 and 110 kDa SR-related proteins of the U4/U6.U5 tri-snRNP are essential for the assembly of mature spliceosomes. EMBO J *20*, 2553-2563.

Masucci, M.G. (2004). Epstein-Barr virus oncogenesis and the ubiquitin-proteasome system. Oncogene *23*, 2107-2115.

Matsuoka, S., Ballif, B.A., Smogorzewska, A., McDonald, E.R., 3rd, Hurov, K.E., Luo, J., Bakalarski, C.E., Zhao, Z., Solimini, N., Lerenthal, Y., *et al.* (2007). ATM and ATR substrate analysis reveals extensive protein networks responsive to DNA damage. Science *316*, 1160-1166.

Maul, G.G., and Everett, R.D. (1994). The nuclear location of PML, a cellular member of the C3HC4 zinc-binding domain protein family, is rearranged during herpes simplex virus infection by the C3HC4 viral protein ICP0. J Gen Virol *75 (Pt 6)*, 1223-1233.

McDonald, W.H., Tabb, D.L., Sadygov, R.G., MacCoss, M.J., Venable, J., Graumann, J., Johnson, J.R., Cociorva, D., and Yates, J.R., 3rd (2004). MS1, MS2, and SQT-three unified, compact, and easily parsed file formats for the storage of shotgun proteomic spectra and identifications. Rapid Commun Mass Spectrom *18*, 2162-2168.

Meisenhelder, J., Hunter, T., and van der Geer, P. (2001). Phosphopeptide mapping and identification of phosphorylation sites. Curr Protoc Mol Biol *Chapter 18*, Unit 18 19.

Meredith, M., Orr, A., Elliott, M., and Everett, R. (1995). Separation of sequence requirements for HSV-1 Vmw110 multimerisation and interaction with a 135-kDa cellular protein. Virology *209*, 174-187.

Meredith, M., Orr, A., and Everett, R. (1994). Herpes simplex virus type 1 immediate-early protein Vmw110 binds strongly and specifically to a 135-kDa cellular protein. Virology *200*, 457-469.

Minter-Dykhouse, K., Ward, I., Huen, M.S., Chen, J., and Lou, Z. (2008). Distinct versus overlapping functions of MDC1 and 53BP1 in DNA damage response and tumorigenesis. J Cell Biol *181*, 727-735.

Mohni, K.N., Livingston, C.M., Cortez, D., and Weller, S.K. (2010). ATR and ATRIP are recruited to herpes simplex virus type 1 replication compartments even though ATR signaling is disabled. J Virol *84*, 12152-12164.

Moyal, L., Lerenthal, Y., Gana-Weisz, M., Mass, G., So, S., Wang, S.Y., Eppink, B., Chung, Y.M., Shalev, G., Shema, E., *et al.* (2011). Requirement of ATM-dependent monoubiquitylation of histone H2B for timely repair of DNA double-strand breaks. Mol Cell *41*, 529-542.

Munoz, M.A., Saunders, D.N., Henderson, M.J., Clancy, J.L., Russell, A.J., Lehrbach, G., Musgrove, E.A., Watts, C.K., and Sutherland, R.L. (2007). The E3 ubiquitin ligase EDD regulates S-phase and G(2)/M DNA damage checkpoints. Cell Cycle *6*, 3070-3077.

O'Neill, T., Dwyer, A.J., Ziv, Y., Chan, D.W., Lees-Miller, S.P., Abraham, R.H., Lai, J.H., Hill, D., Shiloh, Y., Cantley, L.C.*, et al.* (2000). Utilization of oriented peptide libraries to identify substrate motifs selected by ATM. J Biol Chem *275*, 22719-22727.

Oh, J., and Fraser, N.W. (2008). Temporal association of the herpes simplex virus genome with histone proteins during a lytic infection. J Virol *82*, 3530-3537.

Panier, S., and Durocher, D. (2009). Regulatory ubiquitylation in response to DNA double-strand breaks. DNA Repair (Amst) *8*, 436-443.

Parkinson, J., Lees-Miller, S.P., and Everett, R.D. (1999). Herpes simplex virus type 1 immediate-early protein vmw110 induces the proteasome-dependent degradation of the catalytic subunit of DNA-dependent protein kinase. J Virol *73*, 650-657.

Paull, T.T. (2010). Making the best of the loose ends: Mre11/Rad50 complexes and Sae2 promote DNA double-strand break resection. DNA Repair (Amst) *9*, 1283-1291.

Pawson, T., and Scott, J.D. (1997). Signaling through scaffold, anchoring, and adaptor proteins. Science *278*, 2075-2080.

Pei, H., Zhang, L., Luo, K., Qin, Y., Chesi, M., Fei, F., Bergsagel, P.L., Wang, L., You, Z., and Lou, Z. (2011). MMSET regulates histone H4K20 methylation and 53BP1 accumulation at DNA damage sites. Nature *470*, 124-128.

Peng, J., Elias, J.E., Thoreen, C.C., Licklider, L.J., and Gygi, S.P. (2003). Evaluation of multidimensional chromatography coupled with tandem mass spectrometry (LC/LC-MS/MS) for large-scale protein analysis: the yeast proteome. J Proteome Res *2*, 43-50.

Perng, G.C., Jones, C., Ciacci-Zanella, J., Stone, M., Henderson, G., Yukht, A., Slanina, S.M., Hofman, F.M., Ghiasi, H., Nesburn, A.B.*, et al.* (2000). Virus-induced neuronal apoptosis blocked by the herpes simplex virus latency-associated transcript. Science *287*, 1500-1503.

Pignatti, P.F., and Cassai, E. (1980). Analysis of herpes simplex virus nucleoprotein complexes extracted from infected cells. J Virol *36*, 816-828.

Placek, B.J., and Berger, S.L. (2010). Chromatin dynamics during herpes simplex virus-1 lytic infection. Biochim Biophys Acta *1799*, 223-227.

Plans, V., Scheper, J., Soler, M., Loukili, N., Okano, Y., and Thomson, T.M. (2006). The RING finger protein RNF8 recruits UBC13 for lysine 63-based self polyubiquitylation. J Cell Biochem *97*, 572-582.

Poffenberger, K.L., and Roizman, B. (1985). A noninverting genome of a viable herpes simplex virus 1: presence of head-to-tail linkages in packaged genomes and requirements for circularization after infection. J Virol *53*, 587-595.

Polo, S.E., and Jackson, S.P. (2011). Dynamics of DNA damage response proteins at DNA breaks: a focus on protein modifications. Genes Dev *25*, 409-433.

Prudden, J., Pebernard, S., Raffa, G., Slavin, D.A., Perry, J.J., Tainer, J.A., McGowan, C.H., and Boddy, M.N. (2007). SUMO-targeted ubiquitin ligases in genome stability. EMBO J *26*, 4089-4101.

Querido, E., Blanchette, P., Yan, Q., Kamura, T., Morrison, M., Boivin, D., Kaelin, W.G., Conaway, R.C., Conaway, J.W., and Branton, P.E. (2001). Degradation of p53 by adenovirus E4orf6 and E1B55K proteins occurs via a novel mechanism involving a Cullin-containing complex. Genes Dev *15*, 3104-3117.

Quinlan, M.P., Chen, L.B., and Knipe, D.M. (1984). The intranuclear location of a herpes simplex virus DNA-binding protein is determined by the status of viral DNA replication. Cell *36*, 857-868.

Ren, S., Yang, G., He, Y., Wang, Y., Li, Y., and Chen, Z. (2008). The conservation pattern of short linear motifs is highly correlated with the function of interacting protein domains. BMC Genomics *9*, 452.

Richardson, C., Horikoshi, N., and Pandita, T.K. (2004). The role of the DNA double-strand break response network in meiosis. DNA Repair (Amst) *3*, 1149-1164.

Roberts, C.W., and Orkin, S.H. (2004). The SWI/SNF complex--chromatin and cancer. Nat Rev Cancer *4*, 133-142.

Robins, P., and Lindahl, T. (1996). DNA ligase IV from HeLa cell nuclei. J Biol Chem *271*, 24257-24261.

Rodriguez, M., Yu, X., Chen, J., and Songyang, Z. (2003). Phosphopeptide binding specificities of BRCA1 COOH-terminal (BRCT) domains. J Biol Chem *278*, 52914-52918.

Rogakou, E.P., Boon, C., Redon, C., and Bonner, W.M. (1999). Megabase chromatin domains involved in DNA double-strand breaks in vivo. J Cell Biol *146*, 905-916.

Rogakou, E.P., Pilch, D.R., Orr, A.H., Ivanova, V.S., and Bonner, W.M. (1998). DNA double-stranded breaks induce histone H2AX phosphorylation on serine 139. J Biol Chem *273*, 5858-5868.

Roizman, B. (1979). The structure and isomerization of herpes simplex virus genomes. Cell *16*, 481-494.

Roizman, B., and Knipe, D.M. (2001). Herpes simplex viruses and their replication. In Fields Virology, D.M. Knipe, and P.M. Howley, eds. (Philadelphia, Lippincott, Williams & Wilkins), pp. 2399-2459.

Ropke, A., Buhtz, P., Bohm, M., Seger, J., Wieland, I., Allhoff, E.P., and Wieacker, P.F. (2005). Promoter CpG hypermethylation and downregulation of DICE1 expression in prostate cancer. Oncogene *24*, 6667-6675.

Samaniego, L.A., Neiderhiser, L., and DeLuca, N.A. (1998). Persistence and expression of the herpes simplex virus genome in the absence of immediate-early proteins. J Virol *72*, 3307-3320.

Sanders, S.L., Portoso, M., Mata, J., Bahler, J., Allshire, R.C., and Kouzarides, T. (2004). Methylation of histone H4 lysine 20 controls recruitment of Crb2 to sites of DNA damage. Cell *119*, 603-614.

Sandri-Goldin, R.M. (2003). Replication of the herpes simplex virus genome: does it really go around in circles? Proc Natl Acad Sci U S A *100*, 7428-7429.

Santos, M.A., Huen, M.S., Jankovic, M., Chen, H.T., Lopez-Contreras, A.J., Klein, I.A., Wong, N., Barbancho, J.L., Fernandez-Capetillo, O., Nussenzweig, M.C*., et al.* (2010). Class switching and meiotic defects in mice lacking the E3 ubiquitin ligase RNF8. J Exp Med *207*, 973-981.

Sarisky, R.T., and Weber, P.C. (1994). Requirement for double-strand breaks but not for specific DNA sequences in herpes simplex virus type 1 genome isomerization events. J Virol *68*, 34-47.

Scaglioni, P.P., Yung, T.M., Cai, L.F., Erdjument-Bromage, H., Kaufman, A.J., Singh, B., Teruya-Feldstein, J., Tempst, P., and Pandolfi, P.P. (2006). A CK2-dependent mechanism for degradation of the PML tumor suppressor. Cell *126*, 269-283.

Scaglioni, P.P., Yung, T.M., Choi, S., Baldini, C., Konstantinidou, G., and Pandolfi, P.P. (2008). CK2 mediates phosphorylation and ubiquitin-mediated degradation of the PML tumor suppressor. Mol Cell Biochem *316*, 149-154.

Scheffner, M., Huibregtse, J.M., Vierstra, R.D., and Howley, P.M. (1993). The HPV-16 E6 and E6-AP complex functions as a ubiquitin-protein ligase in the ubiquitylation of p53. Cell *75*, 495-505.

Schimmel, J., Balog, C.I., Deelder, A.M., Drijfhout, J.W., Hensbergen, P.J., and Vertegaal, A.C. (2010). Positively charged amino acids flanking a sumoylation consensus tetramer on the 110kDa tri-snRNP component SART1 enhance sumoylation efficiency. J Proteomics *73*, 1523-1534.

Serrano, M., Lin, A.W., McCurrach, M.E., Beach, D., and Lowe, S.W. (1997). Oncogenic ras provokes premature cell senescence associated with accumulation of p53 and p16INK4a. Cell *88*, 593-602.

Severini, A., Morgan, A.R., Tovell, D.R., and Tyrrell, D.L. (1994). Study of the structure of replicative intermediates of HSV-1 DNA by pulsed-field gel electrophoresis. Virology *200*, 428-435.

Shanbhag, N.M., Rafalska-Metcalf, I.U., Balane-Bolivar, C., Janicki, S.M., and Greenberg, R.A. (2010). ATM-dependent chromatin changes silence transcription in cis to DNA double-strand breaks. Cell *141*, 970-981.

Shichijo, S., Nakao, M., Imai, Y., Takasu, H., Kawamoto, M., Niiya, F., Yang, D., Toh, Y., Yamana, H., and Itoh, K. (1998). A gene encoding antigenic peptides of human squamous cell carcinoma recognized by cytotoxic T lymphocytes. J Exp Med *187*, 277-288.

Shirata, N., Kudoh, A., Daikoku, T., Tatsumi, Y., Fujita, M., Kiyono, T., Sugaya, Y., Isomura, H., Ishizaki, K., and Tsurumi, T. (2005). Activation of ataxia telangiectasia-mutated DNA damage checkpoint signal transduction elicited by herpes simplex virus infection. J Biol Chem *280*, 30336-30341.

Showalter, S.D., Zweig, M., and Hampar, B. (1981). Monoclonal antibodies to herpes simplex virus type 1 proteins, including the immediate-early protein ICP 4. Infect Immun *34*, 684-692.

Sibanda, B.L., Critchlow, S.E., Begun, J., Pei, X.Y., Jackson, S.P., Blundell, T.L., and Pellegrini, L. (2001). Crystal structure of an Xrcc4-DNA ligase IV complex. Nat Struct Biol *8*, 1015-1019.

Sivachandran, N., Cao, J.Y., and Frappier, L. (2010). Epstein-Barr virus nuclear antigen 1 Hijacks the host kinase CK2 to disrupt PML nuclear bodies. J Virol *84*, 11113-11123.

Skaliter, R., Makhov, A.M., Griffith, J.D., and Lehman, I.R. (1996). Rolling circle DNA replication by extracts of herpes simplex virus type 1-infected human cells. J Virol *70*, 1132-1136.

Sobhian, B., Shao, G., Lilli, D.R., Culhane, A.C., Moreau, L.A., Xia, B., Livingston, D.M., and Greenberg, R.A. (2007). RAP80 targets BRCA1 to specific ubiquitin structures at DNA damage sites. Science *316*, 1198-1202.

Songyang, Z., Shoelson, S.E., Chaudhuri, M., Gish, G., Pawson, T., Haser, W.G., King, F., Roberts, T., Ratnofsky, S., Lechleider, R.J*., et al.* (1993). SH2 domains recognize specific phosphopeptide sequences. Cell *72*, 767-778.

Spycher, C., Miller, E.S., Townsend, K., Pavic, L., Morrice, N.A., Janscak, P., Stewart, G.S., and Stucki, M. (2008). Constitutive phosphorylation of MDC1 physically links the MRE11-RAD50-NBS1 complex to damaged chromatin. J Cell Biol *181*, 227-240.

Stewart, G.S., Panier, S., Townsend, K., Al-Hakim, A.K., Kolas, N.K., Miller, E.S., Nakada, S., Ylanko, J., Olivarius, S., Mendez, M.*, et al.* (2009). The RIDDLE syndrome protein mediates a ubiquitin-dependent signaling cascade at sites of DNA damage. Cell *136*, 420-434.

Stewart, G.S., Stankovic, T., Byrd, P.J., Wechsler, T., Miller, E.S., Huissoon, A., Drayson, M.T., West, S.C., Elledge, S.J., and Taylor, A.M. (2007). RIDDLE immunodeficiency syndrome is linked to defects in 53BP1-mediated DNA damage signaling. Proc Natl Acad Sci U S A *104*, 16910-16915.

Stewart, G.S., Wang, B., Bignell, C.R., Taylor, A.M., and Elledge, S.J. (2003). MDC1 is a mediator of the mammalian DNA damage checkpoint. Nature *421*, 961-966.

Stow, N.D., and Stow, E.C. (1986). Isolation and characterization of a herpes simplex virus type 1 mutant containing a deletion within the gene encoding the immediate early polypeptide Vmw110. J Gen Virol *67 (Pt 12)*, 2571-2585.

Stracker, T.H., Carson, C.T., and Weitzman, M.D. (2002). Adenovirus oncoproteins inactivate the Mre11-Rad50-NBS1 DNA repair complex. Nature *418*, 348-352.

Strang, B.L., and Stow, N.D. (2005). Circularization of the herpes simplex virus type 1 genome upon lytic infection. J Virol *79*, 12487-12494.

Stucki, M., Clapperton, J.A., Mohammad, D., Yaffe, M.B., Smerdon, S.J., and Jackson, S.P. (2005). MDC1 directly binds phosphorylated histone H2AX to regulate cellular responses to DNA double-strand breaks. Cell *123*, 1213-1226.

Sun, H., Leverson, J.D., and Hunter, T. (2007). Conserved function of RNF4 family proteins in eukaryotes: targeting a ubiquitin ligase to SUMOylated proteins. EMBO J *26*, 4102-4112.

Tabb, D.L., McDonald, W.H., and Yates, J.R., 3rd (2002). DTASelect and Contrast: tools for assembling and comparing protein identifications from shotgun proteomics. J Proteome Res *1*, 21-26.

Taylor, T.J., and Knipe, D.M. (2004). Proteomics of herpes simplex virus replication compartments: association of cellular DNA replication, repair, recombination, and chromatin remodeling proteins with ICP8. J Virol *78*, 5856-5866.

Umbach, J.L., Kramer, M.F., Jurak, I., Karnowski, H.W., Coen, D.M., and Cullen, B.R. (2008). MicroRNAs expressed by herpes simplex virus 1 during latent infection regulate viral mRNAs. Nature *454*, 780-783.

Uziel, T., Lerenthal, Y., Moyal, L., Andegeko, Y., Mittelman, L., and Shiloh, Y. (2003). Requirement of the MRN complex for ATM activation by DNA damage. EMBO J *22*, 5612-5621.

van der Geer, P., and Hunter, T. (1994). Phosphopeptide mapping and phosphoamino acid analysis by electrophoresis and chromatography on thin-layer cellulose plates. Electrophoresis *15*, 544-554.

Vertegaal, A.C., Andersen, J.S., Ogg, S.C., Hay, R.T., Mann, M., and Lamond, A.I. (2006). Distinct and overlapping sets of SUMO-1 and SUMO-2 target proteins revealed by quantitative proteomics. Mol Cell Proteomics *5*, 2298-2310.

Wald, A., and Link, K. (2002). Risk of human immunodeficiency virus infection in herpes simplex virus type 2-seropositive persons: a meta-analysis. J Infect Dis *185*, 45-52.

Wang, B., and Elledge, S.J. (2007). Ubc13/Rnf8 ubiquitin ligases control foci formation of the Rap80/Abraxas/Brca1/Brcc36 complex in response to DNA damage. Proc Natl Acad Sci U S A *104*, 20759-20763.

Wang, H., Wang, L., Erdjument-Bromage, H., Vidal, M., Tempst, P., Jones, R.S., and Zhang, Y. (2004). Role of histone H2A ubiquitylation in Polycomb silencing. Nature *431*, 873-878.

Weiden, M.D., and Ginsberg, H.S. (1994). Deletion of the E4 region of the genome produces adenovirus DNA concatemers. Proc Natl Acad Sci U S A *91*, 153-157.

Weitzman, M.D., Lilley, C.E., and Chaurushiya, M.S. (2010). Genomes in conflict: maintaining genome integrity during virus infection. Annu Rev Microbiol *64*, 61-81.

Whitley, R.J. (2001). Herpes simplex viruses. In Fields Virology, D.M. Knipe, and P.M. Howley, eds. (Philadelphia, Lippincott, Williams, & Wilkins), pp. 2461-2509.

Wilkinson, D.E., and Weller, S.K. (2003). The role of DNA recombination in herpes simplex virus DNA replication. IUBMB Life *55*, 451-458.

Wilkinson, D.E., and Weller, S.K. (2004). Recruitment of cellular recombination and repair proteins to sites of herpes simplex virus type 1 DNA replication is dependent on the composition of viral proteins within prereplicative sites and correlates with the induction of the DNA damage response. J Virol *78*, 4783-4796.

Williams, R.S., Dodson, G.E., Limbo, O., Yamada, Y., Williams, J.S., Guenther, G., Classen, S., Glover, J.N., Iwasaki, H., Russell, P.*, et al.* (2009). Nbs1 flexibly tethers Ctp1 and Mre11-Rad50 to coordinate DNA double-strand break processing and repair. Cell *139*, 87-99.

Wilson, T.E., Grawunder, U., and Lieber, M.R. (1997). Yeast DNA ligase IV mediates non-homologous DNA end joining. Nature *388*, 495-498.

Wu, J., Huen, M.S., Lu, L.Y., Ye, L., Dou, Y., Ljungman, M., Chen, J., and Yu, X. (2009). Histone ubiquitylation associates with BRCA1-dependent DNA damage response. Mol Cell Biol *29*, 849-860.

Wysocka, J., and Herr, W. (2003). The herpes simplex virus VP16-induced complex: the makings of a regulatory switch. Trends Biochem Sci *28*, 294-304.

Yao, F., and Schaffer, P.A. (1995). An activity specified by the osteosarcoma line U2OS can substitute functionally for ICP0, a major regulatory protein of herpes simplex virus type 1. J Virol *69*, 6249-6258.

Ye, Y., and Rape, M. (2009). Building ubiquitin chains: E2 enzymes at work. Nat Rev Mol Cell Biol *10*, 755-764.

York, I.A., Roop, C., Andrews, D.W., Riddell, S.R., Graham, F.L., and Johnson, D.C. (1994). A cytosolic herpes simplex virus protein inhibits antigen presentation to CD8+ T lymphocytes. Cell *77*, 525-535.

You, Z., Chahwan, C., Bailis, J., Hunter, T., and Russell, P. (2005). ATM activation and its recruitment to damaged DNA require binding to the C terminus of Nbs1. Mol Cell Biol *25*, 5363-5379.

Yu, X., Chini, C.C., He, M., Mer, G., and Chen, J. (2003a). The BRCT domain is a phospho-protein binding domain. Science *302*, 639-642.

Yu, X., Yu, Y., Liu, B., Luo, K., Kong, W., Mao, P., and Yu, X.F. (2003b). Induction of APOBEC3G ubiquitylation and degradation by an HIV-1 Vif-Cul5-SCF complex. Science *302*, 1056-1060.